Analysing the performance of KHFAC nerve block stimulation parameters

Developing design considerations for blocking the pudendal nerve using a new gate-dependent block-determination model

K.M. Emmer

Master Thesis
Electrical Engineering

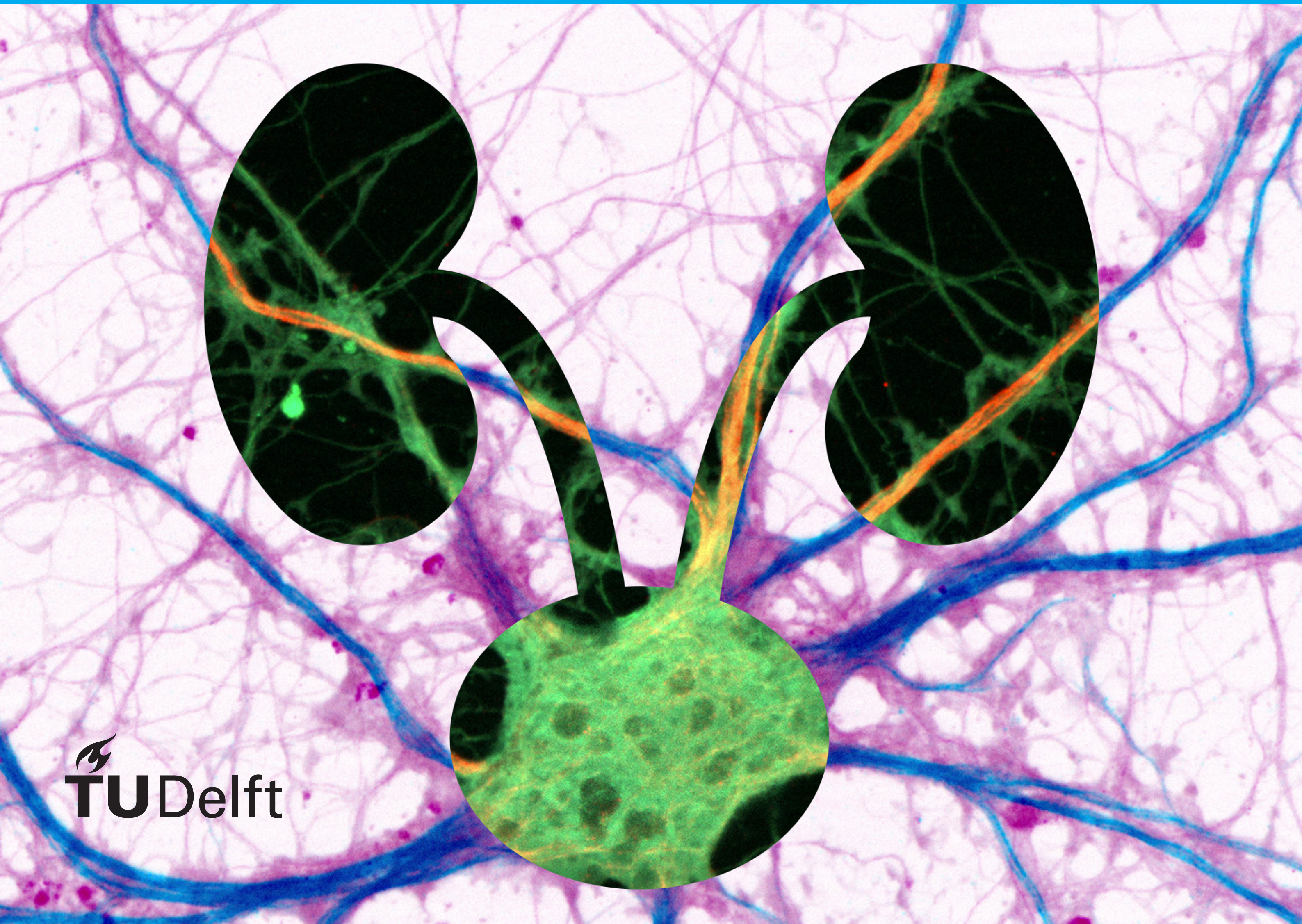

TU Delft

Analysing the performance of KHFAC nerve block stimulation parameters

Developing design considerations for blocking the pudendal nerve using a new gate-dependent block-determination model

by

K.M. Emmer

to obtain the degree of Master of Science
at the Delft University of Technology,
to be defended publicly on Friday May 24, 2019 at 11:00 AM

Student number:	4164156	
Project duration:	August 20, 2018 – May 24, 2019	
Thesis committee:	Prof. dr. ir. W. A. Serdijn,	TU Delft, supervisor
	Dr. ir. R. F. Remis,	TU Delft
	Dr. M. Negrello,	Erasmus MC

An electronic version of this thesis is available at http://repository.tudelft.nl/.

Preface

Dear reader,

It has been almost eight years since I first stepped onto the TU Delft campus as a fresh Electrical Engineering student, not knowing where this adventure would take me. The years after flew by, but graduation always seemed distant.

This changed nine months ago, when I first started working on my thesis: graduation suddenly became a dot that was clearly visible on the horizon. However, the road ahead was though, with many hurdles on the way; sometimes it felt like I was walking in circles, or even taking a few steps back. It even sometimes felt that I completely lost sight of the dot.

Yet here lies my Master's Thesis, which embodies not only the final deliverable, but also the most challenging leg of my journey to become Electrical Engineering student at the Delft University of Technology. A journey I would not have successfully completed without the support of many others. Therefore I would like to thank a number of people in person.

First and foremost, I would like to thank my supervisor Wouter Serdijn for his excellent support. When I encountered a sign that said "straight road to graduation", you challenged me to take another, much more difficult road, which resulted in a thesis that I can without doubt say to be very proud of. Whenever I felt that I was going backwards or felt that I lost sight of graduation, you helped me to identify what I already have accomplished, and showed me that I was well on the way to the finish line. Seeing with how much enthusiasm you help so many students get the best out of themselves, I feel honoured to have graduated at your group, and I hope that in the end I have been able to teach you some things as well.

I would like to thank Mario Negrello and Rob Remis for joining my thesis committee. I felt that this went without hesitation, and the enthusiasm you showed for my project makes me look forward to the interesting discussions we will have during the thesis defence. Thank you also Mario for our discussions on computational neuroscience, which helped me create the foundations of the direction of my thesis, and for introducing me to Brainframe, which made a lot of my thesis work a lot easier.

This thesis project would not have existed without Bertil Blok. I would like to thank you for trusting me with this project, and providing me with the medical insights and information that were needed for my project. I would also like to thank Panagiota and the rest of the Erasmus team for helping me answer all medical questions. I really look forward to hearing in the news about the first REValUE implant.

Past year was made much more interesting and fun by the Bioelectronics group. It was great to learn from so many fields presented by so many incredible researchers. I am confident that the world will see much more of the great work you are doing here. I would like to especially thank the students in the MSc room for making the thesis bearable with the fun distractions and coffee breaks. I would also like to especially thank Marc for reviewing my thesis and Rui for both reviewing my thesis and the many times she could help me answer any questions I had. I am glad that I was able to do something back for the Bioelectronics group by introducing the Friday Afternoon Drinks, or 'VrijMiBio', which is a tradition that I hope will last for decades!

Thanks as well to Harry and Konstantinos from Brainframe for letting me use your technology. I am happy that my feedback on your platform was helpful, and wish you good luck in creating one of the best neural simulation platforms.

Mum, Dad and Tijn, thank you for your confidence and trust over my whole academic career. I know that you have been wanting to hear a graduation date from me for quite some time now, and I was happy that you trusted me and stayed patient when I told you that I had no idea yet.

Dear Femke, thank you for motivating and supporting me whenever necessary, doing some thinking for me when I was unable to, and making sure that I was doing enough fun things to distract me from my thesis work.

Suzanne and Ron, it was great fun to graduating parallel to you, thank you for the distractions during the day. Some of the best ideas I had were at the end of our lunch or extended coffee break.

Finally thanks to all my friends and family that I have not previously mentioned. In many ways you have given me support that all helped to achieve the finish line of an eight year journey.

I would like to conclude this preface by giving a piece of advice to anyone who is starting on his/her thesis, inspired by the motto of Dutch Formula 1 driver Max Verstappen: 'Keep pushing'. Whenever you have the feeling that you are not getting anywhere, that progress is minimal or even absent, even if it lasts for weeks or even months: keep pushing. Not just anywhere, but at the place that you feel is the work environment, whether it is at a company, the MSc room of your department, or even the same table in the library that you go everyday: keep pushing. If at the end of the day you feel that you spent more time watching online videos or browsing your phone than reading meaningful literature, don't worry too much and keep pushing. Cumulatively speaking you have read more meaningful literature today than yesterday, and besides, 'doing nothing' was something you needed, and now it is out of your system: keep pushing. For me the first three months mostly felt like I was getting nowhere, but everyday I kept returning to the TU Delft. Then suddenly it hit me: I realized exactly where I had to go, and the road to graduation seemed as clear as day. All the knowledge that I acquired over the past months, that sometimes seemed useless, I could suddenly envision as chapters and sections of the thesis that lies in front of you. The three month delay I thought I built up, I never saw again: at the start I envisioned to finish the thesis in nine months, and that is exactly what happened.

The road ahead is tough, with many hurdles on the way; it will sometimes feel like you are walking in circles, or even taking a few steps back. It will even sometimes feel that you completely lost sight of the dot at the horizon. Gather the right people around you for support, that can shift your vision back to the dot. You will see that the dot has grown in size, as it moved closer. Because every day you put into your thesis, is you getting one day closer to graduation. Keep pushing, and good luck.

It makes me proud and happy to present you with my Master's Thesis. Enjoy reading!

K.M. Emmer
Delft, May 2019

Abstract

A major cause for voiding dysfunction is the inability to relax the urethral sphincter. KiloHertz Frequency Alternating Current (KHFAC) stimulation can block signals that are travelling through the body; applying this type of stimulation at the pudendal nerve could inhibit the pulses that lead to contraction of the urethral sphincter, and restore voiding ability.

In order to design a successful KHFAC block therapy for the pudendal nerve, it is necessary to understand what impact different stimulation parameters have on efficacy, safety and power-efficiency. This thesis will therefore test earlier researched KHFAC stimulation parameters against a new quality measure, study the impact of new waveform alterations, and study how bipolar electrode design can improve KHFAC therapy.

By utilizing the theory behind the mechanism of the KHFAC nerve block, a new block-determination model was developed that is over thirty times faster than the classic model. The McIntyre-Richardson-Grill model was chosen as the implementation of the axon model, and the bipolar electrode was modelled as an electric dipole.

The simulation experiments revealed that the charge per phase of the KHFAC signal at block threshold could be reduced, without increasing the amplitude of the signal, by introducing interphase delays to the waveforms and by creating asymmetric charge-balanced waveforms. Triangular waveforms were shown to also require less charge per phase than a regular square wave to block, albeit with a higher amplitude. A correctly aligned bipolar electrode set-up with an interpolar distance that was about the same as the electrode-to-axon distance was shown to result in reduced block thresholds.

Overall, this thesis has shown how stimulation parameters can be chosen to develop an effective KHFAC block therapy for the pudendal nerve.

Contents

Preface iii

Abstract v

List of Figures ix

List of Tables xi

1 Introduction 1
- 1.1 Previous research 1
- 1.2 Thesis objectives 2
- 1.3 Thesis outline 2

2 Urinary retention and KHFAC stimulation 5
- 2.1 Urinary Retention 5
- 2.2 KHFAC stimulation 6
  - 2.2.1 Nerve block mechanisms 7
  - 2.2.2 Earlier research on nerve block thresholds 11
- 2.3 High frequency nerve block in the pudendal nerve for treatment of nerve-related urinary retention: REValUE project 13
  - 2.3.1 Design goals 14
  - 2.3.2 Proposed electrode 14
  - 2.3.3 Properties of the human pudendal nerve 14
  - 2.3.4 Goal of this thesis for REValUE 14
- 2.4 Conclusion 15

3 Determination of effectiveness of block 17
- 3.1 Classic method: visualizing the actual block 17
  - 3.1.1 Disadvantages of classic method 18
- 3.2 Proposed method: Measurement of gate quantities 20
  - 3.2.1 Characteristics of sodium channel inactivation variable h during nerve block 21
  - 3.2.2 Implementing the gate-dependent method into a working model 21
  - 3.2.3 Performance of proposed model 23
- 3.3 Conclusion 26

4 Implementation of the simulator 27
- 4.1 Signal generation model 28
- 4.2 Electrode and axon environment model 28
  - 4.2.1 Monopolar set-up 28
  - 4.2.2 Bipolar electrode 29
  - 4.2.3 Improvements for modelling electrodes and axon environment 29
- 4.3 Axon model 31
  - 4.3.1 McIntyre-Richardson-Grill model for simulation of nerve block 31
  - 4.3.2 Properties of axon model 33
- 4.4 Simulation environment 33
  - 4.4.1 Interface with Brainframe 34
- 4.5 Conclusion 34

5 Simulation analysis of stimulation parameters for KHFAC stimulation 35
- 5.1 Simulation set-ups 35
  - 5.1.1 Monopolar set-ups 36
  - 5.1.2 Bipolar set-ups 36

5.2 Monopolar simulation results . . . 38
5.2.1 Influence of waveform . . . 38
5.2.2 Influence of distance along pudendal nerve diameter . . . 41
5.3 Bipolar simulation results . . . 43
5.3.1 Influence of interpolar distance on performance for two bipolar orientations . . . 43
5.3.2 Influence of interpolar distance on axons across the pudendal nerve . . . 44
5.3.3 Bipolar orientation . . . 46
5.4 Discussion . . . 46
5.4.1 Impact of results on design considerations . . . 46
5.4.2 Validity of results . . . 48
5.5 Conclusion . . . 50

6 Conclusions and recommendations 51
6.1 Conclusion . . . 51
6.2 Contributions . . . 52
6.3 Recommendations . . . 53
6.3.1 Recommendations for the REValUE project . . . 53
6.3.2 Recommendations for the gate-dependent block-determination model and future simulations . . . 53
6.3.3 Recommendations for KHFAC block research and applications . . . 53

A Electrode design considerations for kilohertz frequency alternating current nerve conduction block therapy in the human pudendal nerve 57

B Simulation system code 67

Glossary 69

Bibliography 71

List of Figures

2.1 Schematic of normal voiding operation 5
2.2 Block diagram of normal voiding operation 6
2.3 The voltage-gated sodium channel in three phases of the action potential 7
2.4 Membrane voltage and gate variables during an action potential 8
2.5 Membrane gate variables during KHFAC stimulation 9
2.6 Dependencies of h_∞, m_∞, τ_h and τ_m on the membrane voltage 10
2.7 Onset response 11
2.8 Relationship between block threshold and KHFAC frequency 12
2.9 Relationship between block threshold and electrode distance 12
2.10 Influence of asymmetric waveforms on the block threshold 13
2.11 Relationship between block threshold and axon diameter 13
2.12 Proposed electrode for REValUE project 14

3.1 Overview of a block threshold determination process 17
3.2 Typical simulation set-up for classic block-determination method 18
3.3 Example of a successful KHFAC block 19
3.4 Four different KHFAC block-determination simulations 20
3.5 Simulation set-up proposed for gate-dependent block-determination model 22
3.6 Settling time of variables in gate-dependent model 22
3.7 Charge-balanced asymmetrical waveform example 23
3.8 Error margins of gate-dependent block determination method for asymmetrical waveforms 24
3.9 Error margins of gate-dependent block determination method for sine waves 25

4.1 Overview of the complete simulation set-up 27
4.2 Electric field and equipotential lines for a point charge and a dipole 29
4.3 Monopolar simulation set-up 30
4.4 Bipolar simulation set-up 30
4.5 The double cable structure and circuit representation of the MRG model 32

5.1 Interpolar distance 36
5.2 Electrode set-up for the bipolar varying electrode-to-axon distance simulation 37
5.3 Electrode set-up for electrode orientation simulation 38
5.4 Results of basic waveform simulations 39
5.5 Results of stepped waveform simulations 39
5.6 Results of asymmetrical waveform simulations 40
5.7 Results of interphase delay simulations 42
5.8 Results of monopolar electrode distance simulations 42
5.9 Results of bipolar simulations with changing interpolar distances in a parallel and perpendicular configuration 43
5.10 Results of bipolar electrode distance simulations 44
5.11 Higher resolution results for bipolar electrode distance simulations, with focus on interpolar distances between 1 and 10 mm 45
5.12 Optimal interpolar distances for different electrode-to-axon distances 45
5.13 Results for bipolar orientation simulations 46
5.14 Three design options for including interphase delays in a waveform 47
5.15 Validation of interphase delay simulation results 49

List of Tables

4.1 Axon models used in nerve propagation block simulation studies 31
4.2 The MRG model parameters for an axon diameter of 10 µm 33

5.1 Simulation parameters for monopolar simulations 36
5.2 Simulation parameters for bipolar simulations 37

1

Introduction

A 2011 study estimated the worldwide prevalence of lower urinary tract symptoms, and predicted that in 2018 over 1 billion people worldwide would suffer from symptoms related to voiding [1]. Voiding dysfunction can result from multiple symptoms, one of which is the inability to relax the urethral sphincter, the ‘exit’ through which urine can leave the bladder [2]. Its cause can be related to neural damage, but it can also be a psychological problem.

A new type of stimulation, which involves sending an alternating electric signal of frequencies in the kilohertz range, has shown its ability to put a nerve in a ‘blocked’ state, where pulses travelling through the nerve can not propagate past the point where the stimulation is applied. The terminology for this type of stimulation is called KiloHertz Frequency Alternating Current (KHFAC) block, as proposed by Kilgore and Bhadra [3]. This type of induced nerve propagation block has been shown to be quickly reversible; meaning that after ending the stimulation, cells quickly restore to their original state with no signs of tissue damage [4].

KHFAC stimulation has therefore been proposed as a solution to urethral sphincter related voiding dysfunction, as it could create a reversible block of the pulses that originate from the central nervous system to contract the sphincter. The REValUE (REstoring Voiding Urinary rEtention) project, a research collaboration between the Delft University of Technology (TU Delft) and Erasmus University Medical Center (Erasmus MC), aims to apply this theory to create a working implant that can block pulses travelling through the pudendal nerve [5]. To develop an implant that is able to deliver an efficient and safe blocking therapy, knowledge must first be developed on how this implant should be designed.

1.1. Previous research

Since Kilgore and Bhadra demonstrated in 2004 that the nerve block was not a result of muscle fatigue [4], different research groups have been using simulation approaches, often validated by experimental research, to find stimulation parameters that can reduce the block threshold. This block threshold is defined as the minimum required current amplitude that creates a block under specific conditions.

Parameters that have been tested previously are:

- signal frequency [6],
- electrode-to-axon distance [6],
- axon diameter [6],
- a selection of different waveforms [3, 7],
- temperature [8, 9], and
- electrode surface area (for nerve cuff electrodes) [10].

However, not all of these studies have used human-like axon models; other axon models can have different blocking mechanisms, which result in outcomes that can be different and invalid for human nerves.

Furthermore, all of the mentioned simulation studies only focus on monopolar set-ups (set-ups involving a return electrode placed at infinite distance); there is only one research that utilizes a bipolar set-up (a set-up involving a return electrode placed near the active electrode) to examine if block thresholds can be reduced by changing the interpolar distance (the distance between the stimulating and return electrode) [11]. However, this research only examines the case of an electrode that is perfectly aligned at 1.0 mm above the axon; no insight is given on changing electrode orientations or distances.

Thus far, all of these studies only focused on the block threshold as a performance variable. However, the required charge per phase at block threshold is just as important, as this is a measure of how many electrons are actually physically injected into the tissue, and moreover the amount of injected charge at the electrode-tissue interface should be minimized to prevent irreversible Faradaic reactions from occurring [12]. The charge per phase is defined as the area underneath the positive or negative phase of a single signal period of the current wave; it is therefore dependent on the shape and width of the waveform. A waveform with a higher block threshold than another waveform can thus require less charge per phase. Bhadra et al. [6] mentions the charge per phase, but only to compare the behaviour of the KHFAC block thresholds to regular stimulation activation thresholds.

Another thing all previously mentioned KHFAC simulations have in common, is the way they establish whether the simulation parameters lead to a successful block or not. This is a time-consuming process, which has to be repeated until the block threshold has been found.

1.2. Thesis objectives

The main objective of this thesis is to find the important design considerations for building a KHFAC block implant for the pudendal nerve. The main question that thus needs to be answered is:

"What is the impact of different design parameters on the effectiveness of a KHFAC conduction block in the pudendal nerve?"

To answer this question, the following steps will be taken:

1. A new block-determination model for simulations will be developed to reduce simulation time. The new model will use the theory behind the mechanism of the nerve block to achieve this speed-up. The reduced simulation time will allow many more stimulation parameters to be evaluated for their impact on the KHFAC block.
2. Existing research on stimulation parameters will be revisited, using a human-like axon model and with an added focus on the charge per phase. The goal is to find out if some of these previously researched parameters, that were either ignored or seemed to reduce performance as they resulted in increased block thresholds, can compensate by requiring less charge per phase. This could lead to new design possibilities.
3. New waveform alterations, that have not been researched yet, will be tested for their impact on the performance of the KHFAC block.
4. The effect of bipolar electrode design will be further evaluated. It will be observed how different interpolar distances will influence the block threshold at different distances from the nerve, and also how electrode orientation will affect the block thresholds.

The simulations are tailored to the pudendal nerve. The resulting data can then later be used for designing a therapy for the REValUE project, which corresponds with experimentally proven safe and efficacious electrical stimulation limits.

1.3. Thesis outline

The remainder of this thesis will elaborate on the problem of finding the impact of different design parameters for KHFAC stimulation in the pudendal nerve, focus on the simulation approach of this thesis that is used to solve this problem, and present the results that lead to the final conclusions.

Chapter 2 contains the necessary background information to understand the motivation of this work. An elaboration on urinary retention is given, and KHFAC nerve propagation block is introduced. The mechanism behind this phenomenon is explained, and existing research on KHFAC stimulation is presented. The REValUE project [5] is also introduced, which is the original motivation for this thesis and researches if KHFAC stimulation can become a real treatment for urinary retention.

Chapter 3 focuses on the design of a new simulation method for detecting a successful block. First, the classic method is introduced. Then the theory supporting the new method is explained, and step-by-step the method is designed into a fully working model, which is tested against the classic block-detection method.

In Chapter 4, the full simulation system is introduced. The chapter covers the equations describing the different electrode configurations, the explanation and justification of the McIntyre-Richardson-Grill (MRG) model [13], and the simulation software that is used and how it impacts the design. It is also clarified how the previously designed block-detection model is implemented in the simulation system.

The results of the simulations are presented and analysed in Chapter 5. From these analyses, design considerations for KHFAC therapy in the pudendal nerve are derived.

Chapter 6 summarizes the conclusions of this thesis, and points out the contributions of this work. With the knowledge that has been gathered for this thesis, recommendations are made not only for the REValUE project, but for the entire field of KHFAC nerve propagation block.

A glossary is added for convenience at the end of this thesis. This includes both the medical terminology that is important for this thesis work, as well as new terminology that is first introduced in this thesis.

2

Urinary retention and KHFAC stimulation

This chapter presents the literature that is necessary to understand this work, and highlights the higher overall goal to which this thesis contributes. Section 2.1 starts by introducing urinary retention: the high-level problem to which solution this thesis contributes. Section 2.2 introduces KiloHertz Frequency Alternating Current (KHFAC) stimulation as a solution to this problem. The underlying theory is explained, together with the characteristics of this type of inhibiting stimulation that were found in previous studies. In Section 2.3 the REValUE Project is introduced, which is the research project that aims to bring KHFAC stimulation to patients suffering from urinary retention; an insight is given in how this thesis contributes to the REValUE project, and the parameters that are defined by the project and are important for this thesis are discussed.

2.1. Urinary Retention

The normal control of micturition, or urination, can be roughly split up in three actions: (1) the contraction of the bladder, (2) the relaxation of the internal urethral sphincter, and (3) the relaxation of external urethral sphincter [14]; (1) and (3) are shown in Figure 2.1 and Figure 2.2. The external urethral sphincter is voluntarily relaxed during micturition; outside of micturition, the pudendal nerve is continuously stimulating the external urethral sphincter to contract it and prevent leaking [15].

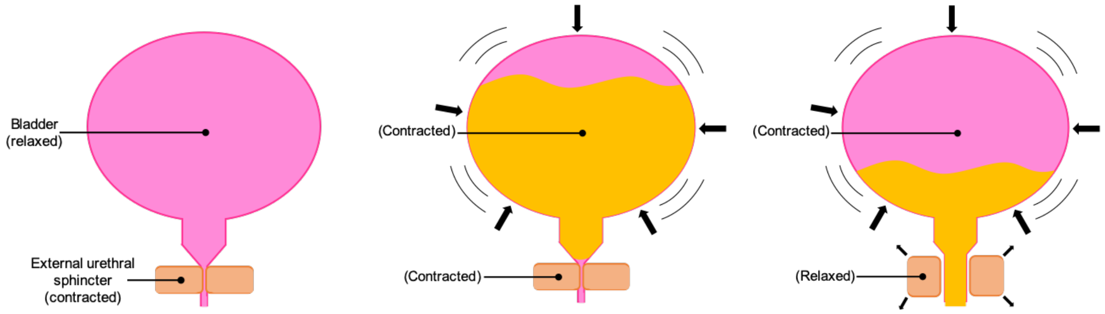

(a) (b) (c)

Figure 2.1: A schematic figure depicting normal voiding operation, focused on the bladder and the external urethral sphincter. (a) Non-voiding operation. The bladder is relaxed; the external urethral sphincter is contracted to prevent urine from leaking out. (b) Contraction of the bladder. Voiding is initiated by contracting the bladder, but urine can't exit the bladder while the external urethral sphincter is contracted. (c) Relaxation of the external urethral sphincter. Due to the increased bladder pressure, the external urethral sphincter is relaxed, and the bladder is emptied.

One of the main causes for voiding dysfunction is the inability to voluntarily relax the external urethral sphincter. Causes can be related to neural damage, such as a spinal cord injury, but can also be psychological, such as paruresis ('shy bladder') [16]. The result is an inability to fully empty the bladder, or even an inability to void at all. Next to causing huge discomfort, not properly voiding the bladder can result in the tearing of the bladder, and urine being pushed back into the kidneys due to increased bladder pressure which can lead to severe health issues in the kidneys [17].

Treatment methods include [2]:

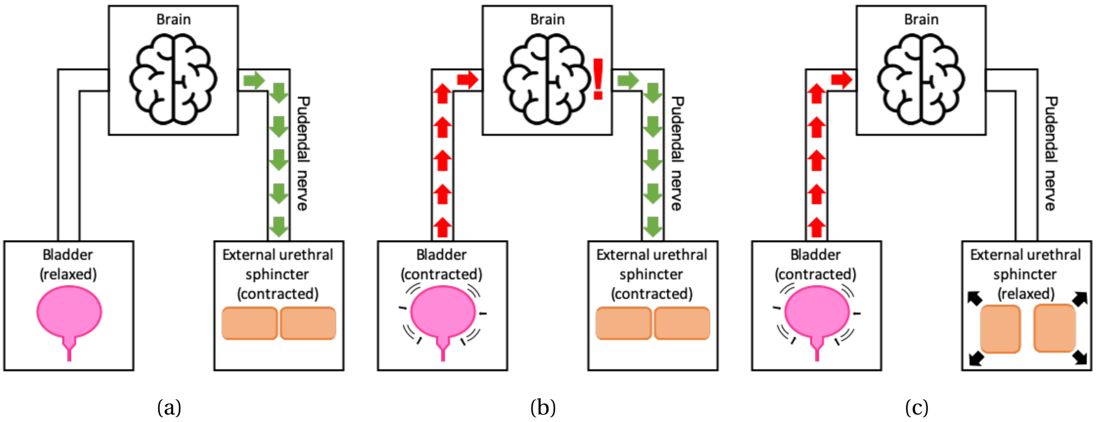

Figure 2.2: Block diagram of voiding operation. (a) Non-voiding operation. The brain is sending pulses via the pudendal nerve to the external urethral sphincter to ensure it is contracted. (b) Contraction of the bladder. Voiding is initiated by contracting the bladder, resulting in an increased bladder pressure, which is signalled to the brain. (c) Relaxation of the external urethral sphincter. The brain reacts to the increased bladder pressure and stops sending pulses to the external urethral sphincter, relaxing it; now voiding of the bladder can take place.

- Mechanically emptying the bladder by, often intermittent, urethral catheterization; this method is the most common, but can lead to a urinary tract infections,

- Relaxation of the external urethral sphincter by injecting botulin toxin; this method is not yet supported by enough evidence,

- Surgery, which is highly invasive, has high costs and can cause irreversible effects.

None of these methods restore the original functionality: a temporary and quickly reversible relaxation of the external urethral sphincter. If such a treatment method would exist, it would be the preferred over all others.

A more elaborate study on urinary retention can be found in the master thesis of Baquer Gómez [18].

2.2. KHFAC stimulation

Electrical stimulation is often related to the elicitation of action potentials in the nerve by the use of electrical current. However, Tanner first mentioned a potential opposite application of electrical stimulation in 1962 [19]: inducing a reversible nerve conduction block. The hypothesis is that when a nerve is stimulated with an alternating current signal of sufficiently high frequency and amplitude, no more action potential propagation can take place inside the nerve. The lowest current amplitude for a specific frequency at which complete block persists is defined as the block threshold for that frequency [3].

In 2004, Kilgore and Bhadra demonstrated through both simulation and experiment, that, for AC waveforms with frequencies in the range of 3 kHz to 10 kHz, a 100% block of action potential propagation in the stimulated nerve could be accomplished [4]. The experiment demonstrated that these were true conduction blocks, which blocking mechanism was different from synaptic and neural conduction fatigue. Their simulations showed that during KHFAC stimulation, the paranode regions become sufficiently depolarised such that action potentials can no longer propagate through them.

Applications of this quickly reversible nerve block involve any treatment where the goal is to stop signals coming in from one end of the nerve to reach the other end. An example is chronic pain treatment, where KHFAC stimulation can be used to stop ‘pain’-signals from reaching the brain. The Nevro Senza System [20] provides such a treatment for people with back pain or leg pain, by applying a 10 kHz signal. Another potential application would be to block signals sent from the central nervous system to the urethral sphincter, to force a relaxation of the sphincter muscle resulting in proper micturition; a treatment for the dysfunction explained in Section 2.1.

This section presents a literature overview of KHFAC nerve blocks. First, the theory behind the mechanism of the nerve block will be discussed. This will be followed by an overview of earlier research that has been done on determining nerve block thresholds.

2.2.1. Nerve block mechanisms

At the moment, there are two different hypotheses on why a nerve block occurs, based on different simulation studies. The reason there's a difference between the two theories, is because the axon models used are based on different species. The two theories on KHFAC induced nerve block are:

- **Outward potassium currents overwhelm the inward sodium currents at the nodes of Ranvier (or axon section in unmyelinated axons)**. This theory was proposed by Zhang et al. [21] in 2006 based on simulations done with the Frankenhaeuser-Huxley (FH) model [22]. Wang et al. [9] found the same result after simulating the nerve block using the Schwarz-Eikhof (SE) equation [23]. However, Wang et al. note that the fast potassium current is small in mammalian myelinated axon, suggesting that KHFAC block for this type of axons is still mostly a result of the inactivation of sodium channels. There is also no experimental confirmation of this theory being the cause of the nerve block.

- **Inactivation of the sodium channel**. In 2007, Bhadra et al. [6] also looked into the mechanism of conduction block, and found that for the McIntyre-Richardson-Grill (MRG) model, the average inward sodium current exceeded the average outward potassium current; the theory of Zhang et al. [21] was thus not applicable. Instead, Bhadra et al. found that the sodium channels are in a state of inactivation during KHFAC stimulation, which causes the conduction block.

The FH model and SE model are based on frog and rat data, respectively, whereas the MRG model is based on data from mammalian axons. This means that for human axons, as the fast potassium current is small, the most likely mechanism for the nerve block is the inactivation of the sodium channel.

Cellular mechanisms

Cell membranes contain ion channels that allow the passing of ions through the membrane. The two most important ions in generating electrical signals are sodium and potassium. The regulation of their in- and outflow is modelled by at least three membrane 'gates', that open or close their respective ion channels. These were first defined and quantitatively described by Hodgkin and Huxley [24]. Two of these gates are related to the voltage-gated sodium channel, and one is related to the voltage-gated potassium channel. The membrane channel gates are described by their state variables: m for the sodium activation gate, h for the sodium inactivation gate, and s for the potassium activation gate. These 'gate' variables are dimensionless and have a value between 0 and 1. A value of 0 means that the gate is 'closed', whereas a value of 1 means that the gate is 'open', and that the ions corresponding to the gate can flow through. A visualization of the sodium channel, containing both activation and inactivation gate, is given in Figure 2.3.

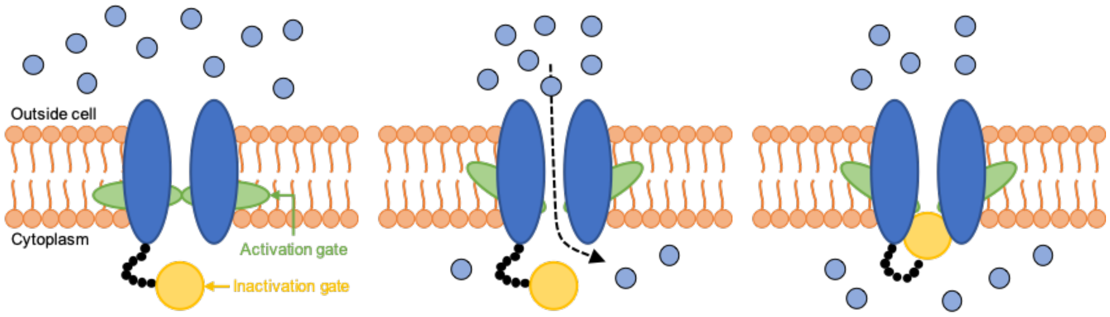

(a) Closed state (b) Open state (c) Inactivated state

Figure 2.3: The voltage-gated sodium channel in three phases of the action potential. (a) The sodium channel at resting potential is in a *closed* state. This is due to the activation gate m (green) being closed. (b) When the membrane voltage becomes higher than the threshold voltage, the activation gate m opens, and positively charged sodium ions start flowing through the membrane, dramatically increasing the membrane voltage. (c) With a small delay the inactivation gate h (yellow) closes, and no more sodium ions flow through the membrane. The sodium channel is now inactivated. By now, the potassium channel s (not in the figure) is opened, restoring the membrane potential to its initial value.

To properly understand the mechanics behind a nerve block, it is important to understand the mechanism behind nerve activation. Signals travel through nerves as 'action potentials', which are short peaks of the membrane potential of the axon, as shown in Figure 2.4.

A typical action potential cycles through four phases [25]:

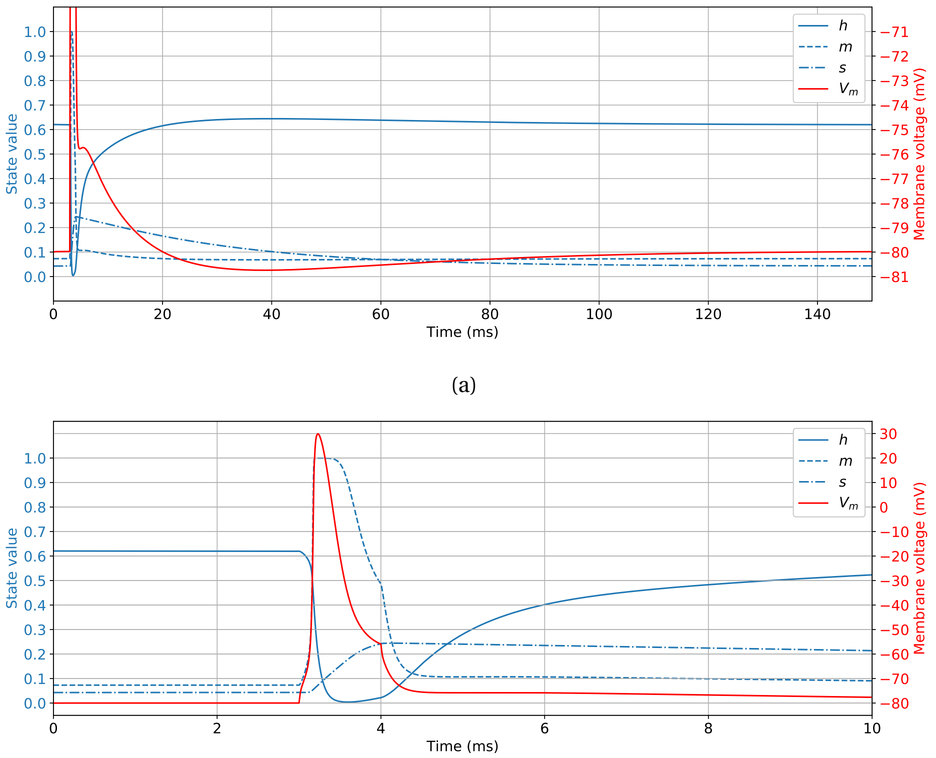

(a)

(b)

Figure 2.4: The membrane voltage V_m, sodium inactivation gate variable h, sodium activation gate variable m, and potassium activation gate variable s during an action potential. The action potential is triggered by a single test pulse delivered at $t = 3$ ms. The axon was modelled by the MRG model such that the simulated behaviour closely resembles that of a human axon. (a) The action potential with the afterhyperpolarization visualized. The scale has been adjusted such that the small afterhyperpolarization is clearly visible. The peak value of V_m, which is 30 mV, is therefore not shown. (b) A close-up of the depolarization and repolarization phase of the action potential. Note the different scale for the membrane voltage; the peak value of V_m is now clearly shown.

1. The membrane starts at the resting potential, where the different components of the membrane current are in equilibrium; this results in a constant resting potential. This state of the membrane is visualized in Figure 2.3a for the sodium channel.
2. When a stimulus is applied, the activation gate of the sodium channel (m) will open, leading to a massive inflow of sodium ions. This leads to a rapid spike in voltage, and is called ‘depolarization’. This state is visualized in Figure 2.3b for the sodium channel.
3. The increased membrane voltage also leads to the closing of the sodium inactivation gate (h), a process that is slightly slower than the opening of the sodium activation gate. The inactivation gate is often modelled as a ‘ball-and-chain’ gate; the massive inflow of sodium ions moves the ball toward the opening of the sodium channel, effectively closing it. At the same time, the slow potassium channel (s) opens, leading to the outflow of potassium ions, decreasing the membrane voltage; this is called ‘repolarization’. This state is visualized in Figure 2.3c for the sodium channel.
4. The outflow of potassium channels leads to an undershoot of the membrane voltage. The sodium and potassium ions redistribute themselves across the membrane, until the resting voltage is restored. This period of undershoot being restored is called ‘afterhyperpolarization’.

When a KHFAC signal is applied at a node of Ranvier, some of the gate variables behave different compared to when an action potential is triggered: it can be observed from Figure 2.5 that, after the inactivation variable h in and around the stimulated node drops close to 0, it does not rise again; whereas m is fluctuating between values above 0.5. These nodes thus remain in a state of inactivation.

Especially the two nodes around the KHFAC stimulated node seem to exhibit this behaviour, with the lowest values for h of the entire axon (visible in Figure 2.5a). These two nodes are referred to in literature as 'virtual anodes' [4, 26].

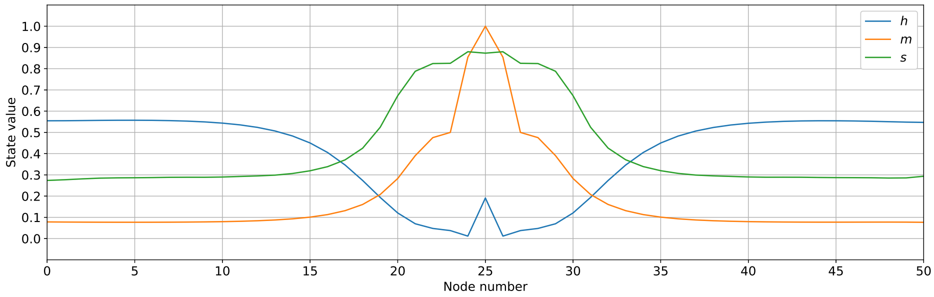

(a)

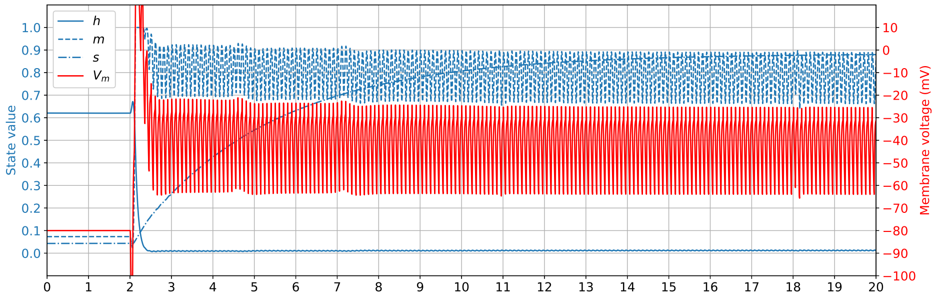

(b)

Figure 2.5: Application of KHFAC stimulation to an MRG axon of 51 nodes (10 kHz, 1.0 mA, 1.0 mm electrode-to-axon distance, 10 µm axon diameter). The KHFAC signal was initiated above node 25 at t = 2 ms. (a) The values of all gate variables at t =20 ms. At the two nodes surrounding the node closest to the KHFAC electrode (nodes 24 and 26), h is closest to 0. These two nodes are referred to in literature as 'virtual anodes' [4, 26]. (b) The membrane voltage and gate parameters over time for node 26, one of the two virtual anodes. After application of the KHFAC signal, h drops to nearly 0 and does not rise again, whereas m is fluctuating between values above 0.5; the sodium channel is thus in a state of inactivation. The membrane voltage is still fluctuating as a result of the varying electric field caused by the KHFAC electrode, but no new action potentials are triggered. Meanwhile, s restores to its original value, as it would do after a regular action potential; the potassium channel thus seems to be unaffected by KHFAC stimulation.

An inactivated sodium channel leads to a nerve block, as it can no longer elicit new action potentials. This can be observed from analysing the sodium current, which is given by the following equation [24]:

$$I_{Na} = g_{Na} * m^3 * h * (V_m - E_{Na}) \tag{2.1}$$

Where g_{Na} is a constant representing the maximum conductance for the sodium channel in Siemens, V_m is the membrane voltage in millivolt, and E_{Na} is the equilibrium potential for sodium ions in millivolt. This equation implies that a low h value (which points to an inactivated sodium channel) results in a small sodium current, which makes it impossible to trigger a new action potential; this would thus result in a blocked axon.

Although it is unclear why the sodium inactivation gate remains closed, an explanation can possibly be found in the definition of the inactivation parameter h [24]:

$$\frac{dh}{dt} = \alpha_h(1-h) - \beta_h h \tag{2.2}$$

where parameters α_h and β_h are rate constants (in ms^{-1}) given by the MRG model as [13]:

$$\alpha_h = \frac{0.34 * -(V_m + 114)}{1 - e^{(V_m+114)/11}} \tag{2.3}$$

$$\beta_h = \frac{12.6}{1 + e^{-(V_m+31.8)/13.4}} \tag{2.4}$$

From these equations, it can be seen that the change in h is a function of the membrane potential V_m. This membrane potential is dependent on the charge concentrations on both the intracellular and extracellular sides of the membrane. When applying a signal on the extracellular side, with high frequency and sufficient amplitude, the charge concentration on the extracellular side continuously changes at a high rate. As a result, the same thing happens to the membrane potential; the inactivation gate is now too slow to keep up, resulting in values for $\frac{dh}{dt}$ that are too low to raise the value of h closer to 1.

From Equation (2.2) there are also two other variables that can be derived, namely the steady-state solution h_∞ and time constant τ_h:

$$h_\infty = \frac{\alpha_h}{\alpha_h + \beta_h} \tag{2.5}$$

$$\tau_h = \frac{1}{\alpha_h + \beta_h} \tag{2.6}$$

Since α_h and β_h are functions of the membrane potential V_m, h_∞ and τ_h are so as well, and they can be plotted against the membrane potential. This results in the plot of Figure 2.6 for the steady-state values and time constants of both h and m (which has mostly the same set of equations as h, but different definitions for α_m and β_m). The most interesting of these curves, is that the time constant of h has a large peak in its dependency of V_m; at a V_m around −75 mV, h changes more than ten times slower than at a V_m of 0 mV.

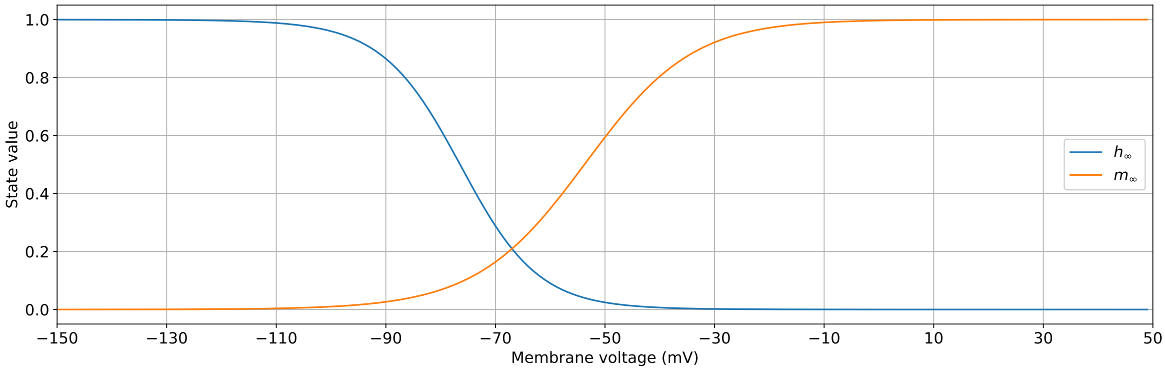

(a)

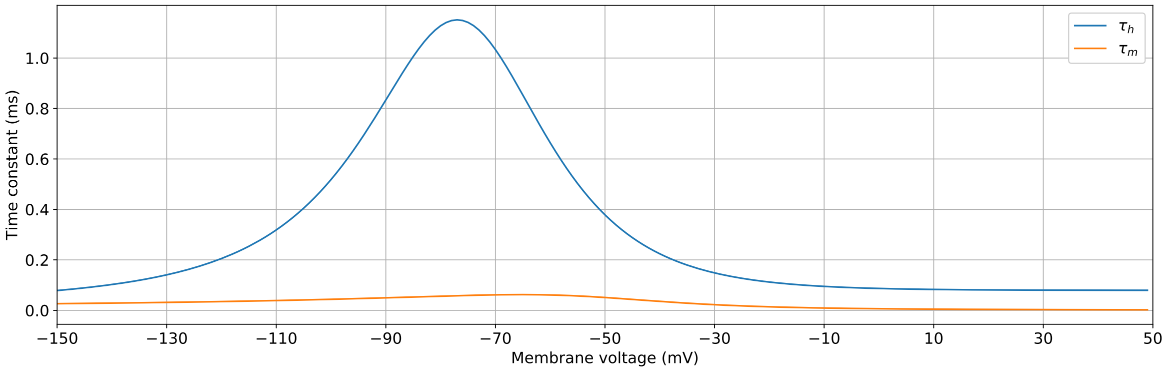

(b)

Figure 2.6: The dependencies of (a) steady-state values h_∞ and m_∞, and (b) time constants τ_h and τ_m on the membrane voltage V_m. Note how inactivation variable h has a relatively small time constant for steady-state values close to 0, whereas h has a relatively high time constant at steady-state values close to 1. This implies that the inactivation gate closes faster than it opens. It can also be seen that m is much faster than h, which allows the sodium channel to be briefly opened during an action potential before being inactivated.

Onset response

In both experimental and computational studies, one or multiple peaks in the membrane potential are visible immediately after applying KHFAC-stimulation; this is called the 'onset response', of which an example is shown in Figure 2.7. There has been no record of applying KHFAC stimulation without this onset response, although some solutions have been provided, such as adding a short DC pulse next to the KHFAC stimulation site [27], or by combining the KHFAC stimulation with infrared light [28].

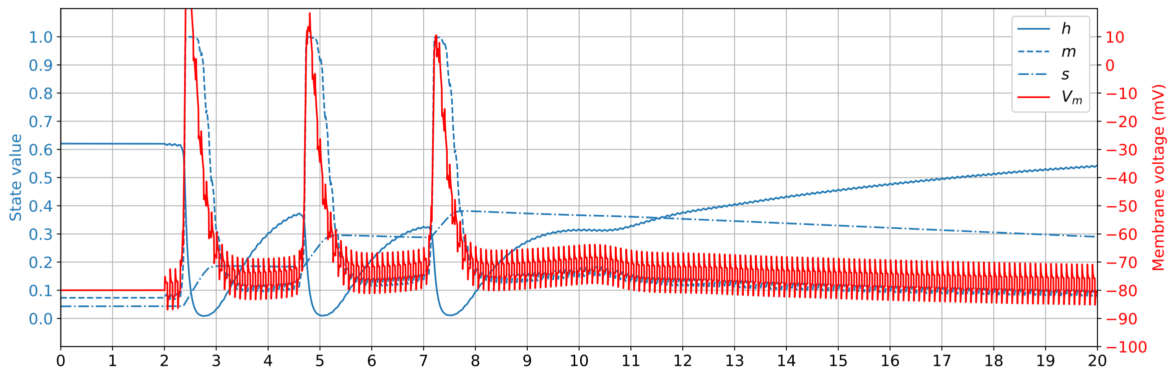

Figure 2.7: Membrane potential and gate parameter state values over time of a node showing the onset response after KHFAC stimulation (10 kHz, 1.0 mA, 1.0 mm electrode-to-axon distance, 10 µm axon diameter). The figure is a result of the same simulation as done in Figure 2.5, and focuses on node 10, and is thus 15 nodes of Ranvier apart from the node above which the KHFAC signal is applied. The KHFAC signal is initiated at node 25 at $t = 2$ ms. For node 10 this results in an action potential triggered with slight delay around $t = 2.5$ ms, and two more at $t = 4.7$ ms and $t = 7.2$ ms; this effect is called the onset response.

It has been found that it is not possible to obtain conduction block without firing at least one action potential [29]. However, once block is obtained, the current amplitude can be adjusted to another level sufficient for block without firing more action potentials. Furthermore, the number of action potentials that were fired at block threshold is higher with smaller diameter axons.

Miles et al. tested the hypothesis that slowly ramping up the amplitude of a KHFAC waveform could produce nerve block without an onset response, both through experiment and simulation [29]. The onset response did not disappear for any of these simulations and experiments, proving that slowly ramping up the amplitude does not prevent the onset response from occurring.

There is no clear evidence yet on why this onset response takes place. However, in order to reach the inactivation state, the sodium channel should first be put in the activation state (as explained in Figure 2.3). Following this line of thought, the application of a KHFAC signal should always trigger at least one action potential before it blocks the axon.

The aforementioned research by Miles et al. does show that the onset response causes a peak twitch force in muscle tissue [29], most likely due to that the onset response often consists of multiple rapid action potentials after another. The presence of this onset response is important, as the rapid pulses can result in unwanted muscle twitches (in the efferent path) or possibly the feeling of pain (in the afferent path). The true severity of this problem is however yet to be proven, and should be weighed against the potential benefit of KHFAC nerve block.

2.2.2. Earlier research on nerve block thresholds

There are already many simulation and experimental studies that have been performed on the block thresholds for changing conditions. So far, most simulation studies involve a monopolar set-up, where the return electrode is placed at infinity. It has been studied how blocking frequency, electrode distance, waveform and axon diameter affect the blocking threshold; however, detailed simulation results are sometimes missing.

KHFAC frequency

From the lowest possible KHFAC frequency to 10 kHz, the blocking threshold current increased in a non-linear manner [6]. Above 10 kHz, the block threshold increases linearly. This behaviour can be observed in Figure 2.8.

KHFAC electrode distance

Williamson and Andrews first attempted in 2005 to derive general relationships for current versus diameter, frequency and sinusoidal source location for nerve block [30]. They stated that a full nerve block through the entire cross section of the nerve, would require blocking axons of different diameters, with different distances between the source of the KHFAC electrode and the closest node of Ranvier of each axon. The relationship between the block threshold and the axon diameter was derived to fit:

$$I = b + \left(\frac{D}{d}\right)^{-m} \tag{2.7}$$

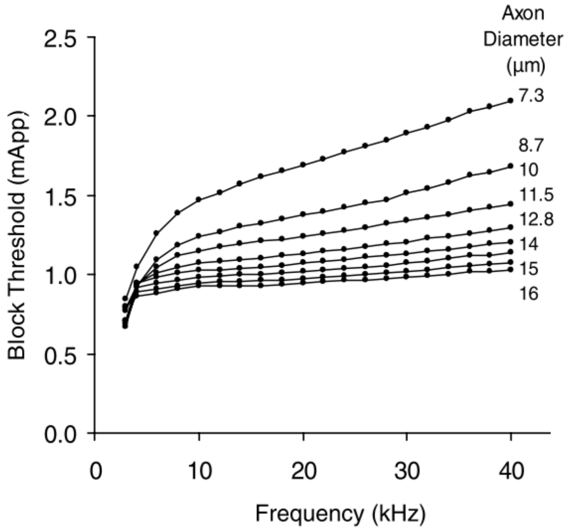

Figure 2.8: The relationship between the frequency used for the KHFAC signal and the block threshold, as found by Bhadra et al. [6]. The set-up used a 1 mm electrode to axon distance.

with I the current in μA and d the diameter of the axon in μm. Offset b, diameter constant D and exponent m were fitted based on the data found.

The relationship between the block threshold and perpendicular distance from the blocking stimulus source to the axon was derived to fit:

$$I = Ae^{mz} \tag{2.8}$$

with I the current threshold, z the perpendicular distance between the KHFAC electrode and axon, and m and A constants, that were fitted based on the data found.

Bhadra et al. [6] researched the influence of the electrode distance as well, but by using the MRG model, and also found an approximately square relationship between the block threshold and the perpendicular distance between blocking electrode and axon. It was stated that when the electrode was moved to closer than 1 mm to the axon, the distance of the electrode to the nearest node became the predominant factor influencing block threshold. This can be observed from Figure 2.9. However, in a real clinical application it is unlikely that the electrode will be this close to the axons that need to be blocked, and the minimal effect of the parallel distance can be ignored.

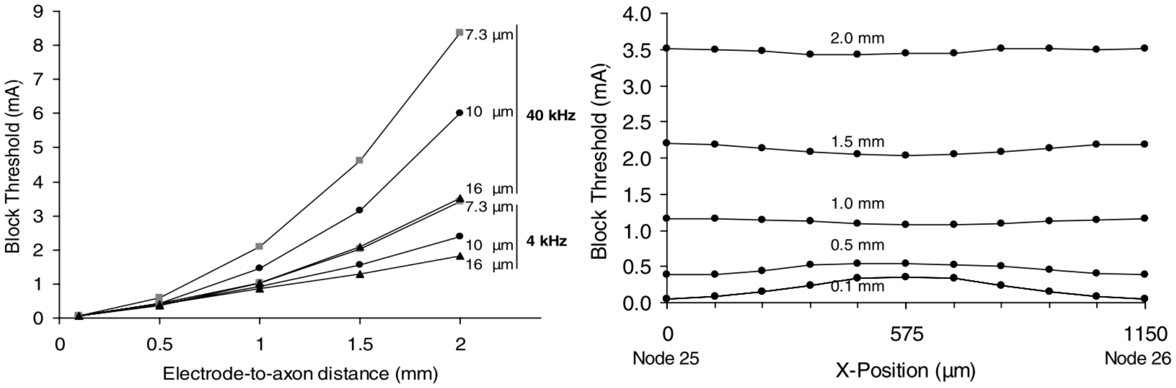

(a) (b)

Figure 2.9: The relationship between the KHFAC electrode distance and the block threshold, as found by Bhadra et al. [6]. (a) The influence of changing the perpendicular distance between the KHFAC electrode and the axon. (b) The influence of changing the parallel location of the KHFAC electrode along the axon for different perpendicular distances.

KHFAC signal waveform

According to Kilgore and Bhadra [3], there are no significant differences between rectangular, sinusoidal, or triangular waveforms, except that the block thresholds are lowest for square waves and highest for triangular waves.

Zhao et al. [7] researched the influence of using asymmetric waveforms in the blocking signal by using the FH-model. A symmetric square wave was compared to a waveform that had a positive pulse that was 1 µs or 2 µs longer than the negative pulse, and to a waveform that had a negative pulse that was 1 µs or 2 µs longer than the positive pulse. However, the amplitudes were not corrected to maintain charge balance. The result can be found in Figure 2.10.

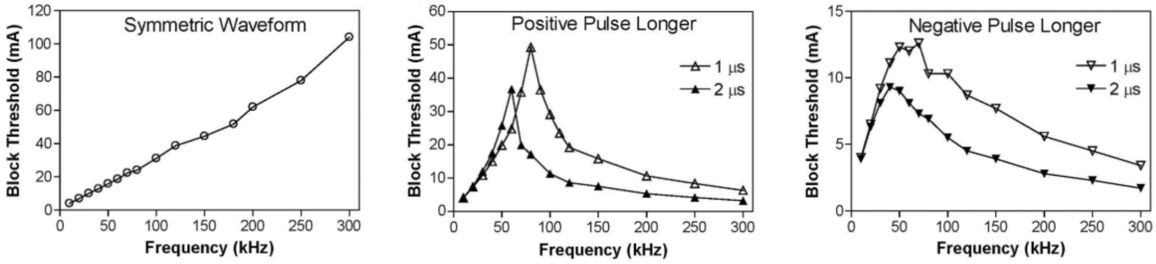

(a) (b) (c)

Figure 2.10: The influence of using asymmetric waveforms on the block threshold, as researched by Zhao et al. [7].

Axon diameter

Larger axon diameters result in lower block thresholds, as was shown in the research by Bhadra et al. [6] (Figure 2.11). This effect was stronger at higher KHFAC frequencies, as with the lower frequencies the block threshold was approximately constant with changing axon diameters.

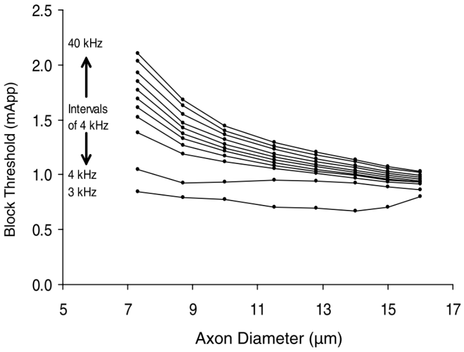

Figure 2.11: The relationship between the axon diameter and the block threshold at different frequencies, as found by Bhadra et al. [6]. The set-up used a 1 mm electrode to axon distance.

2.3. High frequency nerve block in the pudendal nerve for treatment of nerve-related urinary retention: REValUE project

As stated in Section 2.1, urinary retention can be caused by an inability to voluntarily relax the urethral sphincter. A KHFAC-induced nerve propagation block, introduced in Section 2.2, can be used to stop action potentials from propagating through a nerve. Theoretically, by applying a KHFAC signal to the pudendal nerve, the signals coming from the central nervous system that are on their way to the external urethral sphincter can be blocked 'by the press of a button', returning voluntary control over the relaxation of the urethral sphincter. This theory is the motivation behind the REValUE (REstoring Voiding Urinary rEtention) project [5], a collaboration between Erasmus MC and TU Delft.

This section will start by discussing the project design goals. The electrode that is preferred for the project has been determined before, and the location of implantation as well: this leads to constraints, which will be discussed next. The section will conclude with how this thesis will contribute to the project.

2.3.1. Design goals

The goal of the REValUE project is to develop a neurostimulator for humans that produces a temporary, quickly reversible action potential propagation block in the pudendal nerve, which should result in relaxation of the urethral sphincter. The patient should be able to control when the block is initiated. The stimulation therapy should be efficacious, power-efficient and safe (i.e., it should not result in nerve damage). The stimulation signal should be controllable, such that the settings can be adjusted to work best for a specific patient. A full nerve block may not always be necessary, as different bladder pressures require different urethral pressures for optimal operation. Ideally, the signal is adjusted during voiding to produce a block that corresponds to the bladder pressure.

2.3.2. Proposed electrode

The electrode that is proposed for the stimulator, is the Medtronic Spinal Neurostimulation Lead [31], shown in Figure 2.12. The lead has four cylindrical electrodes, and is part of the Medtronic InterStim system. This lead has the advantage that it can be implanted relatively easy, by making a small incision and from there positioning it next to the pudendal nerve, as it offers fluoroscopy and positioning with visual aids. This is a surgical operation that can be completed within half an hour. This makes it highly preferred to a cuff-type electrode, which is placed around a nerve. Placing a cuff-type electrode is a surgically much more invasive operation, requiring multiple doctors working on a single patient for multiple hours.

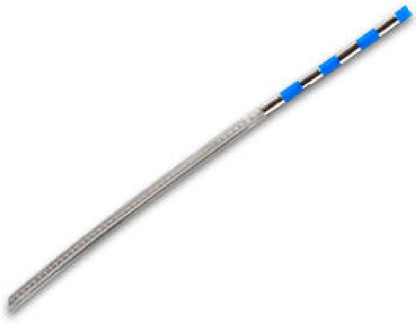

Figure 2.12: The Medtronic Spinal Neurostimulation Lead 3889, that is the proposed electrode for the REValUE project. Source: Medtronic [31].

2.3.3. Properties of the human pudendal nerve

The human pudendal nerve is a mixed nerve (meaning that it contains both afferent and efferent nerves) that consists of myelinated axons. The proposed stimulation site for the REValUE project is Alcock's canal (also named pudendal canal), a fascial compartment containing the pudendal nerves, arteries and veins. Alcock's canal is preferred, as it can hold the electrode in place, such that electrode migration is minimized. The average diameter of the pudendal nerve at the proposed stimulation site is 4.67±1.17 mm [32].

Axons within the pudendal nerve that are responsible for the pressure in the urethra are constantly being stimulated when not voiding, such that the urethra is closed. This means that an onset response should have no effect in these axons. However, since the pudendal nerve is a mixed nerve, that also carries afferent axons, the onset response can potentially cause sensations such as pain each time stimulation is turned on. The severity of this should be further examined from experimental research, preferably on humans as they can tell whether these sensations are felt or not.

2.3.4. Goal of this thesis for REValUE

In order to create an effective KHFAC stimulation protocol for blocking the pudendal nerve, one of the steps that needs to be taken is to find which simulation parameters influence the effectiveness of the nerve block. As noted in Section 2.2.2, this already has been researched for stimulation frequency, electrode distance and some alterations of the waveform. However, the effect of waveform alterations are missing documented results, or have been executed in a way that results in charge-imbalanced waveforms; this adds a DC component to the signal, which might have resulted in an unwanted influence on the research results. Moreover, none of these analyses have focused on the specific case of the pudendal nerve. Finally, most results so far have been achieved using a monopolar set-up, with a return electrode placed at infinity.

This research focuses on finding how the stimulation parameter relationships impact the effectiveness of the KHFAC block, specifically in the pudendal nerve. Note that all variations are charge-balanced, to ensure that no DC component exists.

The stimulation parameters that are researched for their impact on effectiveness are:

- Waveform-related parameters
    - Square waveforms
    - Sine waveforms
    - Triangular waveforms
    - Step function waveforms
    - Asymmetrical square waveforms
    - Addition of inter-phase delays
- Electrode-to-axon distance as-is in the pudendal nerve

In order to achieve a complete picture of the impact of the different waveforms, not only the block threshold will be measured, but also the minimum charge per phase that is necessary to create a block.

This will be followed by bipolar simulations (with a return electrode placed close to the KHFAC electrode), where the following parameters are tested:

- Effect of interpolar distance for various electrode-to-axon distances
- Electrode orientation

The exact block thresholds are not realistic in a clinical context, as the simulation does not fully model all elements that are in the body surrounding the stimulation site, which can alter the electric fields generated. However, the trends that are found through stimulation can be very helpful, as they can guide both the circuit designer and the clinician in finding a set of optimal stimulation parameters. These trend lines can reveal how the stimulation parameters can be adjusted such that the block remains successful, but less energy is needed or safer stimulation is achieved.

2.4. Conclusion

In this chapter one of the fundamental causes for urinary retention, an inability to voluntarily relax the sphincter, was given. An anatomical and physiological simplification was made, to highlight the root of this problem: the constant pulse train that travels from the brain via the pudendal nerve to the external urethral sphincter, contracting the latter.

KHFAC stimulation was introduced as a potential solution. This type of stimulation encompasses alternating current stimulation signals with a frequency in the kilohertz range, which may result in an inhibition of action potentials propagating down a nerve, called a ‘nerve block’. Simulation analysis has shown that the most likely reason for this effect to appear in mammals is the inactivation of the sodium channel: a state where the sodium activation gate, described by gate variable m, is open, whereas the sodium inactivation gate, described by gate variable h, is closed. In a normal action potential, the inactivation state of the sodium channel is related to repolarization. When initiating KHFAC stimulation, this always leads to an ‘onset response’, which consists of a series of one to five pulses that quickly travel down the axon in both ways, away from the point where the KHFAC stimulation was initiated. It can theoretically lead to muscle twitches as a result of the pulses in the efferent path, and a short sensation of pain as a result of the pulses in the afferent path. The latter might not be a severe problem for stimulation in the pudendal nerve, as action potentials created by the onset response will meet the action potentials that were travelling down the brain to the sphincter, resulting in a collision block.

Previous research examined the influence of frequency, electrode-to-axon distance, waveform asymmetry and axon diameter on the block threshold, which is the minimum current necessary to inhibit the nerve under a set of circumstances.

Finally, the REValUE Project was introduced, which aims to bring KHFAC stimulation to urinary retention patients, by implanting a lead electrode in the Alcock's canal. It was explained how this thesis contributes to the project. The trends that are found for changing simulation parameters are more important than exact block thresholds, as the latter can differ greatly depending on the specific anatomy of a patient.

3

Determination of effectiveness of block

When searching for the influence of different stimulation parameters on the effectiveness of a nerve propagation block, a simulation method is needed that can determine block thresholds. Figure 3.1 represents the standard approach for finding the block threshold for a specific set of stimulation (and environmental) parameters. A simulation environment is built up for the set of parameters, on which a nerve block simulation is repeated with increasing KHFAC amplitude until a successful nerve block is registered; the KHFAC amplitude that causes this block is the block threshold.

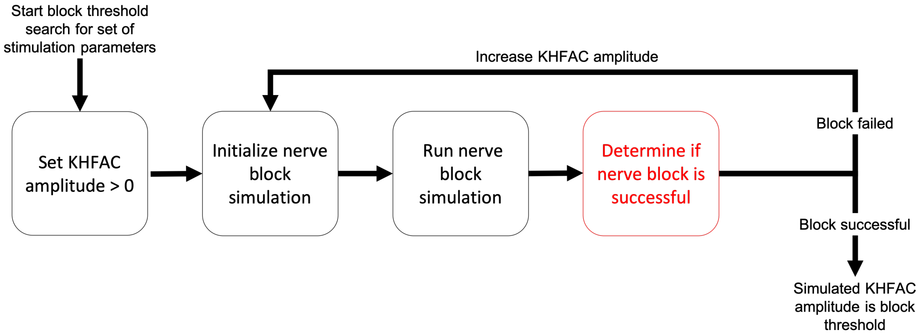
Start block threshold search for set of stimulation parameters
Increase KHFAC amplitude
Set KHFAC amplitude > 0
Initialize nerve block simulation
Run nerve block simulation
Determine if nerve block is successful
Block failed
Block successful
Simulated KHFAC amplitude is block threshold

Figure 3.1: Overview of a block threshold determination process using simulations. For a set of stimulation parameters, a simulation environment is initialized, and a small initial KHFAC amplitude is chosen. A nerve block simulation is executed, and the results are checked to determine whether the nerve block was successful. If not, the simulation has to be repeated, with an increased KHFAC amplitude. If the block was successful, the KHFAC amplitude is registered as the block threshold for the set of stimulation parameters. This chapter focuses on the block-determination model (coloured red) of the process, and how it can be altered to reduce the time necessary for a nerve block simulation.

The most extensive part of this process is running the nerve block simulation and is part of the process that is being repeated. Reducing the time to run a single nerve block simulation can thus drastically reduce total simulation time. However, the size of the nerve block simulation is dependent on the block determination model, which checks if the nerve block simulation resulted in a 'successful' block.

Previous research has only used one method to determine the effectiveness of a block, which is discussed in Section 3.1. To be able to reduce the nerve block simulation size, Section 3.2 introduces a new method for determining a successful nerve block, that utilizes the gate variables of the sodium channel. The proposed method is used to build a working model, and its performance is compared with a model using the classic method.

3.1. Classic method: visualizing the actual block

The classic method of determining whether a successful block has occurred in a simulation, often involves a set-up as shown in Figure 3.2, and is used by many studies [4, 6–9, 21, 29, 33]. An axon of sufficient length is modelled (51 nodes of Ranvier for the MRG model [6]), and somewhere in the middle, at a small distance from the axon, an electrode is placed that will deliver the blocking signal. The return electrode is placed at infinity, such that the KHFAC electrode can be modelled as a point source. After application of the KHFAC signal, an onset response will occur, such that the axon needs a few milliseconds to settle. Then, at one end of the axon, an intracellular test pulse is delivered; on the other end of the axon, the membrane voltage is measured to see if the test pulse arrives. A step-by-step demonstration of a successful block can be seen in Figure 3.3, whereas the time-spatial result of the simulation described for an unsuccessful and successful block can be seen in Figure 3.4a and Figure 3.4b, respectively.

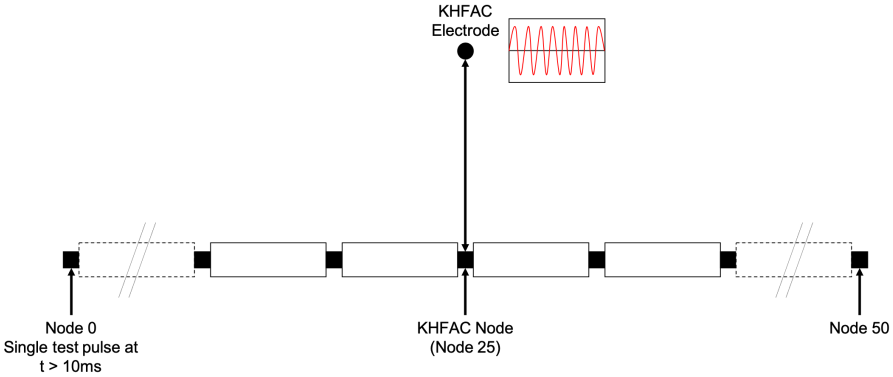

Figure 3.2: The simulation set-up used in the classic method. An axon of 51 nodes of Ranvier is modelled, with an extracellular electrode placed somewhere above the middle node. This electrode, modelled as a point source, generates a KHFAC signal. After at least 10 ms (when the onset response is over), an intracellular test pulse is generated at one end of the axon (node 0). The membrane voltage of the node at the other end of the axon (node 50) is being measured to see if the action potential has passed the KHFAC node, or if it has been blocked.

A variation of this simulation can be done by replacing the single test pulse by a pulse train. This can much more accurately determine the effectiveness of the block, as it can also distinguish a partial block (where some of the pulses are blocked and some are not), which is demonstrated in Figure 3.4c. If these parameters were used in the single pulse test, the partial block could be mistakenly identified as either a full block or as non-blocking.

For all simulations, the amount of pulses at the receiving end can be counted. In the intracellular pulse train simulations, the amount of received pulses over time can be compared to the amount of pulses that are received when no blocking signal is applied, as to develop a measure for the exact degree of effectiveness of a partial block.

3.1.1. Disadvantages of classic method

Simulations like the ones done in Figure 3.4 are quite extensive. Many nodes of Ranvier are necessary, as the depolarization profile in KHFAC block modelling extends 17 to 21 nodes in the region under the electrode, which for a too small axon model can lead to exaggerated onset firing from the two ends of the axon, under-estimation of block thresholds and inaccuracies in the electrode-to-axon distance and axon diameter relationships [6].

Another factor is a result of the onset response, that was discussed in Section 2.2.1. Before the effectiveness of the block is determined, the onset response should have passed. The duration of the onset response can differ based on simulation parameters, so often a relatively long settling time is chosen between the initiation of the KHFAC blocking signal and the determination of the effectiveness of the block. This increases the simulation time frame. Moreover, because the KHFAC signal is at a relatively high frequency, many more simulation time steps are necessary compared to simulations that study low frequency stimulation (at least ten time steps per signal period).

As an example, the simulations that were done in Figure 3.4 each consisted of 51 nodes of Ranvier. The model used was the McIntyre-Richardson-Grill model [13], where every section between two nodes is modelled by 10 internodal segments (this is more elaborately explained in Section 4.3.1). Thus the axon is modelled by a total of $51 + 50 \times 10 = 551$ segments. The simulation time frame in these simulations was 40 ms. The frequency of the KHFAC signal was 20 kHz, and thus had a period of 0.05 ms. In order to simulate at least 10 samples of each signal period, the time step should thus be set to 0.005 ms. That is a total of 8000 time steps in one simulation, where in each time step calculations are done for 551 segments.

When checking for a few standard situations, this is not a problem. However, when searching for the block

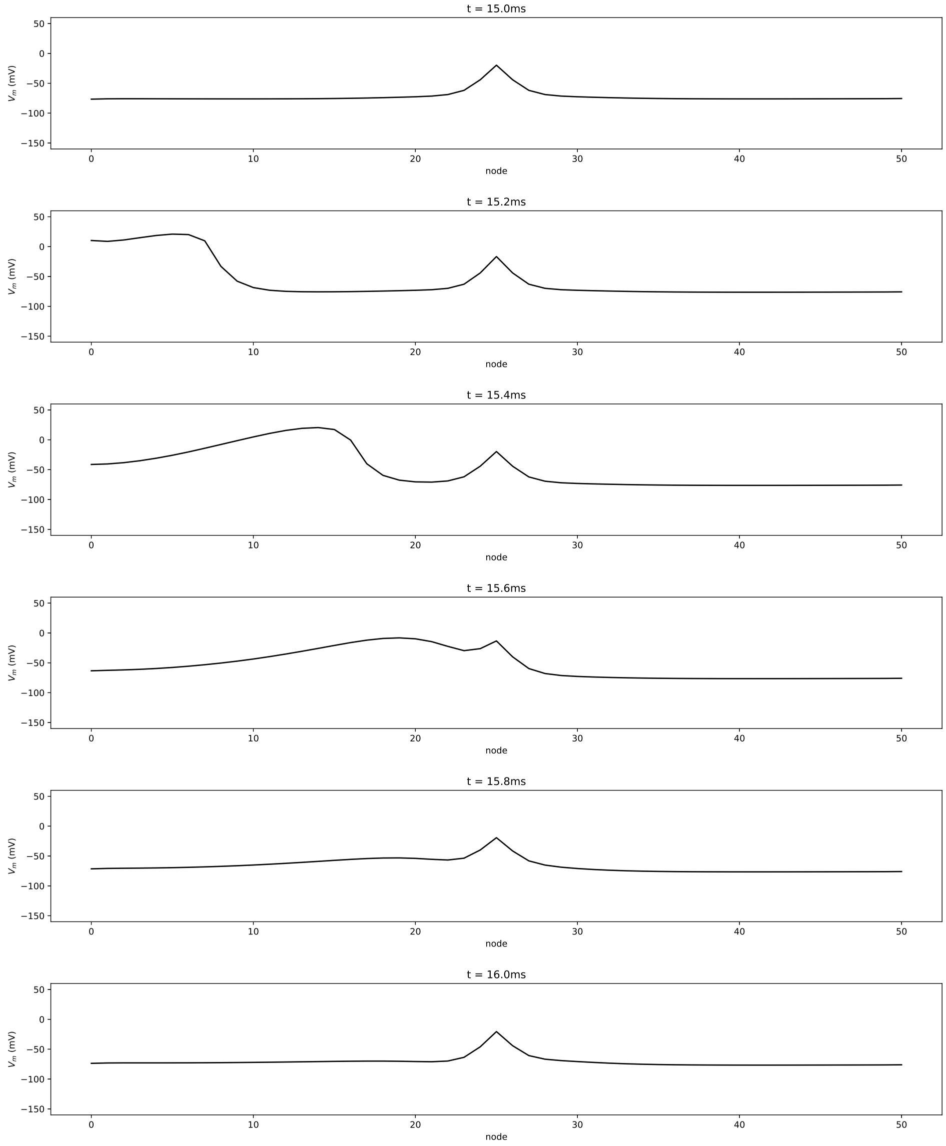

Figure 3.3: Example of a successful KHFAC block. The figure at t =15.0 ms displays that most of the axon is at resting potential, except the middle node of Ranvier, where the KHFAC signal is applied. At t =15.2 ms an action potential has been initiated at node 0, and has started propagation further down the axon. At t =15.4 ms, the propagation can be clearly seen, and at t =15.6 ms, the pulse has propagated towards the KHFAC node. At t =15.8 ms it can be seen that the pulse is not able to pass the KHFAC node, which is confirmed by the image at t =16.0 ms, as the axon has now been reset fully to the original state.

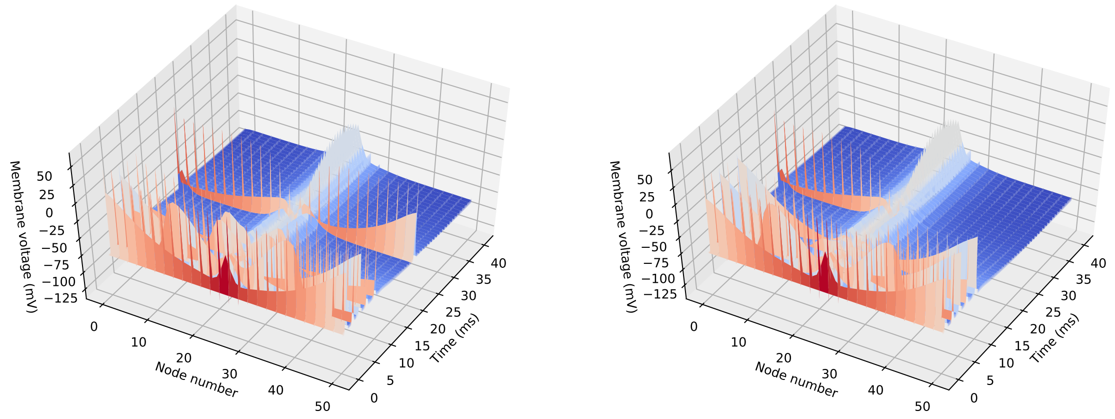

(a) KHFAC amplitude = 0.53 mA. No block.

(b) KHFAC amplitude = 0.6 mA. Successful block

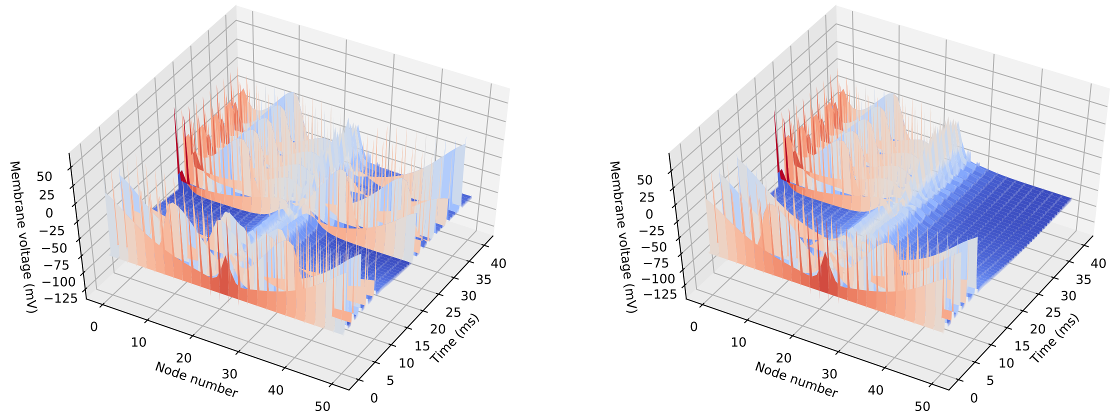

(c) KHFAC amplitude = 0.53 mA. Partial block

(d) KHFAC amplitude = 0.6 mA. 100% block

Figure 3.4: Four different KHFAC block-determination simulations. The axon is modelled to consist of 51 nodes of Ranvier, with a 10 µm axon diameter. The KHFAC signal for each simulation is sinusoidal with a frequency of 20 kHz, and is initiated directly above the middle node at a distance of 1 mm. The simulation time step size used was 0.001 ms. (a) A KHFAC signal with a 0.53 mA amplitude is initiated at $t = 0$ ms. A single test pulse is delivered at node 0 at t=20 ms. The block is unsuccessful. (b) A KHFAC signal with a 0.6 mA amplitude is initiated at $t = 0$ ms. A single test pulse is delivered at node 0 at $t = 20$ ms. The block is successful. (c) A KHFAC signal with a 0.53 mA amplitude is initiated at $t = 0$ ms. A pulse train starts from node 0 at $t = 20$ ms. Close inspection shows that the block is slightly successful, with a few pulses not reaching the other end of the axon. This simulation thus nuances the result observed in Figure (a), as an amplitude of 0.53 mA apparently is able to block some of the pulses. (d) A KHFAC signal with a 0.6 mA amplitude is initiated at $t = 0$ ms. A pulse train starts from node 0 at $t = 20$ ms. The block is 100% successful.

threshold under specific conditions, these simulations have to be repeated until the minimum KHFAC amplitude is found that results in a block. If a higher accuracy is necessary, the number of simulations is further increased. Then, when the minimal KHFAC blocking amplitude for different frequencies, waveforms, axon diameters or other parameters needs to be found, the number of simulations starts growing exponentially.

3.2. Proposed method: Measurement of gate quantities

In this research, the effectiveness of KHFAC stimulation is studied for multiple signal parameters. It is thus desirable to minimize the simulation time of a single nerve block determination simulation as much as possible.

This section will introduce a new method, based on the sodium channel ‘gate’ variables. First, the behaviour of the sodium channel inactivation gate during KHFAC stimulation will be described, and how this can be used to develop a new block determination method. Next, this section will describe step-by-step how this theory was used to develop a fully functioning gate-dependent block determination model. The section will conclude by analysing the performance of the newly developed model.

3.2.1. Characteristics of sodium channel inactivation variable h during nerve block

As stated in Section 2.2.1, a KHFAC nerve block is most likely the result of the sodium channel being forced into the inactivation state. This can be observed from plotting the gate variables, as was done in Figure 2.5. After applying the KHFAC signal, the variable describing the state of the sodium channel activation gate, m, was above 0.5 for the virtual anodes, meaning the activation gate was mostly opened. The variable describing the state of the sodium channel inactivation gate, h, dropped to a value close to 0 and remained nearly constant, meaning the inactivation gate was closed. These values reveal that the membrane is in a state of inactivation.

The most important aspect however, is the relative constant value h takes on after the initiation of the KHFAC signal. This leads to the suspicion that a nerve block may be identified by simply studying variables such as the mean and variance of h. If clear conditions can be found for h, for which blocking will occur, the need for sending an intracellular pulse across the axon can be taken out. Moreover, the amount of nodes of Ranvier can possibly be reduced.

3.2.2. Implementing the gate-dependent method into a working model

Theory hints to a solution for determining nerve block effectiveness without having to simulate an entire axon, followed by checking if pulses can travel from one end of the axon to the other. In order to apply the proposed method to real simulations, it first needs to be implemented as a working model. That means determining the size of both the axon model and the simulated time frame, and finding the threshold conditions which, if met, indicate a successful nerve block.

Selecting the number of nodes of Ranvier

In the classic method, the number of nodes needs to be sufficient to prevent the depolarization profile in the region under the electrode from influencing the results. However, this assumes that a simulation set-up is used as in Figure 3.2, where a pulse is sent from one end to the axon, to see whether it reaches the other end of the axon. Whereas the extended depolarization profile can definitely influence the propagation of this pulse, it is hard to see how it would influence the behaviour of the individual nodes if such a pulse is left out; as is the case with the proposed method.

It is therefore expected that the amount of nodes of Ranvier can be reduced to a minimum for the proposed method. As stated in Section 3.2.1, the virtual anodes are just as important for the existence of the block as KHFAC node. This means that at least the virtual anodes should be fully modelled, meaning that the internodal segments on each side of the virtual anodes should be taken into account as well. Thus, at least five nodes of Ranvier should be included in the proposed model, with the middle node acting as the KHFAC node.

Since every node of Ranvier that is added to the model, also adds a total of 10 segments that need to be evaluated in every simulation time step, the total simulation time could be greatly reduced by minimizing the number of nodes of Ranvier that are modelled. Therefore, the proposed model shall be developed to use the minimum of five nodes of Ranvier; the resulting set-up is shown in Figure 3.5.

Selecting the measurement time frame

Figure 3.6 is the result of a single KHFAC simulation using the set-up of Figure 3.5. It can be seen that the mean values of the membrane voltage V_m and gating variables h and m of the virtual anode are slowly changing, but after about 15 milliseconds the mean values seem to reach a steady state value. The measurement time frame should be selected to only measure the membrane voltage and gating variables during this steady state; this best represents the state of the axon during most of the real stimulation. The total simulation time frame thus becomes the sum of the 'settling' time frame and the measurement time frame. In this implementation a total simulation time frame of 20 milliseconds is chosen, with the last two milliseconds being the measurement time frame.

Calibrating the model: selecting threshold conditions

With the time frame and number of nodes of Ranvier for the proposed model selected, the model is ready to run simulations. This can be used to develop the most important aspect of the model: the threshold conditions that decide whether a block is effective or ineffective.

Promising candidate variables that form the basis for threshold conditions are gate variables h and m, as they can reveal whether the sodium channel is in a state of inactivation, and the membrane voltage V_m, since

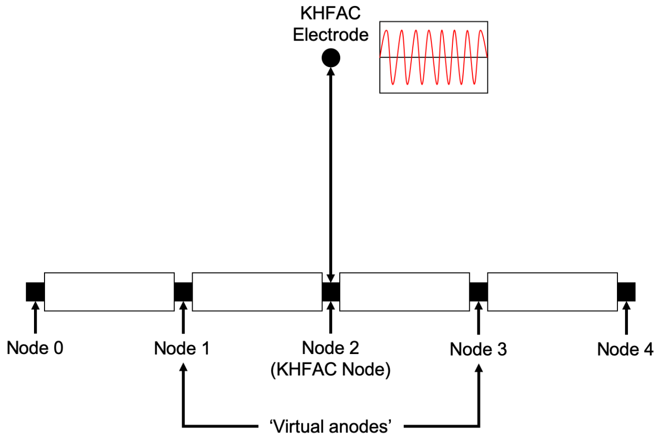

Figure 3.5: The basic simulation set-up used for the proposed block effectiveness determination method. The model is simplified to 5 nodes. The KHFAC electrode is situated above node 2, which is called the KHFAC node. Nodes 1 and 3 are the 'virtual anodes', the two nodes that have the lowest, most stable values for h when the KHFAC signal is initiated, as was observed in Figure 2.5.

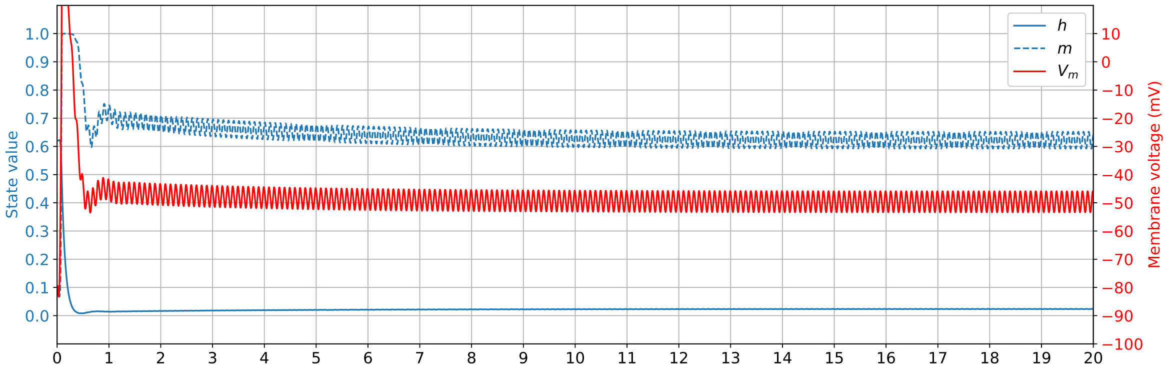

Figure 3.6: Gating variables h and m and the membrane voltage V_m of a virtual anode after applying a KHFAC signal, using 5 nodes of Ranvier. After the KHFAC stimulation signal is applied at $t = 0$ ms, it can be seen that the mean values of the membrane voltage V_m and gating variables h and m are slowly moving to a steady state value, which is reached after about 15 ms.

it is directly related to h_∞, m_∞, τ_h and τ_m (as explained in Section 2.2.1), and thus projects to which values h and m are changing at which speed.

In order to find the exact threshold conditions, at first the classic method (described in Section 3.1) was applied to different charge-balanced asymmetrical waveforms (described in Figure 3.7), to determine the corresponding block thresholds for frequencies between 3 and 40 kHz. This implementation of the classic method consisted of a pulse train that was introduced at $t = 10$ ms, which is directly after the onset response ends. The pulse train brought in one pulse at one end of the axon every 2 ms. The simulation ended after a total simulation time frame of 51 ms, equal to 21 pulses. A successful nerve block was perceived if less than 90% of the pulses were measured at the other end of the axon.

The same waveforms with the same frequencies where simulated using the proposed gate-dependent model, and were kept running after the block threshold (retrieved from the classic method) was reached; for every single repetition, the maximum, minimum, mean and variance values were stored for the variables h, m and V_m.

With these two datasets available, the threshold conditions could be found. First, a 'filter' was created consisting of a group of thresholds that were conditions for a successful block. The starting point for these threshold conditions was made by comparing the results of the classic method to the values measured with the proposed model. The dataset retrieved from the proposed method was pulled through this filter, and the resulting block thresholds were plotted against the block thresholds derived using the classic method (as shown in Figure 3.8). The resulting curves of the proposed model were brought closer to the classic curves by adjusting the values of the threshold variables, whereas anomalies (e.g. peaks) in the curve of the proposed

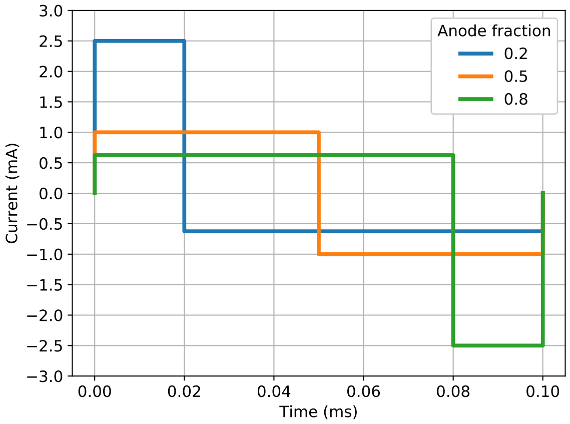

Figure 3.7: An example of two charge-balanced asymmetrical waveforms and one symmetrical waveform, all three with the same charge per phase. The fraction that represents the anodal pulse, given by $\frac{T_{\text{anodal}}}{T_{\text{anodal}}+T_{\text{cathodal}}}$, is called 'anode fraction'. For the anode fraction of 0.2, the anodal (positive) pulse lasts $1/5^{\text{th}}$ of the signal time period ($T_{hi} = 0.2T_{\text{signal}}$), whereas the cathodal (negative) pulse lasts for $4/5^{\text{th}}$ of the signal period. The cathodal pulse is thus four times as long. To achieve charge-balance, the anodal pulse has an amplitude that is 4 times as high as the cathodal pulse, or 2.5 times as high as the amplitude for a symmetrical square wave with the same charge per phase. For the anode fraction of 0.2, this thus results in an anodal amplitude of 2.5 mA and cathodal amplitude of 0.625 mA, if the charge is matched to a symmetrical square wave with amplitude 1 mA. For the pulse with an anode fraction of 0.8 the inverse description is true. The figure also clearly shows that an anode fraction of 0.5 results in a regular symmetrical square wave.

model were taken out by introducing new threshold variables or taking old ones out. This resulted in the following condition:

$$\text{Successful block if: } max(h_{\text{virtualanode}}) < 0.04 \text{ AND } \begin{pmatrix} max(V_{m,\text{virtualanode}}) & > -22mV \\ \text{OR} & \\ min(V_{m,\text{virtualanode}}) & > -51.5mV \\ \text{OR} & \\ min(V_{m,\text{KHFACnode}}) & < -90mV \end{pmatrix} \tag{3.1}$$

Where h is the dimensionless variable that describes the state of the inactivation gate of the sodium channel, V_m is the membrane voltage, 'KHFACnode' is the node of Ranvier closest to the external KHFAC electrode, and 'virtualanode' is one of the two nodes of Ranvier directly next to the 'KHFACnode'. Qualitatively, the condition described in Equation (3.1) categorizes a nerve block as 'successful', if:

- The maximum value of h in the virtual anode is almost zero,
- The membrane voltage in the virtual anode is either never too negative, such that the value of h could potentially climb to a value close to 1 too fast, or that the membrane voltage has it's peaks at sufficiently high voltage to pull the value of h back to zero at high speed to compensate for rising values of h.

The condition concerning $V_{m,\text{KHFACnode}}$ can not be explained from theory; this has been introduced as an 'override' condition, as the lower frequencies had trouble with meeting the other two conditions in the OR block (the right part of Equation (3.1)), leading to large over-estimations of the block thresholds. Moreover, the membrane voltage in the KHFAC node does not become as negative as −90 mV for higher frequencies. The introduction of this override condition thus had no effect on the results found in higher frequencies.

3.2.3. Performance of proposed model

Now that a working model that implements the proposed method is introduced, the performance should be evaluated in order to determine if this model is worth using for the rest of the research.

Error margins of proposed model design

The proposed nerve block effectiveness determination model with the settings described in Equation (3.1) was tested against the classic model to analyse the reliability. The classic model data points were found by simulating an axon model of 51 nodes of Ranvier, with an axon diameter of 10 μm, an electrode-to-axon distance of 1 mm, and a pulse train introduced at one end of the axon starting at 10 ms that initiates an action potential once every 2 ms. The data points represent the minimum charge per phase necessary to have at least 90% of all pulses blocked after a simulated time of 50 ms.

The settings of Equation (3.1) were created by calibrating for the asymmetrical waveforms with anode fractions ranging between 0.1 and 0.9. The resulting block thresholds are compared with the classic model in Figure 3.8 for a selection of the anode fractions. It can be seen that for the two extremes, the anode fractions of 0.1 and 0.9, the proposed gate-dependent model approaches the results of the classic model very closely. Same goes for an anode fraction of 0.5, which essentially is a regular square wave. For an anode fraction of 0.8, the model underestimates the block threshold charge per phase up until 21 kHz, after which it starts overestimating up to about 30% at 40 kHz.

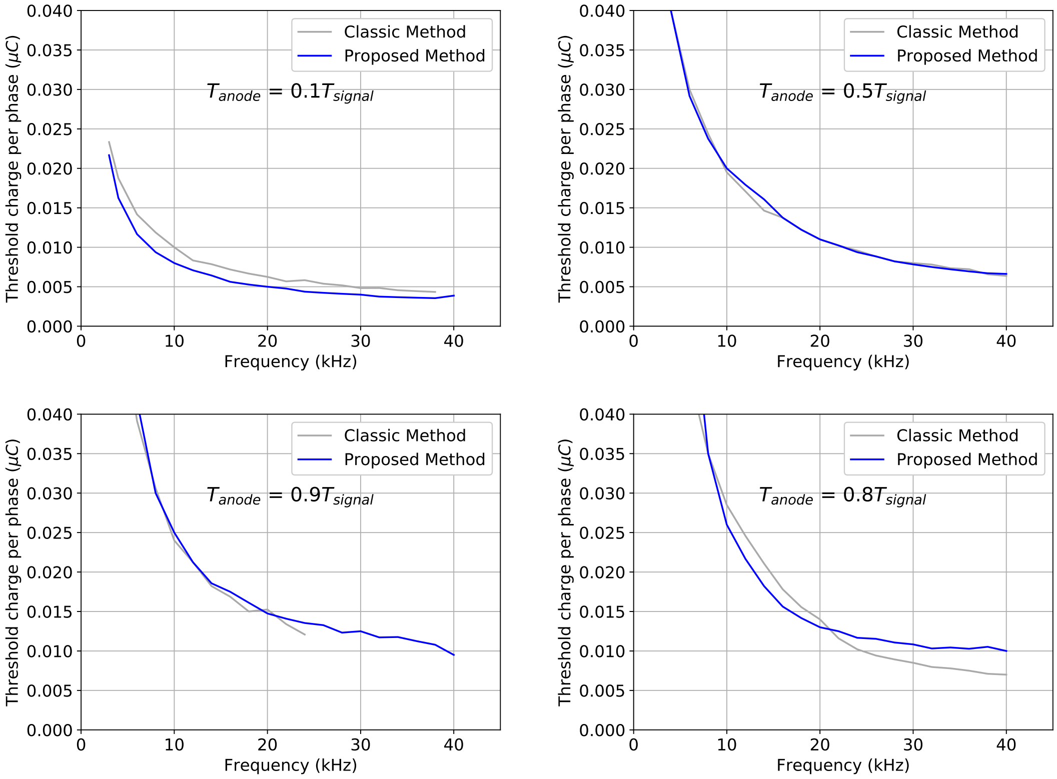

Figure 3.8: Comparison of block thresholds resulting from the classic block determination method and the proposed gate-dependent block determination method for asymmetrical waveforms (described in Figure 3.7) with anode fractions of 0.1, 0.5 (a symmetrical square wave), 0.9, and 0.8, for frequencies between 3 and 40 kHz. The block thresholds are presented as threshold charge per phase, which is the total charge of a single anodic or cathodic pulse at block threshold, and is chosen as the comparison value as the asymmetrical waveforms have a different anodal and cathodal amplitude. For an anode fraction of 0.9, results for frequencies above 24 kHz are missing, most likely due to the simulation boundaries that were chosen to limit the time of the total simulation.

The same comparison was made for a regular sine wave, and the result can be found in Figure 3.9 (for both block threshold and charge per phase at block threshold). The proposed model underestimates the block thresholds by about 10% to 15%. However, the trend at which the threshold changes over frequency closely matches that of the classic model.

Advantages of proposed model

The biggest advantage of the gate-dependent model is the speed-up. The model design as described in Section 3.2.2 runs over 30 times faster than the model design based on the classic method that was used to find the 90% block thresholds in Section 3.2.2 (which simulated a total time of 50 ms), and over 14 times faster than when 20 ms are simulated in the classic model (which is the same simulation time frame used for the proposed model); this is a significant speed-up, and useful when performing larger and more complex simulations that are closer to reality. For example, for a nerve bundle consisting of 30 axons, all block thresholds can be found in about the same time that it takes the classic model to find the block threshold for a single axon.

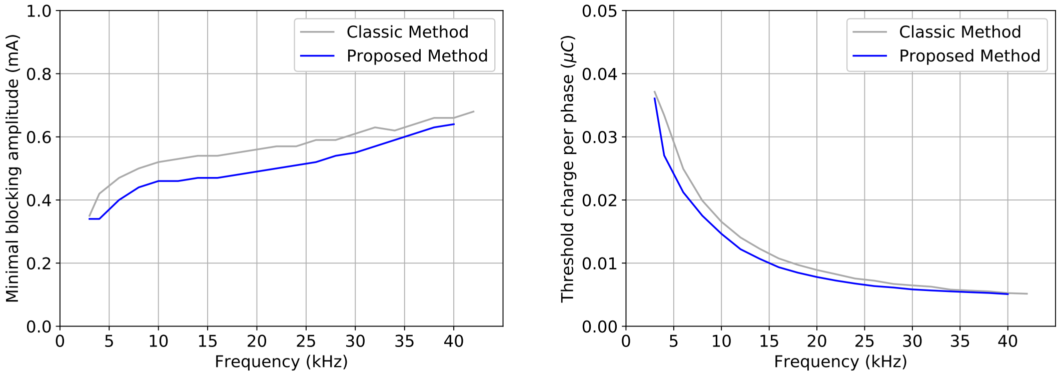

(a) (b)

Figure 3.9: Comparison of block thresholds resulting from the classic block determination method and the proposed gate-dependent block determination method for sine waves with frequencies between 3 and 40 kHz. (a) The resulting block thresholds. (b) The resulting block thresholds as charge per phase.

Weaknesses of proposed model

The proposed method for determining blocking effectiveness uses a more abstract vision on what is considered a nerve block, leading to a loss of information. As explained in Section 3.2.2, many steps are necessary to determine the model threshold conditions for one blocking efficiency level (in this case: 90% block). It is also unsure how well the threshold conditions will work under extremely different conditions, such as waveforms that have multiple anodal and cathodal components in a single period (for example, the waveform that is the result of the work of Baquer Gómez [18]), different axon diameters, or the effect of added noise.

As can be seen in Figure 3.8 and Figure 3.9, the model produces a small error compared to the results that were retrieved via the classic method. This error is biggest for the sinewave, as the thresholds from Equation (3.1) originate from a calibration done on the asymmetrical waves. Even though the error margin is acceptable, this clearly shows that the model contains flaws, and that the results need some validation when circumstances are changed greatly. A combination of the proposed model and the classic method comes to mind, where the proposed model can scan quickly over a large range of amplitudes, and the most promising values are validated using the classic method to determine the exact block threshold.

Finally, this nerve block effectiveness determination method is only applicable to the MRG axon model [13], or any other model which produces a nerve propagation block as a result of the inactivation of the sodium channel. It would not work for example on models based on frog or rat data, as these models have a different mechanism for block (explained in Section 2.2.1).

Justification of proposed model

Extracting exact stimulation parameters through simulation does not make sense, as the characteristics of the stimulation site can differ greatly depending on the patient and the exact placement of the electrode during surgery. In state-of-the-art implantable neurostimulators, the doctor tests different settings to see which set of stimulation parameters have the desired effect. Thus, more interesting would be to know the trends; for example, by how much can the blocking amplitude be decreased, if the stimulation frequency is halved? With this in mind, the error margins introduced by the gate-dependent model are even less significant. Some caution must be taken when comparing, for example, a sine wave to a square wave, due to the slight difference in error margin; but for most simulations so far, the resulting trends are close to trends found with the classic method, justifying the use of the gate-dependent model.

Potential of proposed model

The model design of Section 3.2.2 implements only one blocking efficiency (90% of incoming pulses blocked). However, using an extensive dataset, acquired from the classic method (which has different efficiencies stored and the corresponding minimum blocking amplitudes), threshold conditions for many more efficiency levels could be developed. An extended version of the model would be then able to make much more accurate estimations, without needing to increase the simulation time.

Even though the thresholds as described in Equation (3.1) are imperfect, it is able to produce results with trends and values resembling those of the classic model. There is most likely much more to be gained from to this approach of determining an effective block than has been found in this study. The solution to a more accurate model might be a threshold condition that also takes the length and amplitude of the separate positive and negative cycles of the KHFAC waveform into account, since these are connected to the values of h_∞ and τ_h. Moreover, in this implementation m was left out of the condition due to its varying value which did not reveal any consistency yet for different anodal fractions; if a consistency could be found for m, this could also make the model more accurate. If more stable threshold conditions can be found, this could lead to an even more accurate model, that can also increase the general understanding of the origins of the nerve propagation block.

3.3. Conclusion

To determine which stimulation parameters perform better than others, the block thresholds for different settings are compared. The classic method used to find these thresholds involves an extensive time-spatial simulation that needs to be repeated until the blocking threshold for a specific setting is found.

An alternative method was proposed, that measures the membrane voltage V_m and the state of the inactivation variable h. In a simulation set-up involving five nodes of Ranvier and a simulated time of 20 milliseconds, the values of V_m and h during the last two milliseconds were measured. A block was perceived as successful when these variables met the following condition:

$$\text{Successful block if: } max(h_{virtualanode}) < 0.04 \text{ AND } \left(\begin{array}{rl} max(V_{m,virtualanode}) & > -22mV \\ \text{OR} & \\ min(V_{m,virtualanode}) & > -51.5mV \\ \text{OR} & \\ min(V_{m,KHFACnode}) & < -90mV \end{array} \right)$$

The performance of the proposed model was tested against the classic method. For most of the waveforms tested, no errors larger than 15% were found compared to the results of the classic method, and the shape of the resulting curves closely resembled those acquired with the classic method. Most important however, was the dramatic increase in speed, as the proposed model runs a single simulation more than 30 times faster than the classic model.

Even though the proposed model is less accurate than the classic model, and only implements one blocking efficiency (90% of pulses blocked), the fact that it can generate results that are closely resembling the results of the classic model is promising. A deeper analysis in the threshold conditions could potentially lead to a much deeper understanding of the dynamics that result in a nerve propagation block.

For this research, the model performs well enough, as it is able to find the correct trends on the effectiveness of different stimulation parameters.

4

Implementation of the simulator

This chapter focuses on the full implementation of the simulator on which different stimulation parameters are tested for their effectiveness. The full system implementation can be seen in Figure 4.1.

The signal generation model converts waveforms to a format that can be interpreted by the simulation environment, and is explained in Section 4.1. The source of the current waveform is given spatial locations by the electrode model, and transformed into extracellular voltages at the axon segments via the axon environment model, which models the space surrounding the axon. In this implementation, the electrode and axon environment models are implemented together as one model, described in Section 4.2. The axon model offers a circuit representation of the axon with dynamics based on experimental results, and is explained in Section 4.3. When everything is set up, the simulation environment can then run the actual simulations. The simulation environment is shortly discussed in Section 4.4. The results of the simulation are then finally interpreted by the block determination model, which implementation has been broadly discussed in Chapter 3. Based on the results of the block determination model, the system decides which waveform or electrode set-up to simulate next, and saves the simulated values if a successful block was detected.

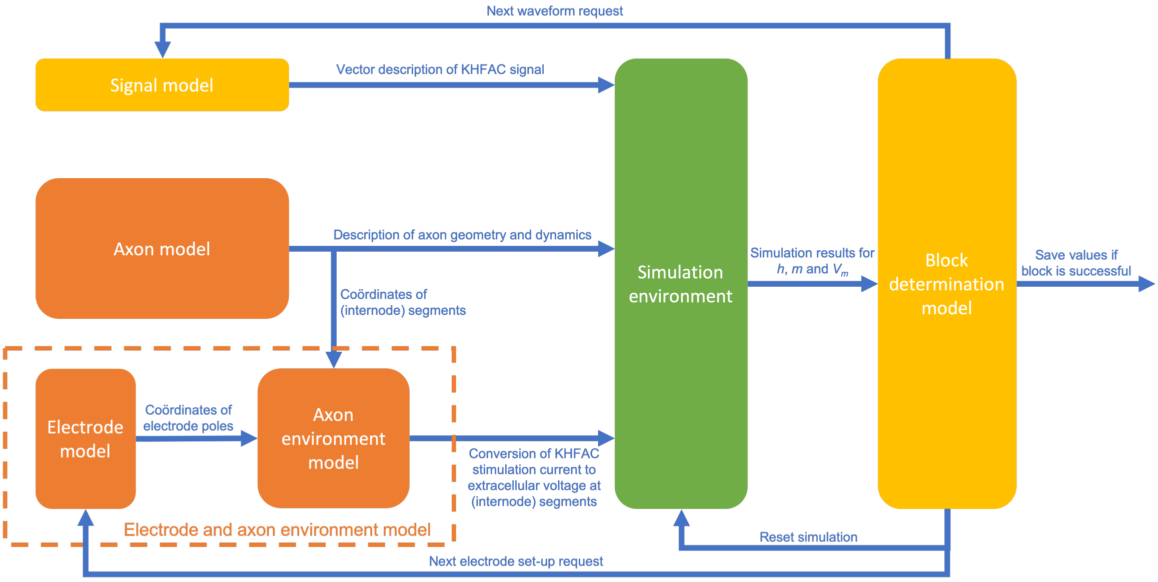
Next waveform request
Signal model
Vector description of KHFAC signal
Axon model
Description of axon geometry and dynamics
Coördinates of (internode) segments
Simulation environment
Simulation results for h, m and V_m
Block determination model
Save values if block is successful
Electrode model
Coördinates of electrode poles
Axon environment model
Conversion of KHFAC stimulation current to extracellular voltage at (internode) segments
Electrode and axon environment model
Reset simulation
Next electrode set-up request

Figure 4.1: An overview of the complete simulation set-up. The yellow blocks represent code written in Python 2.7 [34], the orange blocks represent code written in the hoc (High Order Calculator) programming language [35], and green represents the Neuron simulation environment (version 7.6) [36]. The arrows with text describes which data is sent in which direction.

4.1. Signal generation model

The waveforms need to be generated in a way that they can be interpreted by the simulator. Neuron [36], the simulator that is used in this thesis, uses vectors to interpret signals, specifically a time and amplitude vector. An example set of these two vectors can look as follows:

$$\begin{aligned} t &= \begin{bmatrix} 0 & 0 & 1 & 1 & 2 & 2 \end{bmatrix} \\ i &= \begin{bmatrix} 0 & 1 & 1 & -1 & -1 & 0 \end{bmatrix} \end{aligned} \tag{4.1}$$

This means that at $t = 0$ ms, the amplitude rises from 0 mA to 1 mA. Then the amplitude stays 1 mA until $t = 1$ ms, when it drops to -1 mA. The amplitude then stays -1 mA until $t = 2$ ms. when it returns to 0 mA. This creates a square wave.

Another example can look like this:

$$\begin{aligned} t &= \begin{bmatrix} 0 & 0.5 & 1.5 & 2 \end{bmatrix} \\ i &= \begin{bmatrix} 0 & 1 & -1 & 0 \end{bmatrix} \end{aligned} \tag{4.2}$$

With this set of vectors, the waveform increases amplitude from 0 mA to 1 mA until t =0.5 ms. Then it immediately starts decreasing until -1 mA is reached at t =1.5 ms is reached. From there it increases back to 0 mA at t =2 ms. This results in a triangle wave.

For Neuron, vector representations like in Equation (4.1) and Equation (4.2) are necessary to represent any kind of waveform. Sinusoidal waveforms can thus only be approximated by sampling. The sample size should then preferably be equal to at least the simulation step size.

4.2. Electrode and axon environment model

In this thesis, the electrode model and the axon environment model are implemented as one code block in the simulation environment. The conversion from the KHFAC signal at the electrode(s) to extracellular voltages at the axon segments consists of a set of equations from a simplified model. Two electrode set-ups are implemented:

- A monopolar set-up. In this set-up, the return electrode is placed at infinity. This leads to that the KHFAC electrode can be modelled as a point charge, which results in the electric field and equipotential lines (lines on which the electric potential is equal) of Figure 4.2a.
- A bipolar set-up. In this set-up, the return electrode is placed close to the KHFAC electrode. A simplified model of this set-up is an electric dipole, which results in the electric field and equipotential lines of Figure 4.2b. These altered equipotential lines affect the potentials at the different nodes of Ranvier, which can lead to a decrease in block thresholds.

In this section, the equations that implement both set-ups will be discussed. It will also be explained how the axon environment is modelled as part of the equations, and suggestions for a different implementation of the axon environment are as well.

4.2.1. Monopolar set-up

The first electrode implementation is a monopolar configuration, one that has been used by most previous research. Figure 4.3 displays the model and the different geometrical variables that are involved.

With this model, the extracellular voltages for all the internodal segments (V_e in the MRG Model [38]) can be calculated from the stimulation current. Assuming the electrode is modelled as a single point source placed in an infinite homogeneous isotropic medium, and the return electrode is placed at infinity, the electric potential at any (inter)nodal segment is given by:

$$V_{e,n}(t) = \rho_e \left[\frac{I_{\text{block}}(t)}{4\pi r} \right] \tag{4.3}$$

where $I_{\text{block}}(t)$ is the KHFAC current delivered to the block electrode, ρ_e is the extracellular resistivity, and r is the distance between the electrode and the internodal segment. When the axon is modelled to be on the y-axis, such that $x = 0$ and $z = 0$ for all axon segments, r can be rewritten to:

$$\sqrt{(y_n - y_e)^2 + x_e^2 + z_e^2} \tag{4.4}$$

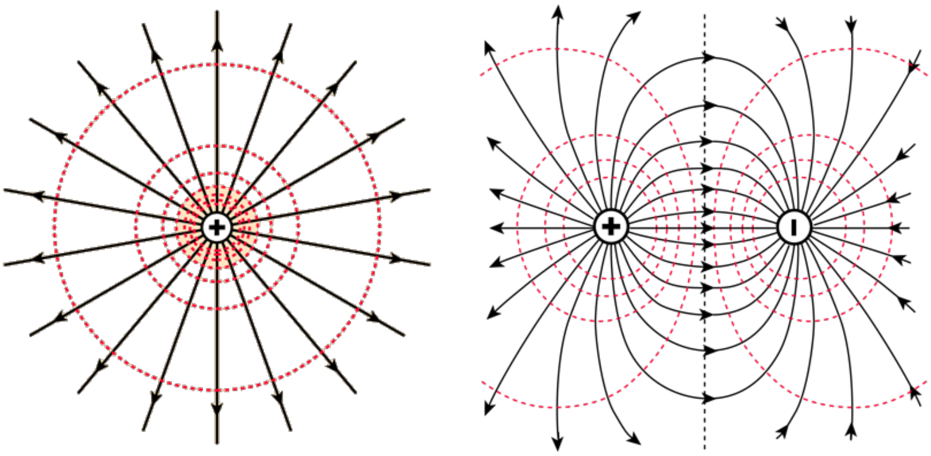

(a) Point charge

(b) Electric dipole

Figure 4.2: Electric field lines (black arrows) and equipotential lines (red dotted lines) for (a) a point charge, which is how the electrodes of the monopolar set-ups are modelled, and (b) an electric dipole, which is how the electrodes of the bipolar set-ups are modelled. Source: Graham, 2003 [37].

with y_n being the location of the axon (inter)nodal segment on the y-axis, and y_e, x_e and z_e being respectively the y-, x- and z-position of the electrode. This can be plugged back into Equation (4.3):

$$V_{e,s}(t) = \rho_e \left[\frac{I_{\text{block}}(t)}{4\pi\sqrt{(y_n - y_e)^2 + x_e^2 + z_e^2}} \right] \tag{4.5}$$

The value of extracellular resistivity ρ_e is taken from the MRG model to be 500 Ω cm [38].

4.2.2. Bipolar electrode

The second electrode implementation that will be researched is a bipolar configuration, which models the influence of both the KHFAC electrode and the return electrode. Figure 4.4 displays the model and the different geometrical variables that are involved.

Assuming again that the electrodes are placed in an infinite homogeneous isotropic medium, and modelling the bipolar electrode lead as a dipole, the voltage at any (inter)nodal segment is given by the sum of the electric potential resulting from the active electrode and from the return electrode. These potentials are given by Equation (4.3). However, for the return electrode, the current flows in opposite direction compared to the active electrode; this results in the following equation:

$$V_{e,n}(t) = \rho_e \left[\frac{I_{\text{block}}(t)}{4\pi r_+} + \frac{-I_{\text{block}}(t)}{4\pi r_-} \right] \tag{4.6}$$

With r_+ being the distance to the anode and r_- being the distance to the cathode. Implementing the x-, y- and z-location for both poles, as was done in Equation (4.4), yields the following result:

$$V_{e,n}(t) = \frac{\rho_e I_{\text{block}}(t)}{4\pi} \left[\frac{1}{\sqrt{(y_n - y_{e,+})^2 + x_{e,+}^2 + z_{e,+}^2}} - \frac{1}{\sqrt{(y_n - y_{e,-})^2 + x_{e,-}^2 + z_{e,-}^2}} \right] \tag{4.7}$$

The value of extracellular resistivity ρ_e is again 500 Ω cm, the same as in the monopolar set-up.

4.2.3. Improvements for modelling electrodes and axon environment

Both electrode set-ups are simplified, such that only an equation is left that transforms the KHFAC current at any point in time to the respective extracellular voltages at the (inter)nodal segments. The axon environment is modelled only as an infinite homogeneous isotropic medium with resistivity ρ_e. To gain more accurate results, both the electrode and the axon environment could be modelled with software like COMSOL. By implementing these two environments as separate models, different electrode configurations could be tested

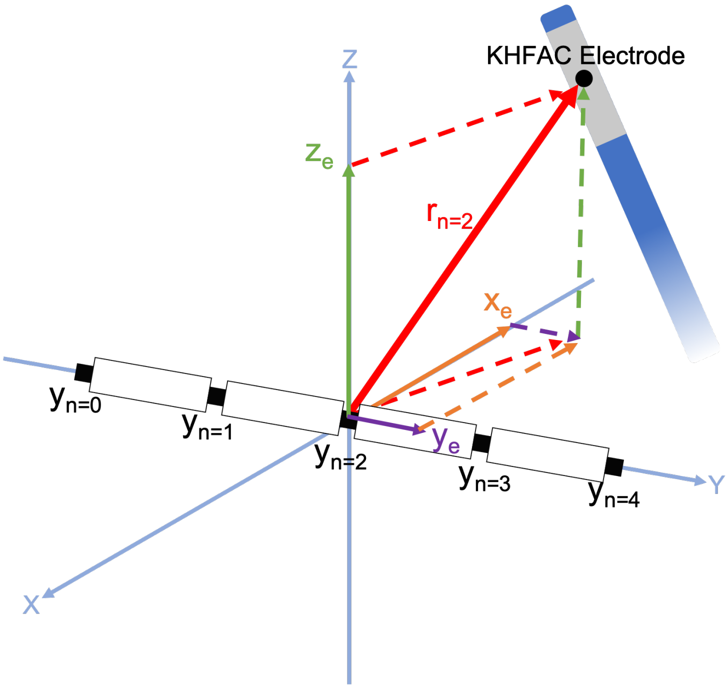
Z
KHFAC Electrode
z_e
$r_{n=2}$
x_e
$y_{n=0}$
$y_{n=1}$
$y_{n=2}$
y_e
$y_{n=3}$
$y_{n=4}$
Y
X

Figure 4.3: The simulation set-up for a monopolar electrode configuration. The axon is situated on the y-axis. Variables z_e, x_e and y_e represent the coordinates of the monopolar electrode, and y_n represents the location of a node of Ranvier. The distance vector between a node and the electrode signal source is given by r_n.

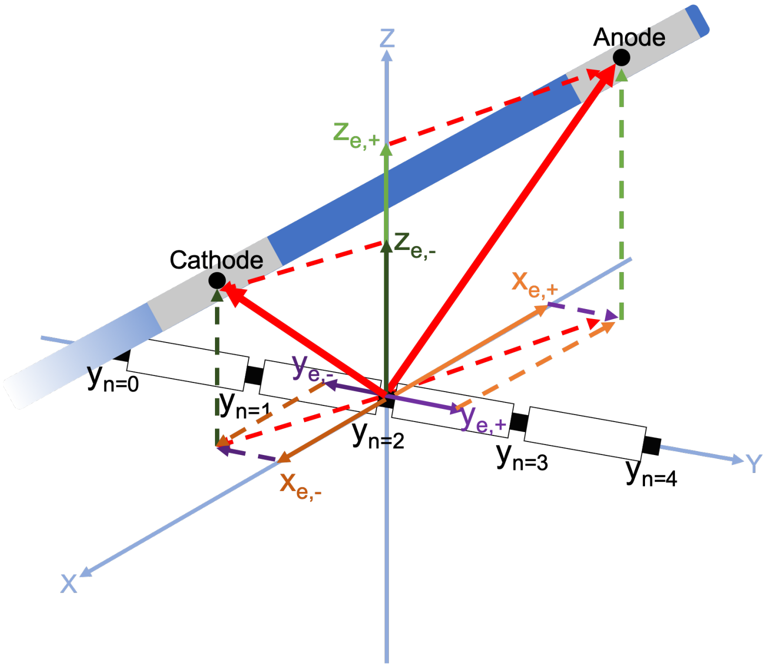
Z
Anode
$z_{e,+}$
Cathode
$z_{e,-}$
$x_{e,+}$
$y_{e,-}$
$y_{n=0}$
$y_{n=1}$
$y_{n=2}$
$y_{e,+}$
$y_{n=3}$
$y_{n=4}$
Y
$x_{e,-}$
X

Figure 4.4: The simulation set-up for a bipolar electrode configuration. The axon is situated on the y-axis. Variables $z_{e,+}$, $x_{e,+}$ and $y_{e,+}$ represent the coordinates of the anode of the bipolar electrode; $z_{e,-}$, $x_{e,-}$ and $y_{e,-}$ represent the coordinates of the cathode of the bipolar electrode; y_n represents the location of a node of Ranvier.

on different models for the axon environment, and parameters such as (electrode) material characteristics can be included.

4.3. Axon model

The simulator needs a model of the axon to describe the dynamics of the ion channels and the behaviour of propagation of signals along the axon. Moreover, not all models include extracellular stimulation.

The first model was developed by Hodgkin and Huxley [24] based on an unmyelinated giant squid axon. In 1976, McNeal [39] published the McNeal cable model, which can be used to describe the effect of extracellular stimulation on a myelinated axon. This model is the foundation for many future myelinated axon models that include extracellular stimulation. In 2001, McIntyre et al. [13] published a myelinated axon model based on human, cat and rat experimental data, that utilized a double-cable structure, and implemented an accurate description of the myelin attachments. This model, named the McIntyre-Richardson-Grill (MRG) model, has become the state-of-the-art axon model in simulation studies that focus on KHFAC nerve block in humans. An overview of other models that are used in KHFAC nerve block simulation studies can be found in Table 4.1.

Table 4.1: Axon models used in nerve propagation block simulation studies

Axon model	Axon type	Based on data of:	Characteristics:
Hodgkin-Huxley (HH) [24]	Unmyelinated	Giant squid	Describes ion channels and membrane capacity
Frankenhaeuser-Huxley (FH) [22]	Myelinated	Frog (Xenopus Laevis)	First myelinated adaptation of the HH model.
McNeal Cable model [39]	Myelinated	Frog (Xenopus Laevis)	First nerve model for myelinated fibre that allows stimuli from extracellular electrodes.
Chiu-Ritchie-Rogart-Stagg-Sweeney (CRRSS) [40, 41]	Myelinated	None	Chiu et al. [40] acquired data for rabbit axons, which Sweeney et al. [41] used to publish the first model for warm blooded nerves.
Schwarz-Eikhof (SE) [23]	Myelinated	Rat	Describes sodium currents.
Schwarz-Reid-Bostock (SRB) [42]	Myelinated	Human	Models human node of Ranvier.
McIntyre-Richardson-Grill (MRG) [13]	Myelinated	Human, cat and rat	A double cable model that includes explicit representations of the myelin sheath (useful for studying the effect of extracellular stimulation) and the internodal segments (including myelin attachments).

This research is focused on the human pudendal nerve, which contains myelinated axons. A model of a myelinated axon based on human data is therefore preferred. The model must also include an option for extracellular stimulation. With this in mind, the MRG model is the preferred model for this research.

4.3.1. McIntyre-Richardson-Grill model for simulation of nerve block

The MRG model models the axon as a double-cable structure, and includes the nodes of Ranvier, the paranodal sections (where the myelin sheaths connect to the nodes) and the internodal sections (the myelin compartments between the nodes) [13]. Between each node of Ranvier, 10 segments are used: 2 paranode myelin attachment segments (MYSA), 2 paranode main segments (FLUT) and 6 internode segments (STIN), making the connections between two successive nodes:

-NODE(i)-MYSA-FLUT-STIN-STIN-STIN-STIN-STIN-STIN-FLUT-MYSA-NODE(i+1)-

The different internodal regions were discovered by Berthold and Rydmark [43]. ‘STIN’ stands for the ‘stereotype internodal segment’, and is the internodal region where the axon is tightly ensheathed by myelin. ‘FLUT’ stands for the ‘paranodal main segment characterized by a fluted axon’, and corresponds to a fluted region near the node of Ranvier; the fluting becomes increasingly deeper near the node. ‘MYSA’ stands for the ‘paranodal end segment characterized by the myelin sheath attachment to the axolemma’ and corresponds to the region where the paranode is abruptly terminated by the attachment of the myelin sheath to the axon.

The nodes of Ranvier itself are modelled as a combination of a fast sodium channel, persistent sodium channel, slow potassium channel, a leakage channel and the membrane capacitance C_n. The sodium channels and potassium channels are represented as nonlinear conductances Na_f, Na_p and K_s; the leakage channel as a linear conductance L_k. All of these conductances are in a parallel combination, as can be observed from Figure 4.5a.

The paranodal and internodal segments are all built up of an axolemma circuit representation in series with a myelin sheath circuit representation. The axolemma, which is the cell membrane surrounding the axon, is represented by an internodal axolemma capacitance C_i in parallel with the series connection of the internodal conductance G_i and the rest potential V_{rest}, as can be seen from Figure 4.5b. The myelin sheath is represented by the myelin capacitance C_m in parallel with the myelin conductance G_m, as can be seen in Figure 4.5c.

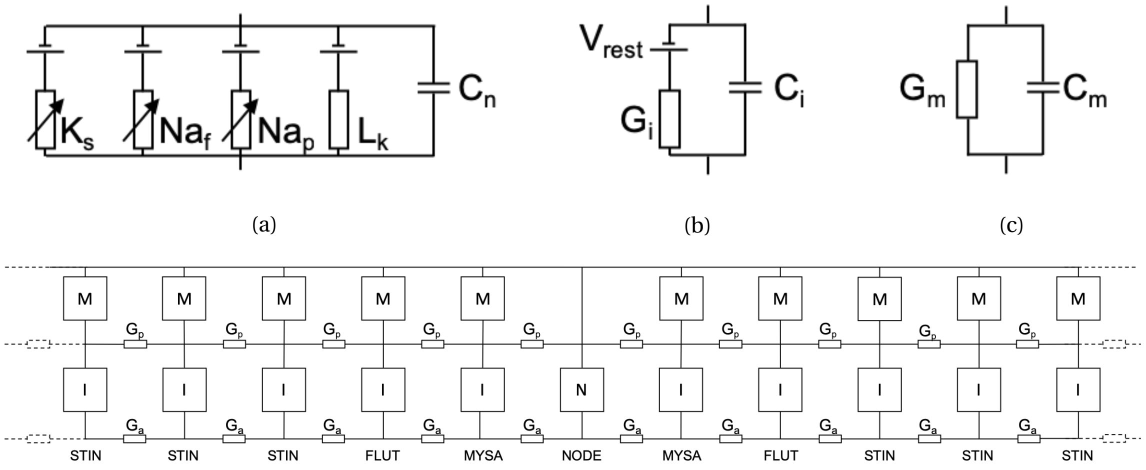

(a) (b) (c)

(d)

Figure 4.5: The double cable structure and circuit representation of the McIntyre-Richardson-Grill model [13]. (a) The circuit representation for the nodes of Ranvier (N-blocks in the complete structure). K_s represents the slow potassium channel, Na_f the fast sodium channel, Na_p the persistent sodium channel, L_k the leakage channel, and C_n the membrane capacitance. (b) The circuit representation for the axolemma of the internodal and paranodal segments (I-blocks in the complete structure). G_i represents the internodal conductance, C_i the internodal axolemma capacitance, and V_{rest} the rest potential. (c) The circuit representation for the myelin sheath of the internodal and paranodal segments (M-blocks in the complete structure). G_m represents the myelin conductance, C_m the myelin capacitance. (d) The complete structure of a node of Ranvier with all 10 segments surrounding it (2 MYSA segments, 2 FLUT segments and 6 STIN segments). It can be repeated to form an axon consisting of multiple nodes. G_a represents an axoplasmic conductance, G_p a periaxonal conductance.

Finally, all nodal, paranodal and internodal segments are connected via axoplasmic conductances G_a and periaxonal conductances G_p, as can be seen from Figure 4.5d. Most of the variables given are quickly deduced from the MRG Model geometric and electrical parameters, found in Table 4.2, only the periaxonal conductances are a little more complicated. The periaxonal space is defined as the space between the axolemma and the myelin sheath, and the inverse of the periaxonal conductances, the periaxonal resistances, are described by the following formulas:

$$R_{p,NODE}[\mathrm{M\Omega/cm}] = \frac{\rho_p}{\pi((r_{NODE} + w_{MYSA-perioaxonal-space})^2 - r_{node}^2)} \tag{4.8}$$

$$R_{p,MYSA}[\mathrm{M\Omega/cm}] = \frac{\rho_p}{\pi((r_{MYSA} + w_{MYSA-perioaxonal-space})^2 - r_{MYSA}^2)} \tag{4.9}$$

$$R_{p,FLUT}[\mathrm{M\Omega/cm}] = \frac{\rho_p}{\pi((r_{FLUT} + w_{FLUT-perioaxonal-space})^2 - r_{FLUT}^2)} \tag{4.10}$$

$$R_{p,STIN}[\mathrm{M\Omega/cm}] = \frac{\rho_p}{\pi((r_{STIN} + w_{STIN-perioaxonal-space})^2 - r_{STIN}^2)} \tag{4.11}$$

In these formulas, r represents radius, w represents width, and ρ_p represents the periaxonal resistivity which is defined as 70 Ω cm in the MRG Model [13]. As can be interpreted from these formulas, the periaxonal space is represented as a cylinder, and by dividing the periaxonal resistivity by the area of the periaxonal space cylinder profile, the periaxonal resistance per centimetre can be derived.

4.3.2. Properties of axon model

There is no published research on the axon sizes within the pudendal nerve. For simulations done in this thesis, an axon diameter of 10 µm will be used, as was agreed on with the medical specialists of the REValUE Project, who stated that axons in the pudendal nerve are between 10 µm and 15 µm. As described in Figure 2.11, earlier research shows higher block thresholds for axons with a smaller diameter; the worst-case results for the pudendal nerve are thus found at an axon diameter of 10 µm, which is therefore the preferred diameter to be used. This axon diameter results in the MRG model parameters shown in Table 4.2.

Table 4.2: The MRG model parameters for an axon diameter of 10 µm [13].

(a) Model geometric parameters (in µm)

Axon diameter	10.0
Node-node separation	1150
Number of myelin lemella	120
Node length	1
Node diameter	3.3
MYSA length	3
MYSA diameter	3.3
MYSA periaxonal space width	0.002
FLUT length	46
FLUT diameter	6.9
FLUT periaxonal space width	0.004
STIN length	175.2
STIN diameter	6.9
STIN periaxonal space width	0.004

(b) Model electrical parameters

Nodal capacitance (c_n)	2 µF/cm^2
Internodal capacitance (c_i)	2 µF/cm^2
Myelin capacitance (c_m)	0.1 µF/cm^2
Axoplasmic resistivity (ρ_a)	70 Ω cm
Periaxonal resistivity (ρ_p)	70 Ω cm
Myelin conductance[a] (g_m)	0.001 S/cm^2
MYSA conductance (g_a)	0.001 S/cm^2
FLUT conductance (g_f)	0.0001 S/cm^2
STIN conductance (g_i)	0.0001 S/cm^2
Maximum fast Na$^+$ conductance (g_{Naf})	3.0 S/cm^2
Maximum slow K$^+$ conductance (g_{ks})	0.08 S/cm^2
Maximum persistent Na$^+$ conductance (g_{Nap})	0.01 S/cm^2
Maximum leakage conductance (g_{Lk})	0.007 S/cm^2
Na$^+$ Nernst potential (E_{Na})	50 mV
K$^+$ Nernst potential (E_K)	−90 mV
Leakage reverse potential (E_{Lk})	−90 mV
Rest potential (V_{rest})	−80 mV

[a] Per lamella membrane (2 membranes per lamella)

4.4. Simulation environment

For this thesis the simulation environment of Neuron [36] was chosen. Neuron contains its own programming language, based on the hoc (High Order Calculator) programming language [35], that is focused on modelling neuronal models, and has a large online database available containing existing models, such as the MRG model.

When simulating, Neuron uses spatial discretization to reduce the cable equation to a set of ordinary differential equations with first order derivatives in time. It then offers backward Euler as integration method to solve these equations.

Another simulation environment option could be Matlab, but Matlab implementations of neuronal models such as the MRG model are much more computationally expensive. Neuron also has the option to interface with Python, meaning that it can also communicate with other software that is Python compatible. In the implementation of this thesis, most of the preparations and the interpretations of results are done via Python (version 2.7) [34], while only the actual axon simulations runs on Neuron.

4.4.1. Interface with Brainframe

As large simulations can still take up large chunks of time in which the computer running the simulation is mostly unavailable, there is a preference to run the simulations externally. The larger simulations in this thesis are therefore not run locally, but on Brainframe [44]: a cloud platform for running simulations with Neuron. Interfacing with Brainframe does not require any special additions, as it just involves uploading project files to the online platform.

4.5. Conclusion

In this chapter an overview of the full implementation of the simulation platform was given with which the different stimulation parameters, described in Section 2.3.4, are evaluated.

Neuron [36] was chosen as the main software on which to simulate the neuronal dynamics, which requires the KHFAC waveforms to be converted to a format consisting of a time and amplitude vector.

The electrode model and axon environment model are implemented as one and the same model. A monopolar electrode is modelled as a single point source placed in an infinite homogeneous isotropic medium, with a return electrode placed at infinity. A bipolar electrode is modelled as two point sources, placed in the same medium.

The McIntyre-Richardson-Grill model [13] is chosen as the implementation of the axon model, as this model is the state-of-the-art representation of a myelinated mammalian axon, with representations for the myelin attachments. With information missing on axon diameters in the pudendal nerve, an axon diameter of 10 µm is chosen for simulations, as agreed with the clinical specialist.

The simulations will be performed on the newly developed cloud Neuron simulation platform ’Brainframe’ [44]. As Brainframe is still in a bèta-phase, the research of this thesis serves as one of the pilot studies performed on Brainframe.

5

Simulation analysis of stimulation parameters for KHFAC stimulation

For the design of the pudendal nerve block stimulator of the REValUE project it is important to understand which stimulation parameters can improve its performance. Section 2.2.2 explored some of the earlier research that was done on nerve block thresholds. In this chapter, some of this research is re-evaluated for the case of the pudendal nerve; the knowledge on KHFAC blocks is also further extended by simulating stimulation parameters that have not been studied before.

The performance of different geometrical and electrical stimulation parameters is compared by looking at two quality measures:

- Block threshold: this is the minimum required current amplitude to create a successful nerve block at the set stimulating conditions. The block threshold can be used to compare efficacy, as it reveals which stimulation parameters should be changed to bring the stimulation conditions in the area where a block occurs most effectively. It can also be related to power consumption, as power is proportional to current squared.
- Block threshold charge per phase: this is the charge carried by a single anodic or cathodic pulse when the current amplitude is equal to the block threshold. This charge is dependent of the surface area under the anodic or cathodic pulse; a higher frequency pulse with a larger block threshold can thus still require less charge per phase. Also the shape of the waveform can have a large influence, e.g. a square wave has more area in a single phase than a sine of the same amplitude. The charge per phase is an important parameter when evaluating safety, as building up too much charge at the electrode-tissue interface can lead to irreversible reactions [12]. It also provides a more realistic view on what is physically happening, as the charge per phase is actually a measure for the amount of electrons that are injected into the tissue.

Section 5.1 explains the final simulation parameters that were used in the experiments done in this chapter. In Section 5.2, results are presented for monopolar simulation set-ups; waveform alterations and the effect of the pudendal nerve diameter are studied. In Section 5.3, results are presented for bipolar stimulation set-ups; the effect of the distance between the two poles on effectiveness is evaluated for all distances across the pudendal nerve diameter, and the effect of different orientations of the bipolar electrode lead are tested as well. The results are evaluated from both a clinical and a circuit design perspective in Section 5.4, in order to set a direction for the design of the REValUE stimulator.

5.1. Simulation set-ups

For all simulations, the axon parameters of Table 4.2 are used. As explained in Section 3.2.2, at least five nodes of Ranvier are necessary for the proposed model of Chapter 3 to work. To minimize simulation time, the minimum of five nodes of Ranvier are used in each of the simulations. The axon is modelled on the y-axis, and centred on the x- and z-axis; thus, every node is at $x = 0$, $z = 0$, $y = y_{\text{node}}$. This is equal to the set-up shown in Figure 4.3 and Figure 4.4. Furthermore, the simulation time-step size used is 1 µs. All KHFAC waveforms used are charge-balanced, meaning that the anodic pulse contains the same charge as the cathodic pulse.

5.1.1. Monopolar set-ups

The monopolar simulations consist mostly of simulations that concentrate on waveform types or alterations on which no data is present. First, the performance of three standard waveforms are tested, namely a square, sine and triangular wave. The sine and triangular waveform are also further explored in their stepped variants. Next, asymmetrical charge-balanced waveforms were tested (explained in Figure 3.7). The final alteration that is made on the waveform, is the addition of interphase delays, both after the anodic and cathodic pulse, of which the length is varied. The results of the waveform simulations can be found in Section 5.2.1.

To understand how well KHFAC stimulation would perform in the pudendal nerve, the electrode-to-axon distance simulation performed by Bhadra et al. [6] is repeated, but for distances that equal the diameter of the pudendal nerve. This gives insight in how much the block thresholds increase if, for example, the full nerve needs to be blocked instead of half the nerve. The result can be found in Section 5.2.2.

The monopolar set-ups consist of one electrode which is situated at $(x, y, z) = (0, 0, 1000)$ [unit = µm] except for the simulation that models the block thresholds across the pudendal nerve diameter, where the location along the z-axis is altered. The rest of the simulation parameters can be found in Table 5.1.

Table 5.1: Simulation parameters for monopolar simulations

Simulation type	Waveform type	Frequency range	Electrode to axon distance(s)	Other variables changed
Standard waveforms	Square, sine and triangular	4 to 40 kHz (2 kHz spacing) + 3 kHz	1 mm	
Stepped waveforms	Stepped sine and stepped triangular	4 to 40 kHz (2 kHz spacing) + 3 kHz	1 mm	4 to 200 steps per period (4 steps spacing)
Asymmetrical waveforms	Asymmetrical square waves	4 to 40 kHz (2 kHz spacing) + 3 kHz	1 mm	Anode fraction ranging from 0.1 to 0.95 (0.05 spacing)
Interphase delays	Square with interphase delays	4 to 40 kHz (2 kHz spacing) + 3 kHz	1 mm	Anodal and cathodal interphase delay ranging from 0.1 to 0.9 (0.05 spacing) with: $T_{\text{ipd\_anodal}} + T_{\text{ipd\_cathodal}} < 1.0$
Perpendicular distance	Square	10 kHz	0.1 to 58.5 mm (0.1 mm spacing)	

5.1.2. Bipolar set-ups

The bipolar simulations are aimed to understand how the performance of the KHFAC block can be optimized by placing the two electrodes at different distances from each other; the separation distance between the two electrodes is referred to as interpolar distance, and is shown in Figure 5.1.

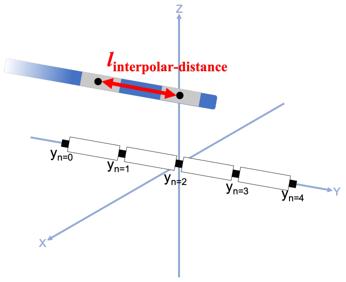

Figure 5.1: The interpolar distance is the distance between the two electrodes. For most bipolar simulations, this distance is increased to study how KHFAC stimulation can be optimized by choosing an optimal interpolar distance.

Section 5.3.1 explores the initial influence of the interpolar distance, and how this varies between a lead electrode that is aligned in parallel with the axon, and a lead electrode that is aligned perpendicular to the axon. The active electrode on the lead is called the anode, and is placed at $(x, y, z) = (0, 0, 1000)$. The return electrode, which is called the cathode, is placed at $(x, y, z) = (0, -l_{\text{interpolar-distance}}, 1000)$ for the parallel set-up, or $(x, y, z) = (l_{\text{interpolar-distance}}, 0, 1000)$ for the perpendicular set-up (these two positions are also shown in Figure 5.3a); $l_{\text{interpolar-distance}}$ represents the distance between the two electrodes. The minus sign in the parallel set-up for the y coordinate is used to place the cathode in the direction of nodes 0 and 1; node 3 can then be used as the 'virtual anode', which values are being read to predict if a block is successful or not. This way, the node is mostly unaffected by the potential reduction of the cathode.

For the simulation in Section 5.3.2, the set-up was mostly the same as for the parallel case, except that z for both anode and cathode was increased from 1000 to 60 000 µm, 'lifting the electrode', as shown in Figure 5.2. The interpolar distance was increased from 0 to 60 mm for each z.

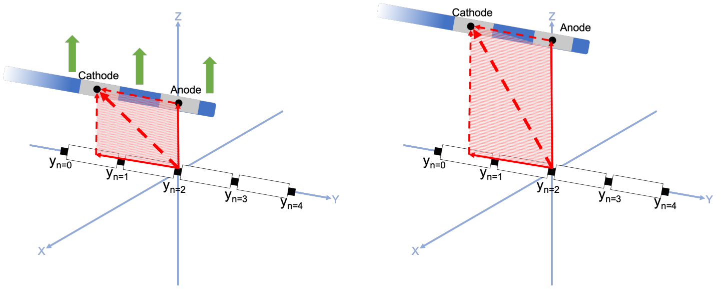

(a) (b)

Figure 5.2: Electrode set-up for the bipolar varying electrode-to-axon distance simulation. The z-coordinate of the anode and cathode are equally increased, such that the set-up changes from the situation in (a) to the situation in (b).

For the simulation in Section 5.3.3, the set-up of the parallel case was slowly changed into the set-up of the parallel case, by moving the cathode in the xy-plane towards the x-axis. Another orientation study was also performed, where the cathode moved into the yz-plane towards the z-axis until a 90° angle was made between the electrodes and the axon. Both set-ups can be observed in Figure 5.3.

The waveforms used in all bipolar simulations were 10 kHz symmetric square waves. The rest of the bipolar simulation parameters can be found in Table 5.2.

Table 5.2: Simulation parameters for bipolar simulations

Simulation type	Electrode to axon distance(s)	Interpolar distance	Other variables changed
Interpolar distance	1 mm	1 to 60 mm (0.5 mm spacing)	Cathode located in yz-plane for parallel simulations, and in xz-plane for perpendicular simulations
Electrode perpendicular distance and interpolar distance	1 to 6 mm (0.5 mm spacing)	1 to 60 mm (0.5 mm spacing)	Interpolar distance for zoomed variant: 1 to 10 mm (0.1 mm spacing)
Electrode orientation	1 mm (only the anode)	2.2 mm	For angle made in xy-plane, cathode moved in the xy-plane towards x-axis. For angle made in yz-plane, cathode moved in yz-plane towards z-axis. Anode location and interpolar distance were kept equal.

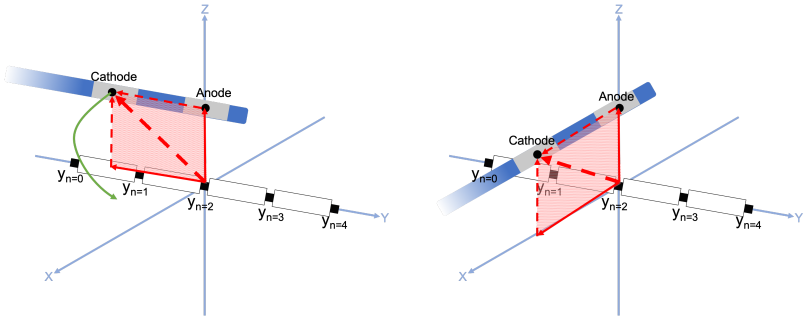

(a) Electrode angle shifted in xy-plane

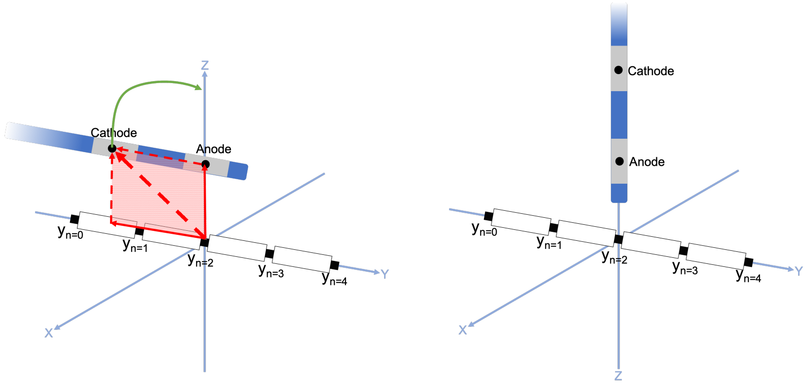

(b) Electrode angle shifted in yz-plane

Figure 5.3: Electrode set-ups for the electrode orientation simulation. The location of the anode remains unchanged for both experiments. (a) An angle is made in the xy-plane, such that the electrode starts parallel to the y-axis, and ends parallel to the x-axis. (b) An angle is made in the yz-plane, such that the electrode starts parallel to the y-axis, and ends parallel to the z-axis.

5.2. Monopolar simulation results

This section focuses on the results of simulations using a single electrode, with a return electrode placed at infinity; this is the set-up used in most other simulation studies on KHFAC blocks (like the ones discussed in Section 2.2.2). Section 5.2.1 discusses the influence of waveform-related parameters to the effectiveness of the KHFAC block. Section 5.2.2 focuses on how the block threshold changes for axons lying at different locations within the pudendal nerve.

5.2.1. Influence of waveform

Waveform alterations can potentially drastically improve performance of KHFAC stimulation. Baquer Gómez [18] found a waveform that minimized potential at the electrode-tissue interface. Although it is complicated to synthesize that waveform on a circuit, and it is questionable how well it performs in conditions that are different from simulation, it does reveal that KHFAC therapy can be improved by altering the waveform shapes that are being used.

In this section, multiple different waveform alterations are tested. First, three basic waveform shapes (square, sine and triangular) are simulated, together with stepped variants of two of these basic waveforms. Next, the effect of charge-balanced asymmetry (earlier described in Figure 3.7) is studied. Finally, the effect of adding interphase delays is explored.

Performance differences between basic waveforms

The performance of a square wave was compared with the performances of a sine and triangular waveform. The results are visible in Figure 5.4. Beneath 15 kHz, the block thresholds are relatively close together. However, due to the shape of the sine and triangular waveforms, the amount of charge that is injected in a single anodic or cathodic phase is significantly lower. Above 15 kHz, the block thresholds of the triangular and sine increase faster than the block threshold of the square wave; this results in that the block threshold charge per phase of all three waveforms at block threshold converge towards each other.

Earlier research only stated the increased block thresholds for sine and triangular waves compared to square waves [3]; this could lead to the conclusion that square waveforms are always the superior choice for a KHFAC signal, which is untrue, as the charge per phase at block threshold is significantly smaller for triangular and sine waves. Thus, when a high KHFAC frequency (above 20 kHz) is implemented, or a low KHFAC amplitude is required, the preference should be to use a square waveform. However, when a low KHFAC frequency (below 10 kHz) is implemented, or a low charge per phase is preferred, a sine waveform or triangular waveform has the preference.

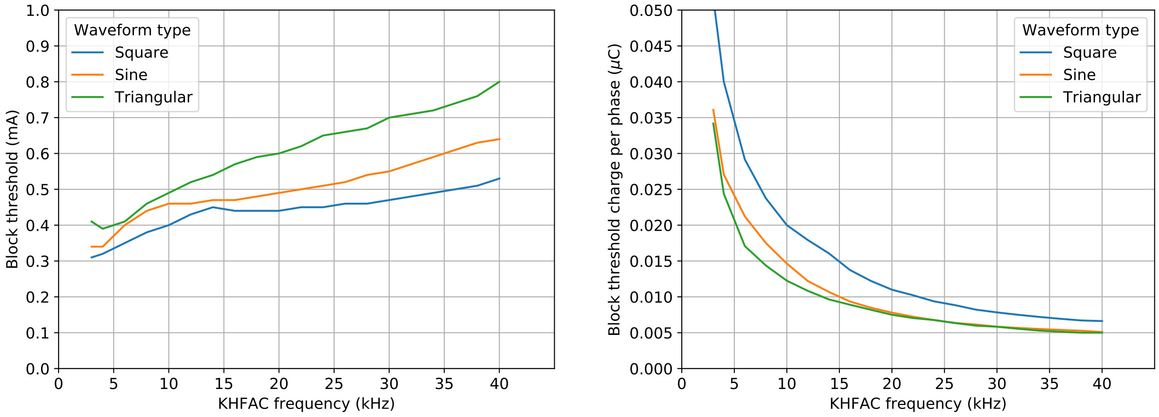

(a)

(b)

Figure 5.4: Comparison of the performance of a square, sine and triangular wave for frequencies ranging from 3 to 40 kHz. (a) The block threshold of all three waveforms. The square wave performs best, as it requires the smallest amplitude, especially at higher frequencies. (b) The block threshold charge per phase for all three waveforms. The triangular waveform is now the best performing waveform, especially at lower frequencies.

In Figure 5.5 two stepped waveforms were compared, as they have the potential to further reduce the block threshold charge per phase. The first was a step function that follows a sine shape, the second has equal step sizes and follows a triangular shape. The performance of both forms were measured as the amount of steps that were taken during each signal period was increased.

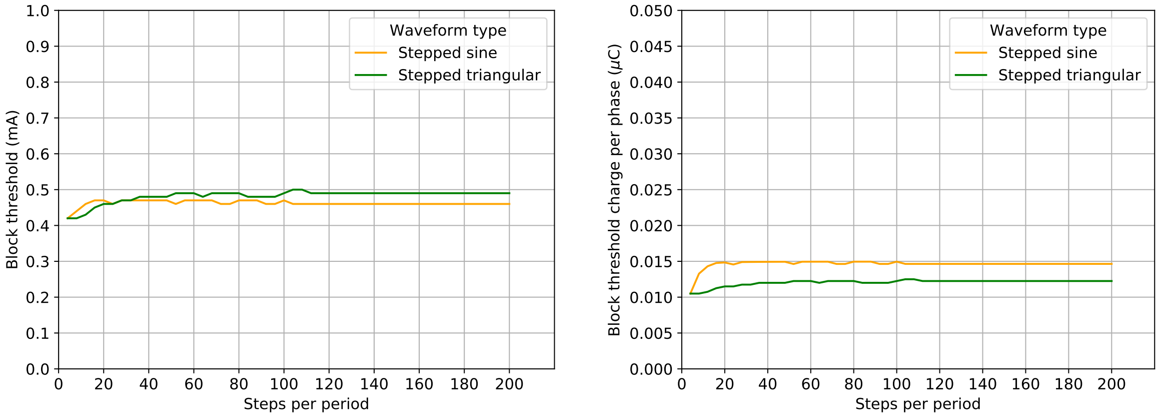

(a)

(b)

Figure 5.5: Comparison of the performance of a stepped sine wave and a stepped triangular wave with a base frequency of 10 kHz, for an increasing amount of steps per period. The block threshold and corresponding charge per phase can be slightly reduced by choosing a smaller amount of steps per period. (a) The block threshold amplitude for both waveform types. (b) The block threshold charge per phase.

The steps per period are increased up until the point where the steps are so small that the stepped signal closely resembles the non-stepped variant. From Figure 5.5a, it can be seen that beneath 25 steps per period, the amplitudes can be reduced by a very small fraction (about 0.05 mA) of the non-stepped variants of the signals. There are also no significant reductions for the necessary charge per phase.

It is also difficult to say whether the reductions are because of the stepped form of the signal, or because of the interphase delays that are also introduced in these type of waveforms, which are relatively large for small step sizes. This will be further examined in Section 5.2.1.

Performance of asymmetric waveforms

Figure 5.6 shows the results of the asymmetrical square (charge-balanced) waveform simulations, with the different anode fractions. As was explained in Figure 3.7, the anode fraction is defined by:

$$\text{anode fraction} = \frac{T_{\text{anodal}}}{T_{\text{anodal}} + T_{\text{cathodal}}} \tag{5.1}$$

with T_{anodal} the period of the anodal phase and T_{cathodal} the period of the cathodal phase. An anode fraction of 0.5 thus results in a regular symmetrical square wave. To maintain charge balance, the amplitude of the anodal phase A_{anodal} is calculated as:

$$A_{\text{anodal}} = \frac{Q_{\text{phase}}}{T_{\text{anodal}}} \tag{5.2}$$

where Q_{phase} represents the charge per phase.

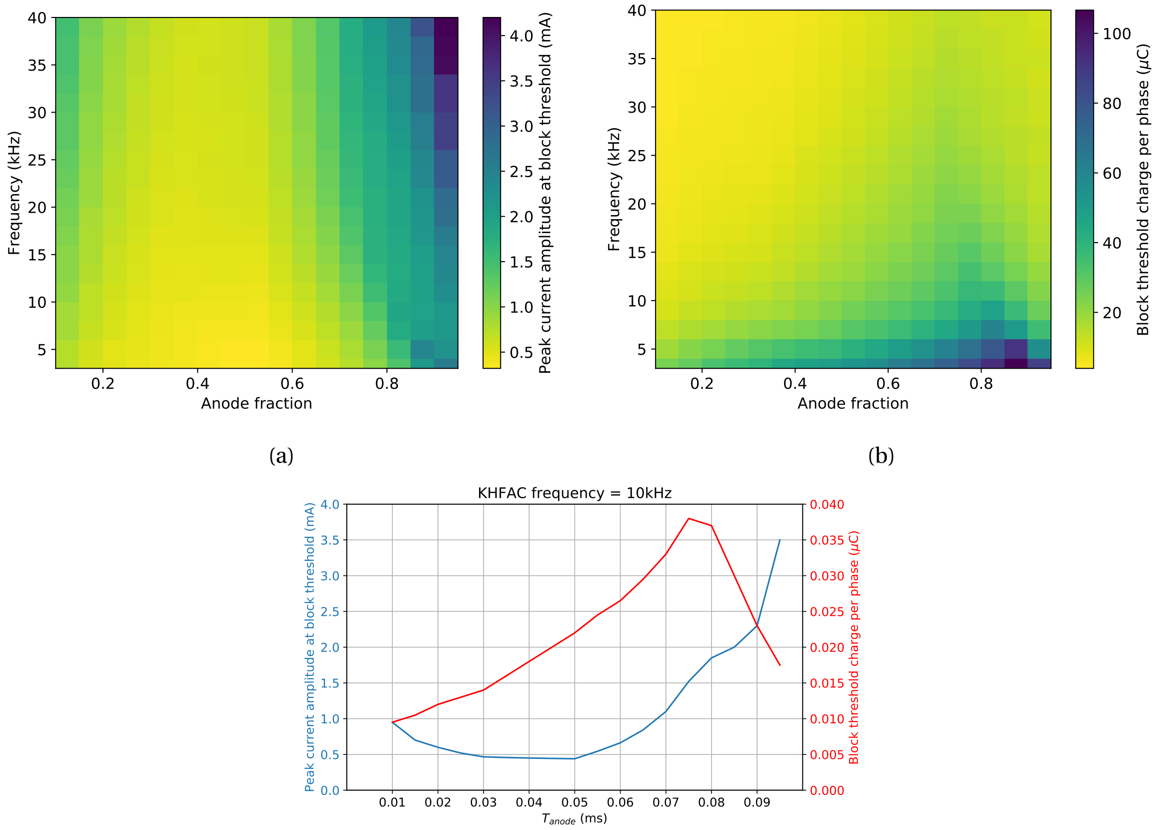

(a)

(b)

(c)

Figure 5.6: Comparison of the performance of different asymmetrical square waveforms, with the anode fraction ranging from 0.1 to 0.95. (a) The block thresholds for the different asymmetrical square waves for frequencies between 3 and 40 kHz. (b) The block threshold charges per phase for the different asymmetrical square waves for frequencies between 3 and 40 kHz. (c) The block threshold and corresponding charge per phase for the different asymmetrical square waves at 10 kHz.

Figure 5.6b is not symmetrical in the line drawn by the anode fraction of 0.5; a shorter, higher amplitude anodal pulse with longer, lower amplitude cathodal pulse (anode fraction< 0.5), requires less charge per phase than the opposite, with signals where the anodal pulse is longer and of lower amplitude than the cathodal pulse (anode fraction > 0.5). This behaviour can be explained when studying the steady-state value and time constant of inactivation variable h, respectively h_∞ and τ_h. Figure 2.6 revealed that at a membrane voltage V_m of −40 mV and higher, the value of h_∞ was close to 0, and τ_h was less than 0.2 ms. Between −40 mV and −110 mV the value of h_∞ increase to 1, but the value of τ_h also peaked above 1.1 ms between −70 mV and −80 mV. At V_m below −110 mV, where h_∞ is 1, τ_h has only reduced to 0.3 ms; h thus converges slower to 1 than to 0.

From Figure 2.5b of Chapter 2, it can also be observed that the membrane voltage V_m for a symmetrical signal fluctuates around −45 mV. The anodal pulse pulls the value of h faster to 0 than the cathodal pulse pulls the value of h to 1.

This explains the result that is observed in Figure 5.6b: a short anodal pulse of high amplitude, will pull the value of h to 0, and thus the membrane into inactivation. This effect is counteracted by the cathodal pulse. However, as the cathodal pulse is of low amplitude, meaning that the resulting membrane voltage V_m will result in τ_h to have it's peak value; thus h will only very slowly diverge away from 0, which allows the long period of the cathodal pulse. With a short high amplitude cathodal pulse however, h is pulled to 1 very fast, which is difficult for the low amplitude anodal pulse to compensate.

This might lead to the conclusion that it would be preferable to minimize the anode fraction of the period as much as possible; however, this leads to a high increase in the amplitude necessary for the anodal pulse. Figure 5.6a shows the maximum amplitude necessary at threshold (given by $\max(A_{\text{anodal}}, A_{\text{cathodal}})$). It can be observed that at an anode fraction lower than 0.3, the necessary amplitude of the anodal pulse needs to be increased again, whereas from Figure 5.6b it can be observed that the necessary charge per phase does not reduce as much any more.

This effect is further examined for a frequency of 10 kHz in Figure 5.6c. This figure emphasizes the suggestion that the anode fraction can be reduced to 0.3 (which is an anodal phase period of 0.03 ms), while the amplitude of the anodal phase is barely increased, but the required charge per phase is significantly reduced compared to a square wave. Figure 5.6a also reveals that at higher frequencies, the amplitude at an anode fraction of 0.3 begins to increase; an anode fraction of 0.4 would be more preferable for implementation if these higher frequencies are used.

Influence of interphase delays on performance

Figure 5.7 shows the results for simulations with increasing interphase delays following anodal pulses ('anodal interphase delays') and cathodal pulses ('cathodal interphase delays') of a square wave with symmetrical anodal and cathodal pulses. Figure 5.7a reveals that the block threshold rises exponentially, and is merely increasing for smaller interphase delays. Apparently, as the anodal and cathodal pulses become shorter with the introduction of interphase delays, the amplitudes can stay the same. This thus results in a decrease of the block threshold charge per phase, as seen in Figure 5.7b. This means that by introducing interphase delays up to a certain length, the required charge per phase can be reduced without increasing the amplitude.

The effect is further studied in Figure 5.7c and Figure 5.7d. From Figure 5.7a it can be observed that the block threshold barely increases for $T_{\text{ipd\_anodal}} + T_{\text{ipd\_cathodal}} \leq 0.06 ms$ ($T_{\text{ipd\_anodal}}$ = anodal interphase delay; $T_{\text{ipd\_cathodal}}$ = cathodal interphase delay); whereas from Figure 5.7d it can be seen that the block threshold charge per phase more than halves (this can also be more precisely confirmed from Figure 5.7b).

Another aspect that can be observed from Figure 5.7c and Figure 5.7d is that the figures are nearly symmetric in the line drawn by $T_{\text{ipd\_anodal}} = T_{\text{ipd\_cathodal}}$; the block threshold increases slightly slower for increased cathodal interphase delay. This suggests that increasing or decreasing the anodal interphase delay will have almost the same effect on the block threshold and corresponding charge per phase as increasing or decreasing the cathodal interphase delay. It also implies that in a bipolar set-up, the effect on performance of the KHFAC signal at the anode and cathode of the lead electrode will be equal.

5.2.2. Influence of distance along pudendal nerve diameter

Figure 5.8 shows the influence of the electrode-to-axon distance on the block threshold and required charge per phase. It was already noted by Bhadra et al. [6] that the block threshold varies approximately as the square of the perpendicular axon. These figures however, show just how much impact this relationship has when designing a KHFAC therapy for the pudendal nerve. In Section 2.3.3 it was mentioned that the pudendal nerve has a diameter of 4.67±1.17 mm. Figure 5.8 shows that for the axon at the furthest distance (about 5.84 mm), a block threshold that is over 600 times larger than the block threshold for the axon closest to the electrode is necessary. Whereas if only half of the nerve needs to be blocked, the block threshold should be 100 times larger than for the axon closest to the electrode.

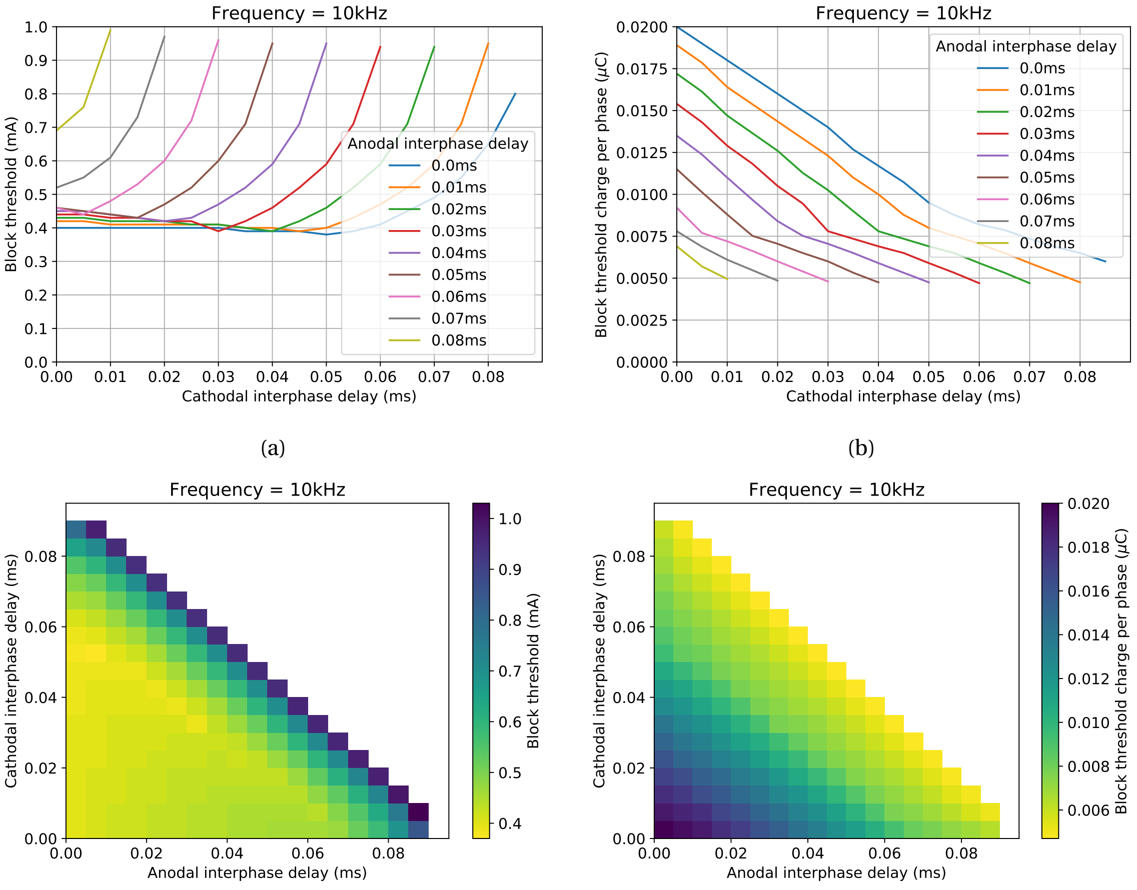

(a)

(b)

(c)

(d)

Figure 5.7: The influence of the addition of interphase delays, with $T_{\text{ipd-anodal}} + T_{\text{ipd-cathodal}} < T_{\text{signal}}$, on the performance of a 10 kHz square waveform. The time of the interphase delays are subtracted from the signal period; the remaining time is split between the anodal and cathodal pulse; this ensures that the frequency of the waveform remains intact. The anodal interphase delay is the interphase delay following the anodal (positive) pulse; the cathodal interphase delay is the interphase delay following the cathodal (negative) pulse. (a) The block thresholds for different interphase delays. It can be seen that the block threshold increases exponentially with a larger total interphase delay. (b) The block threshold charges per phase for different interphase delays. It can be seen that the required charge per phase decreases linearly with a larger total interphase delay. (c) The block threshold for different interphase delays shown as pseudo-colour plot. The plot is nearly symmetrical in $T_{\text{ipd\_anodal}} = T_{\text{ipd\_cathodal}}$. (d) The block threshold charge per phase for different interphase delays shown as pseudo-colour plot. This plot is also nearly symmetrical in $T_{\text{ipd\_anodal}} = T_{\text{ipd\_cathodal}}$.

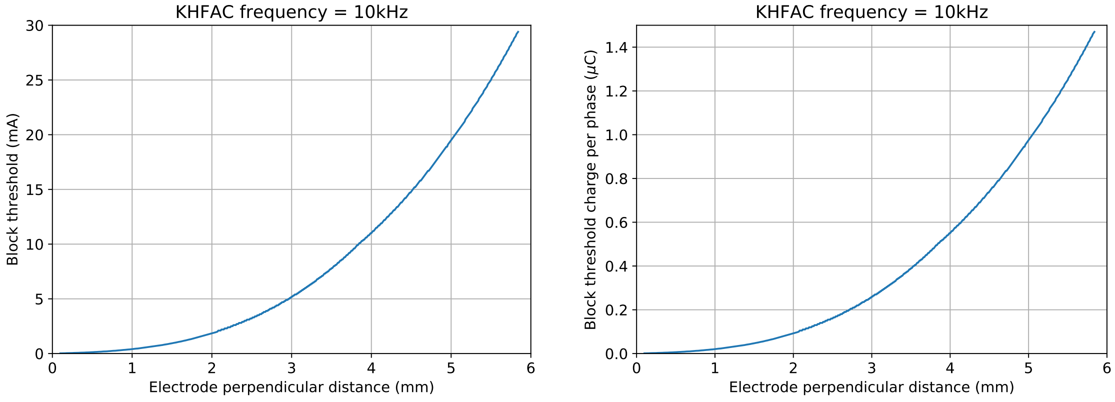

(a)

(b)

Figure 5.8: The block thresholds for the different electrode-to-axon distances that can be found within the pudendal nerve. The block signal is a 10 kHz symmetrical square wave. (a) The block threshold for increasing electrode-to axon distance. (b) The block threshold charge per phase for increasing electrode-to-axon distance.

5.3. Bipolar simulation results

This section focuses on simulations using a bipolar set-up, that has an extra 'inverted' pole close to the original monopole, similar to placing the return electrode close to the active electrode. If this extra pole is placed close enough, the electric field is altered, which can influence the block threshold. Section 5.3.1 explores the effect and compares two different electrode orientations. Section 5.2.2 then further examines how changing the interpolar distance can optimize the KHFAC stimulation.

5.3.1. Influence of interpolar distance on performance for two bipolar orientations

The first analysis of the bipolar set-up was using the set-up often used in monopolar simulations, with an electrode-to-axon distance of 1000 µm; except this time the return electrode, with current in opposite direction, was placed near the (original) active electrode. The return electrode was placed at varying distances of the active electrode; this distance is called the 'interpolar distance'. In Figure 5.9, the results of two lead electrode orientations are shown:

- A parallel orientation, meaning that both electrodes are placed such that the line connecting them is parallel to the axon
- A perpendicular orientation, where one electrode is placed above the axon (the anode), but the other electrode is placed away in the x-direction from the axon (the cathode), such that the line between the two electrodes is perpendicular in the xy-plane (see Figure 4.4).

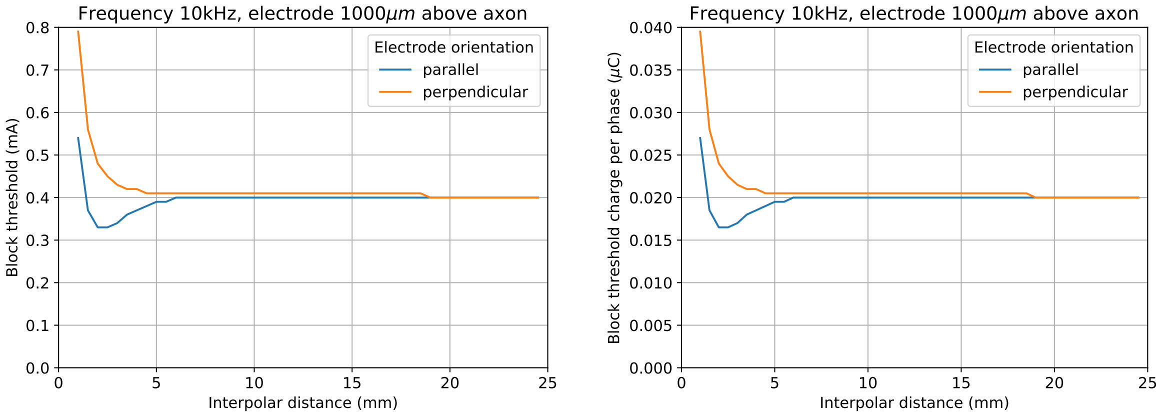

(a) (b)

Figure 5.9: The influence of changing interpolar distances of a bipolar set-up parallel and perpendicular to the axon with a 10 kHz symmetrical square wave. (a) The block threshold for the different interpolar distances in the two set-ups. (b) The block threshold charge per phase for the different interpolar distances in the two set-ups.

The results show that in the mentioned set-up, for an interpolar distance above ±7 mm, the block threshold and corresponding charge per phase converge to values that are also required in a monopolar set-up. The electric field at 1000 mm distance from the anode is thus perceived as equal to the electric field of a monopole.

Beneath 7 mm however, the block threshold has an reduction of more than 0.05 mA for the parallel set-up. In the perpendicular set-up, this improvement is nullified, and the block thresholds and corresponding charges per phase only become worse for smaller interpolar distances.

From this, two conclusions can be drawn:

1. A careful chosen interpolar distance can optimize the block threshold and required charge per phase. This effect is further examined in Section 5.3.2.
2. An electrode with optimized interpolar distance, that is not perfectly aligned with the axons that lie within the pudendal nerve, will have increase block thresholds compared to a perfectly aligned situation (and therefore increased block threshold charges per phase). This effect is further examined in Section 5.3.3.

5.3.2. Influence of interpolar distance on axons across the pudendal nerve

To achieve a better understanding on how the block threshold can be reduced for axons that lie at different distances from the electrode across the pudendal nerve, by changing the interpolar distances, a simulation experiment was done where both variables (electrode-to-axon distance and interpolar distance) were changed. The results are visible in Figure 5.10, and reveal a combination of two effects:

- the quadratic effect of the electrode-to-axon distance, which was shown in Figure 5.8;
- the effect of the interpolar distance, which was described in Figure 5.9.

It can be observed that, for higher electrode-to-axon distances, the reduction of block threshold that an optimized interpolar distance can have increases rapidly. For an electrode-to-axon distance of 100 mm, the reduction was only about 0.05 mA on 0.4 mA, which equals a reduction of about 12.5 percent; for an electrode-to-axon distance of 6 mm, the block threshold can drop from about 30 mA to lower than 12 mA (this is more obvious from Figure 5.11a), which equals a reduction of more than 60 percent.

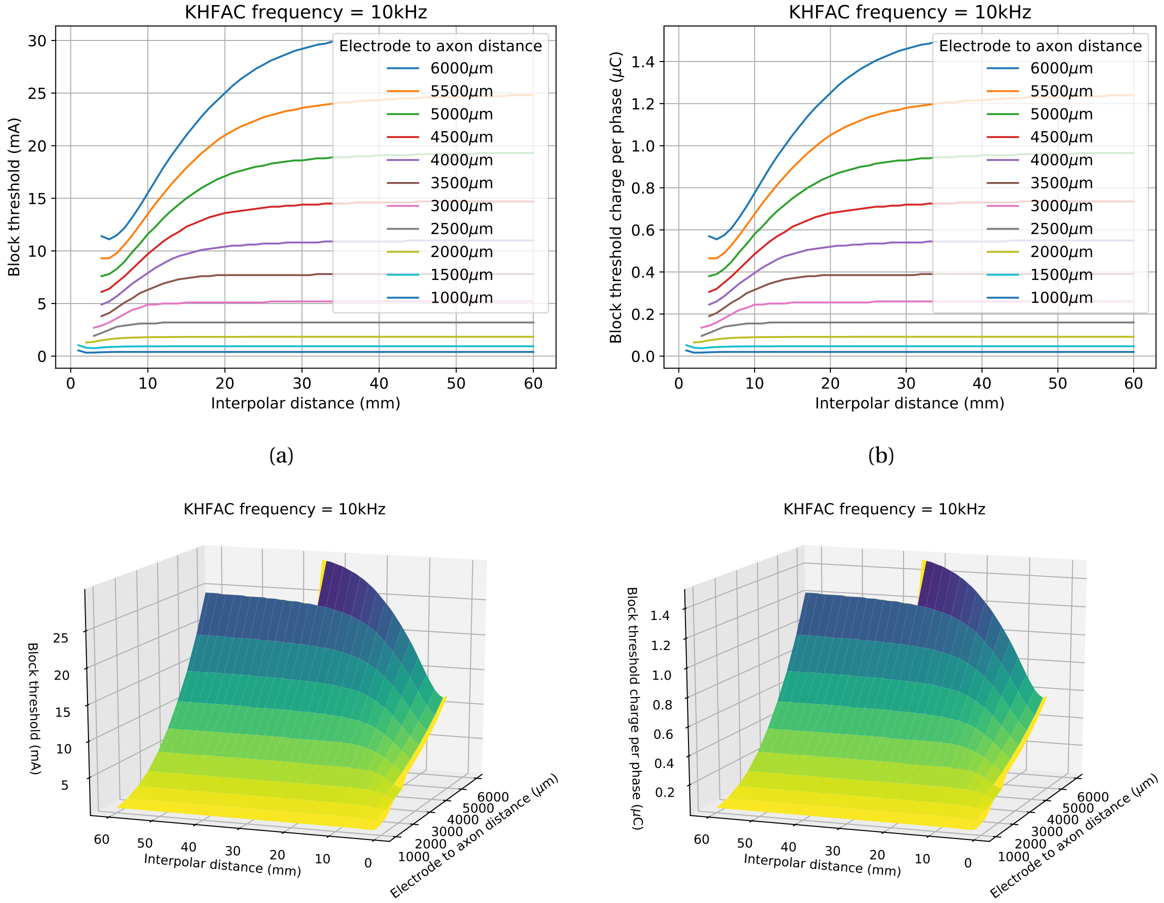

(a) (b)

(c) (d)

Figure 5.10: The performance of different interpolar distances for increasing electrode-to-axon distances for a 10 kHz symmetrical square wave. (a) The block threshold. (b) The block threshold charge per phase. (c) The block threshold shown in a 3D plot, better visualizing the parameter relationship between interpolar distance and electrode-to axon distance. (d) The block threshold charge per phase in a 3D plot.

Figure 5.10 also reveals that block thresholds are lowest with interpolar distances below 10 mm; above 10 mm, the responses of the set-ups converge to their monopolar variations. Figure 5.11 zooms in on the block threshold and required charge per phase for interpolar distances beneath 10 mm. It shows clearly that the block thresholds for blocking the furthest axons is brought much closer to the block thresholds needed for the axons closest to the electrodes. However, there is still a factor of 200 times difference between them, according to the figure.

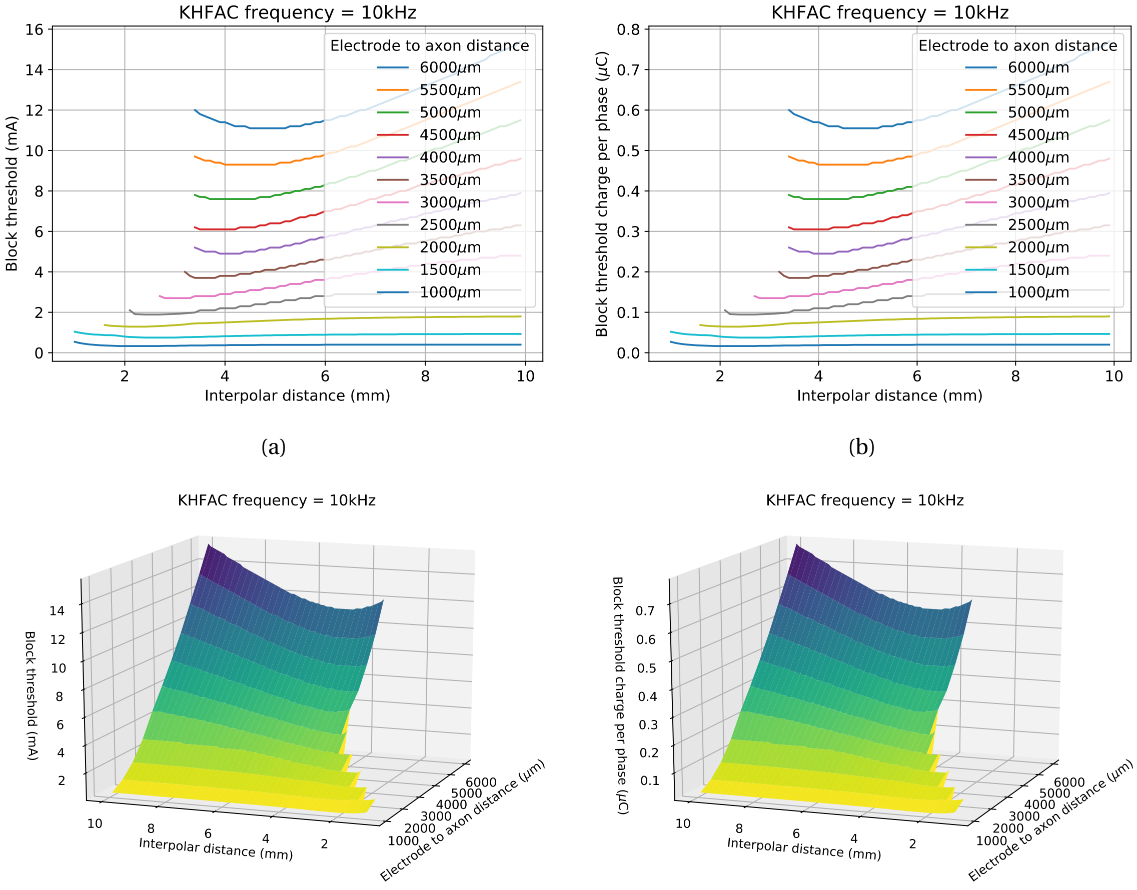

(a) (b)

(c) (d)

Figure 5.11: The performance of different interpolar distances for increasing electrode-to-axon distances for a 10 kHz symmetrical square wave, zoomed in to interpolar distances between 1 and 10 mm. (a) The block threshold. (b) The block threshold charge per phase. (c) The block threshold shown in a 3D plot, better visualizing the parameter relationship between interpolar distance and electrode-to axon distance. (d) The block threshold charge per phase in a 3D plot.

Figure 5.12 plots block thresholds for the optimal interpolar distance (and the corresponding interpolar distance itself) for each electrode-to-axon distance. The results of the optimal interpolar distances has irregularities, but close observation shows that for most datapoints, the optimal interpolar distance almost equals the nerve diameter. For the pudendal nerve, which is 4.67±1.17 mm, the optimal would be between 3.5 mm and 5 mm.

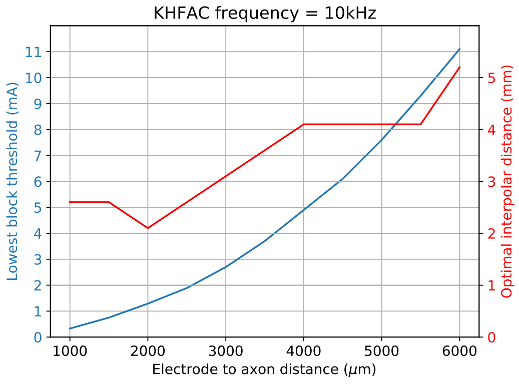

Figure 5.12: The optimal interpolar distances for each electrode-to-axon distance and the corresponding block thresholds, for a 10 kHz square wave.

5.3.3. Bipolar orientation

In a real surgery it will be hard to perfectly align the electrode with the nerve that is stimulated. Even when a perfect alignment would be reached, the axons inside the nerve are not necessarily perfectly aligned. Section 5.3.1 already showed that a misaligned electrode may nullify any improvements to the block threshold that resulted from an optimally chosen interpolar distance.

Figure 5.13 reveals the results of simulating different electrode orientations, both for the electrodes oriented at an angle in the xy-plane (towards the x-axis), and oriented at an angle in the yz-plane (towards the z-axis). Realistically, the angle in the xy-plane will be no more than 10° due to the limited space available in Alcock's canal, and the plot reveals that the block threshold will be stay mostly equal in that area.

The block threshold does increase when the 10° angle is made in the zy-plane. Because the electrode will be implanted in the pudendal canal, the electrode is most likely forced to be aligned in the zy-direction with the pudendal nerve as much as possible, such that this effect is minimized. This will however impact axons that lie within the nerve that are not perfectly aligned with the nerve itself.

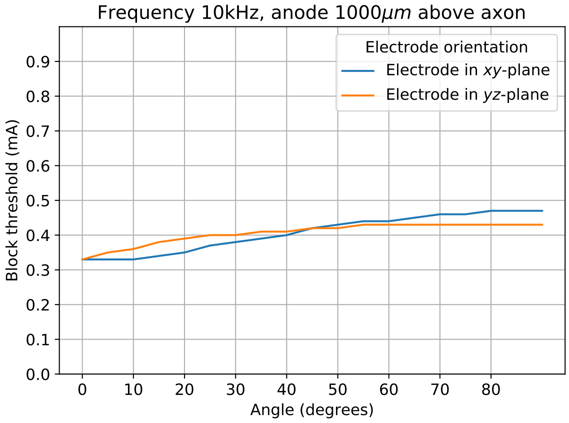

Figure 5.13: The block threshold for two changing bipolar electrode orientations, for a 10 kHz square wave and an interpolar distance of 2200 µm.

5.4. Discussion

The simulations show that amplitudes and required charge per phase for KHFAC block can be reduced by electrode and waveform design. This offers a wide range of design considerations, which will be discussed in this section. The validity of the results will also be discussed in this section.

5.4.1. Impact of results on design considerations

When considering circuit design, the square and triangular waveforms are easiest to synthesize. Depending on if system requirements demand low current amplitude or low charge per phase, it can be decided which of these two waveforms should be implemented.

The stepped variants of the sine and triangular waveforms did not result in significant reductions of the block threshold and charge per phase. The reductions that were visible, could also be a result of the interphase delays that were introduced at low numbers of steps per period. As implementing step waveforms will also increase circuit complexity, and can only accomplish a small reduction in block threshold, it does not seem to be a preferable option for implementation unless truly minimized block thresholds are required.

The asymmetrical charge-balanced square wave seems promising, as with an anode fraction reduced to 0.3, instead of 0.5 (which is equal to a symmetrical square wave), the charge per phase can be reduced while the block threshold does not increase. However, it is unclear how well this asymmetrical wave would perform in a realistic bipolar setting. At the return electrode, the current is travelling in the opposite direction compared to the active electrode (i.e. $I_{\text{stim,cathode}} = -I_{\text{stim,anode}}$); this results in an 'inverted' waveform at the return electrode, which is equal to having an anode fraction of more than 0.5. Thus, block thresholds are increased for the return electrode. This may lead to a failed block at the return electrode, which can result in repetitive firing. This might be very useful if one-way stimulation is needed, where the active electrode blocks stimulation in one direction, and the return electrode stimulates towards the other. However, Section 2.3.3

discussed that the pudendal nerve is a mixed nerve; asymmetrical waves can thus block signals travelling to the urethra, but it is unsure what the result will be of the repetitive firing at the return electrode that are created on the afferent nerves (the signals fired on the efferent nerves at the return electrode will most likely collide with the signals sent from the central nervous system).

The addition of interphase delays present what may be the most useful result, and has not been studied before in papers; most likely because there is no decrease in block threshold, which is the quality measure most studies focus on. Yet the decrease in block threshold charge per phase is significant, making it worthwhile to implement interphase delays in the KHFAC signal. Due to the symmetry that was observed between the effect of adding anodal versus cathodal signals, there is a much wider area of design options:

- A basic design option, which might be the easiest to implement on a circuit, would be to have an anodal and cathodal interphase delay that both make up 25% of the period of the signal, such that the anodal and cathodal pulse also each have a length of 25% of the period of the signal; an example is shown in Figure 5.14a. A clock with a frequency of four times the blocking frequency could be used to control the pulses and interphase delays. Also, the total fraction of the period for the interphase delay is then still 0.5, which is beneath the 0.6 threshold above which the block threshold increases.

- Another design option could be to let the anodic pulse immediately be followed by the cathodic pulse, and then implement one interphase delay that takes up no more than 60% of the period of the signal; an example is shown in Figure 5.14b. This way, the charge balance at the electrode is restored faster by the cathodal pulse. The extended interphase delay that follows, allows the tissue to restore some of the imbalances left. Due to the symmetry, the threshold does not increase compared to an option that has both an anodal and cathodal interphase delay, and the charge-per-phase reduction is also equal.

- A more complex way of utilizing the symmetry, would be to change the distribution of the interphase delays in a single waveform period over time (whilst keeping the total interphase delay per period equal); an example is shown in Figure 5.14c. This could be utilized to decrease predictability of the signal without changing the efficacy of the KHFAC block; this is useful to prevent the body from adapting to the signal, which could lead to habituation.

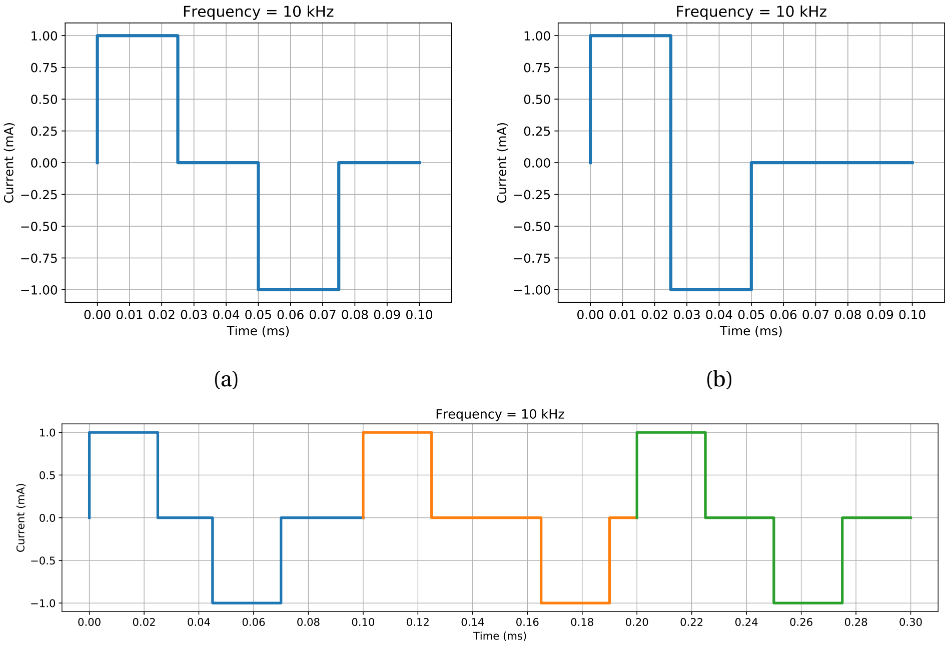

(a)

(b)

(c)

Figure 5.14: Three possible design options for including a 0.05 ms interphase delay in the waveform of a 10 kHz signal, that should result in nearly equal block thresholds. 5.14a A basic design option, where the waveform is split up in four periods of 0.025 ms. 5.14b A design option that focuses on restoring charge-balance as soon as possible. 5.14c A more complex design option, where the length of the anodal and cathodal interphase delays are altered after each signal period. The total interphase delay of each period still amounts to 0.05 ms.

The diameter of the pudendal nerve can become a problem, especially when the goal becomes to fully block the nerve. A bipolar configuration can reduce the block threshold for the axons furthest away of the electrode, but still more than 11 mA is required to block those. These simulations also do not take into account how the varying tissue resistances change the electric field and influence the block threshold; as was explained in Section 4.2, the model that was used assumes an infinite homogeneous isotropic medium instead. In the non-perfect environment where the electrode is implanted, even higher block thresholds are most likely needed. However, the bipolar configuration was also modelled as only two point charges; in the real electrode there are two electrode surfaces. This might alter the electric field to have a positive influence on the thresholds. In a clinical context, the results that show the effect of distance can be a good reason to search where in the pudendal nerve the axons that control the urethra are situated, such that a lead electrode can be placed closer to these axons and block thresholds for relaxing the external urethral sphincter can be decreased. If not the full pudendal nerve has to be blocked, but for example only half of the nerve, then due to the exponential relationship between the block threshold and electrode-to-axon distance, the block threshold reduces by a factor of six (this can be checked from Figure 5.8 by reading out the value at 3 mm). However, it must be realized that the part of the nerve that is not blocked, is instead most likely being constantly stimulated.

5.4.2. Validity of results

All the resulting block thresholds presented in this chapter were acquired via the proposed gate-dependent block determination model introduced in Chapter 3. The proposed model was calibrated such that the block thresholds that resulted for asymmetrical charge-balanced waveforms, matched the block thresholds that were found using the classic model (implemented to identify a 90% effective block). The performance was then further validated by comparing the results for sine waves acquired with the proposed method, to the results for sine waves acquired with the classic method. It was found that the block thresholds for sine waves were slightly underestimated by the gate-dependent model. Section 3.2.3 explained that using waveforms that are very different from the waveforms that were used to develop the model could potentially generate results with a larger error. Therefore it is important to evaluate the results of this chapter.

For the experiments with basic waveforms, that led to the results shown in Figure 5.4, not much will change. Figure 3.8 showed that for square waves (an asymmetrical wave with an anode fraction of 0.5) the results from the proposed model and classic model are almost completely the same. Figure 3.9 showed that the block thresholds of sine waves were slightly underestimated by the proposed method. As the shape of a triangular wave is close to the shape of a sine wave, it is expected that, although the block thresholds might potentially be underestimated even more, this will not lead to a significantly larger error margin. With this in mind, not much will change to the conclusion that was drawn on these basic waveforms. The increased block threshold will also lead to increased values for the block threshold charge per phase for the sine and triangular waveform; however, the sine was shown to have an error-margin of 10% to 15%, whereas the block threshold charge per phase is 50% to 75% higher for the square wave than for the sine and triangular wave at most frequencies. Triangular waveforms will thus still be the preferred waveform when the application requires low charge per phase, whereas square waveforms will be preferred when low amplitude is necessary.

When the same reasoning is applied to the results of the stepped sine waveform and stepped triangular waveform, shown in Figure 5.5, that will presumably again have error margins for the resulting block threshold that are comparable to the error margins of the sine wave, this will still lead to the conclusion that only minor improvements can be made, which are partly caused by the interphase delay that is introduced for a smaller number of steps per period.

As the proposed method is calibrated to resemble the results of asymmetrical charge-balanced waveforms, the results for asymmetrical waveforms, shown in Figure 5.6 can be presumed to be valid.

For results of the interphase delay experiments, shown in Figure 5.7, the validity is more difficult to establish. The gate-dependent model was not calibrated to work with interphase delays; it is unsure if interphase delays influence the gate variables and membrane voltages in such a way that large error margins are introduced. To gain insight in the validity of the results for interphase delays, a simulation using the classic method was done to determine block thresholds for a few sets of interphase delays. The results are presented in Figure 5.15. It can be seen that the resulting curves for the block thresholds still exhibit exponential behaviour, whereas the curves for block threshold charges per phase exhibit the linear behaviour. However, the block threshold increases much faster for an increasing anodal interphase delay than it does for an increasing cathodal interphase delay. Above a total interphase delay of approximately half the KHFAC signal period, the symmetry in block thresholds for adding anodal or cathodal interphase delays is no longer valid. However, the suggested implementations of interphase delays that were shown in Figure 5.14 are still possible, as long as the sum of both interphase delays does not exceed half the signal period.

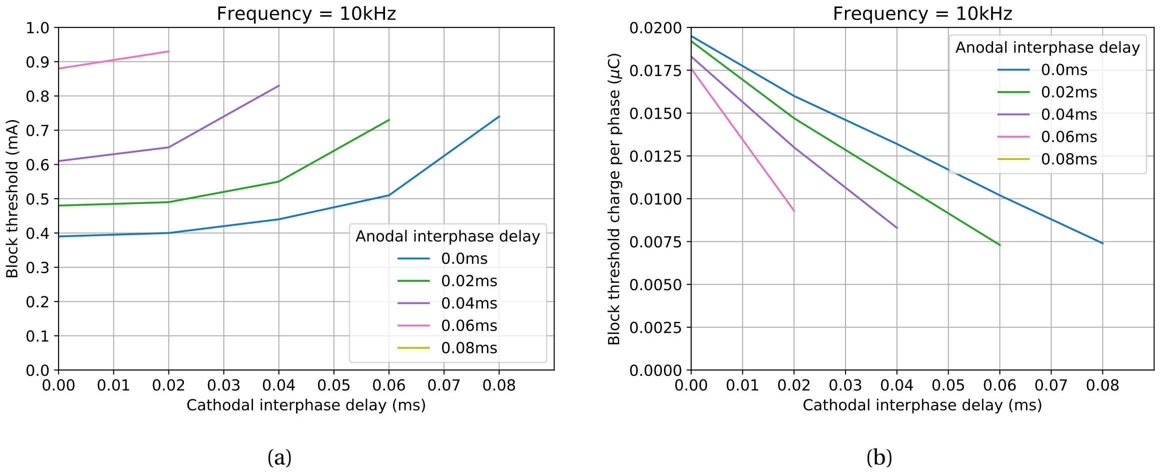

Figure 5.15: Validation of the results for the interphase delay experiments shown in Figure 5.7. The block thresholds presented in this figure were derived using the classic model for 90% block that was used in Section 3.2.2 to find block thresholds that could be used to calibrate the proposed model. (a) The block thresholds acquired with the classic method for different interphase delays. It can be seen that the block threshold increases exponentially with a larger total interphase delay, as was the case in Figure 5.7a. (b) The block threshold charges per phase acquired with the classic method for different interphase delays. It can be seen that the required charge per phase decreases linearly with a larger total interphase delay, as was the case in Figure 5.7b.

For the monopolar electrode distance simulation in Section 5.2.2, the square waveform was used, which was shown to produce almost equal results between the proposed model and classic model. The only thing that changes when increasing the electrode distance, is that the extracellular voltages at the different nodes of Ranvier decrease as well. However, this reduction factor is the same for the entire waveform; the shape of the waveform thus remains unaltered, and a square wave with reduced amplitude remains. From this can be concluded that increasing the electrode-to-axon distance does not influence the results.

For all bipolar simulations in Section 5.3, mostly the same reasoning can be applied as was used for the monopolar electrode distance simulation. However, the introduction of the return electrode and the altered electric field do change the distribution of extracellular voltages along the axon, which could alter the results. To check whether the proposed method creates valid results for a bipolar electrode set-up, the results for the perpendicular set-up, as shown in Figure 5.9, can be compared to the results found in the study by Ackermann et al. published in 2009 [11]. Their resulting curves for increasing interpolar distances have trends that closely resemble the curvature found in Figure 5.9. Thus, based on that:

- the proposed gate-dependent model is shown to produce similar results as the classic model for bipolar electrode set-ups, and
- increasing electrode-to-axon distance does not influence the accuracy of the proposed model,

it can be concluded that the results of Section 5.3 are very accurate to results that would have been acquired using the classic model.

Validity of simulation results for experimental testing

It has been explained that the results of the proposed simulation model are similar to results that would have been produced with the classic simulation model. More important, however, is how well these simulation results predict the results of *in vitro* or *in vivo* trials. In order to understand this, existing literature can be used.

Bhadra and Kilgore found a linear relation for block threshold and frequency, in a frequency range between 10 and 30 kHz, using an experimental set-up [45]; this is the same trend as was found in Figure 5.4a. As the shapes of square and triangular waveforms are not too different from the shape of the sine, it can be expected that these waveforms will also produce linear behaviour, albeit it with a different slope.

Peng et al. found through experiments that asymmetric waveforms, consisting of a short anodic pulse followed by a long cathodic pulse, resulted in more effective block than a symmetric square wave [46]; this means that the block threshold charge per phase was reduced for smaller anode fractions, which is the same result as was found in Figure 5.6c. Their research does not convey enough information to confirm all the trends found in this thesis, especially since the anode fraction that they used is missing. However, the study by Peng et al. shows reductions in block threshold charge per phase of 50%, reductions that can also be observed from Figure 5.6c.

The only research that investigated the effect of bipolar electrode design on block thresholds, which was done by Ackermann et al., also validated the simulation results experimentally, and discovered that the block thresholds acquired through experiments exhibited the same relation to interpolar distance as was found in their simulations [11]; this is the same relation that was found in the results of the parallel set-up of Figure 5.9.

Overall it can be concluded that the stimulation parameter relations that were found in these results are very similar to the relations that will be found through experiments. The only result of which no experimentally validation exists, is the relation of block threshold with interphase delays. The addition of interphase delays, however, is not a drastically different change to the simulated conditions; thus, the expectation is that experimental results for interphase delays will produce similar trends.

Even though the trends between simulation and experimental results will be similar, the experimental trends are expected to be at a much higher current amplitude levels. The study by Ackermann et al. shows a clear example of this, as the observed trends are exactly equal, but the exact block thresholds all are a factor 10 higher [11]. This can be caused by the placement of the electrodes, as they are difficult to place directly next to the nerve; and Figure 5.8 shows that the resulting increased electrode-to-axon distance will lead to an exponential increase in the block thresholds. Furthermore, the simulations in this thesis only simulate a single axon; blocking a complete nerve will require even higher block thresholds.

5.5. Conclusion

The influence of different electrical and geometric stimulation parameters on the effectiveness of the block was evaluated. Both the block threshold, which can be used to compare efficacy of different stimulation parameters and which can be related to power usage, and the block threshold charge per phase at block threshold, which can be related to both safety and the actual amount of electrons that are travelling through the tissue during KHFAC stimulation, were studied.

It was found that square waveforms have lower block thresholds than sine and triangular waveforms, but require more charge per phase.

Asymmetrical charge-balanced square waveforms can decrease the required charge per phase without increasing the peak current amplitude using shorter, high-amplitude, anodal pulses followed by longer, low-amplitude, cathodal pulses. However, it is unsure how well this type of stimulation performs in a bipolar set-up, as the inverted signal is used at the return electrode, which requires a higher charge per phase.

The addition of interphase delays to the waveform can reduce a large amount of the required charge per phase without increasing the block threshold. The effect of an interphase delay after the anodal pulse or after the cathodal pulse is mostly equal.

Simulation showed that to block the entire pudendal nerve, a current amplitude of 600 times the amplitude to block the axon closest to the electrode is necessary. However, this effect can be reduced by using a bipolar set-up. By choosing an electrode where the contacts are separated from each other at a distance that resembles the thickness of the nerve it is used for, the required amplitude can be greatly reduced. In the case of the pudendal nerve, a factor of 200 remained. However, if the electrode is not perfectly aligned with all axons, the effect reduces.

6

Conclusions and recommendations

This chapter summarizes the conclusions that were drawn during this research. The contributions of this thesis are highlighted, and recommendations are given for future work.

6.1. Conclusion

This thesis presented the relations between parameters that impact the effectiveness of a KiloHertz Frequency Alternating Current (KHFAC) block in the pudendal nerve, which were found using a novel simulation approach for detecting a successful nerve block.

As classic nerve block detection simulation methods tend to be slow, a new solution was developed that utilized the key mechanisms that cause the nerve block to speed up simulations. The faster model was utilized to gain more information of the performance of KHFAC blocks in the pudendal nerve, to explore the effect of new KHFAC waveform alterations on the performance of the block, and to study the effects of using a bipolar instead of a monopolar configuration. These results can be applied to electrode and waveform design to create safer and more power-efficient KHFAC nerve conduction blocks.

Chapter 2 explained the basics of KHFAC nerve propagation block, and how it could contribute to the treatment of urinary retention. It was explained that the mechanism of the block in humans is most likely a cause of the axon membrane channels being in a state of inactivation; in mathematical membrane models, this state is recognizable by the inactivation variable h having a value close to 0, and the activation variable m having a value close to 1. An overview was given of literature describing parameter relationships that impact the effectiveness of block. The chapter also focused on some of the anatomical features of the pudendal nerve at the implantation site that is proposed by the REValUE project, which are valuable for the simulations.

In Chapter 3 a new simulation approach for detecting a successful nerve block was proposed. The classic block detection method involves simulating a large part of an axon, initiating an action potential at one end of this axon, and measuring if it arrives at the other end. The proposed method however, only focuses on the nodes of Ranvier which are responsible for the block, and detects a successful block by measuring the values of the gate variables and the membrane voltages. The method was developed into a working model that was calibrated to detect 90% successful blocks. The proposed gate-dependent block detection method was shown to simulate 30 times faster than a model that applied the classic method to detect 90% effective nerve blocks.

Chapter 4 described the full simulation system used to find parameter relations that impact the blocking effectiveness. It discussed how the previously described block detection model fitted into the system, and how the monopolar and bipolar set-ups were implemented. A comparison was made between available axon models that support KHFAC stimulation, of which the McIntyre-Richardson-Grill model [13] was most suitable for this research, as it was partially based on human data. It was explained that the simulation environment was built up from Python code communicating with Neuron [36] in the Brainframe [44] online simulation environment.

Finally, Chapter 5 discussed the results of the simulations. It was shown that the block threshold charge per phase can be reduced without raising the block threshold itself, both by introducing interphase delays to the blocking signal waveforms, and by creating asymmetric charge-balanced waveforms with an anodal fraction lower than 0.5. It was shown that although triangular waveforms have higher block thresholds compared to square waveforms, they also require less charge per phase, which offers a design choice. Stepped variants of sine and square waveforms did not show much improvements. Furthermore, the block threshold necessary to block axons within the pudendal nerve located farthest away from the electrode was shown to be nearly 300 times the block threshold of those closest to the electrode; by choosing the correct interpolar distance of a bipolar configuration, this factor could be reduced to 100. It was also shown that it is important to have the electrode aligned with the nerve, as a misaligned bipolar electrode will increase block thresholds; however, in the suggested implantation site for the REValUE project, the electrode will most likely be forced to be aligned.

In conclusion, a new range of design considerations have been developed that add to previous research, which can be used to design an efficacious, safe and power-efficient stimulation system for creating nerve conduction block in the pudendal nerve, and it has been shown that a reliable block detection model can be developed based on the underlying mechanism of the nerve conduction block.

6.2. Contributions

This thesis put a large focus on the theoretical mechanism of the nerve block, and used this knowledge to draw many new conclusions on developing an efficacious KHFAC stimulation protocol for blocking in the pudendal nerve. This led to to the following main contributions:

A gate-variable-dependent block detection model The knowledge on the theoretical mechanism of the nerve block led to a new fast and reliable block detection model that can be used for KHFAC block simulations. The model is based on the membrane gate variables, and was introduced in Chapter 3. This model is able to simulate significantly faster than the state-of-the-art block detection model, which allows plenty more simulations to be done in shorter time.

Qualitative analysis of nerve block mechanism The mechanism of the nerve block has been identified before as the inactivation of the sodium channel, but this has mostly only been shown through simulations. Chapter 2 provides a first more elaborate qualitative analysis of this mechanism, by also studying the time constants τ_h and τ_m, and the steady state values, h_∞ and m_∞, of the membrane gate variables h and m; this shows it value when later in Chapter 5 the result of asymmetrical charge-balanced square waves is explained. The qualitative analysis also leads to a new explanation on the existence and the inevitability of the onset response.

Charge per phase as a quality measure This thesis focused not only on block thresholds, but also on the charge per phase required for a successful nerve block. The charge per phase has been used before by Bhadra et al. [6], but mostly to compare block threshold trends to trends related to activation of the axon. By using charge per phase as a quality measure, this thesis provides new insights in results from earlier research. For example, this thesis showed in Chapter 5 that the triangular waveform performs better when it comes to the charge per phase that is produced at block threshold, compared to a symmetrical square wave; in earlier research it was only stated that the triangular waveform has higher block thresholds, implicating that it is an inferior waveform for KHFAC stimulation [3]. Due to the better performance in charge per phase, it actually offers a balanced design option.

By focusing at the charge per phase for different waveform alterations, it was also revealed that both asymmetrical charge-balanced square waveforms and the addition of interphase delays to regular square waveforms can decrease the necessary charge per phase, without increasing the block threshold. These are important conclusions for design optimization, that would not have been spotted if only the block threshold was studied.

Simulation study on the performance of new waveform alterations This thesis contributed a first broad simulation analysis on the performance of asymmetrical charge-balanced square waveforms in an MRG modelled axon (Chapter 5), which can improve the required charge per phase.

This thesis also provides the first simulation analysis of the effect of adding interphase delays to a KHFAC waveform on the performance of the block (Chapter 5). The addition of interphase delays resulted in a significant decrease in required charge per phase, without raising the block threshold. It was also shown that the addition of either anodal or cathodal interphase delays have almost the exact same effect, which results in extra design options.

Extensive simulation study on the effect of using a bipolar electrode set-up A bipolar configuration was added to the MRG model in Neuron, which was used to study the influence of the interpolar distance on the block threshold in Chapter 5. This bipolar simulation study has been partly executed before by Ackermann et al. [11], but only for an electrode-to-axon distance of 1.0 mm. This thesis has studied the influence of the interpolar distance for a wide range of electrode-to-axon distances, which gave further insight in how much the relative reduction in block threshold changes for axons that are located further away from the electrode.

This thesis also first studied the effect of how electrode orientation impacts the bipolar block thresholds.

6.3. Recommendations

This thesis has led to valuable conclusions, but it is still a long road until a KHFAC stimulator for treating urinary retention is fully realized. This section aims to give recommendations for the future of the REValUE project, and aims to give insight in the possibilities of KHFAC stimulation.

6.3.1. Recommendations for the REValUE project

Safe charge-injection limits for KHFAC should be evaluated, as well as the maximum current amplitudes that can be used without damaging tissue or causing discomfort to the patient. Depending on these limits, the results of this thesis can be used to create a stimulation therapy with a charge per phase that is within the safe bounds, whilst power consumption is minimized by lowering the block threshold, such that less current is required for efficacious block.

The stimulus waveforms should at least incorporate interphase delays to reduce the required charge per phase, without increasing the block threshold. Square waveforms are most likely going to be the best available option; but if the charge per phase needs to be further reduced, triangular waveforms can be a good alternative.

The electrode used should be designed to have a distance between both electrode contacts that corresponds to the diameter of the nerve. Care should be taken during implantation to align the electrode with the nerve to reduce the block thresholds as much as possible. It should also be tested through clinical experiments how well lead electrodes can create a block in the pudendal nerve, that is large enough to relax the external urethral sphincter such that voiding is possible. It should also definitely be checked if the entire pudendal nerve needs blocking, or if blocking it partially is enough, as this will greatly reduce the block threshold. It could therefore be useful to develop a method with which the location of the axons that control the external urethral sphincter inside the pudendal nerve can be detected, such that the electrode can be placed closer to the correct axons and the block thresholds can be minimized.

6.3.2. Recommendations for the gate-dependent block-determination model and future simulations

The proposed gate-dependent block-determination model has shown that it is possible to determine a successful nerve block based on the gate-variables. However, the model conditions for successful block of Equation (3.1) are imperfect, and only work for detecting a 90% block. A more elaborate analysis on the behaviour of the gate variables during block, which includes for example the signal frequency, could lead to a complete model that can find any blocking percentage with very small error-margins. This could ultimately lead to an improved axon model that accurately describes the blocking conditions, which can help researchers to qualitatively determine the best stimulation conditions for achieving minimized block thresholds.

The decreased simulation time of this model can be useful to do more simulations on nerve bundles (such as the simulations done by Pelot et al. [47]), which more accurately describe the efficacy of the stimulation parameters.

The block-determination model can also be used for researchers that are working with high-frequency signals in their implants, to check whether they do not accidentally induce unwanted nerve blocks.

Finally, it would be interesting to test more non-standard waveforms which can be synthesized on circuits, to see whether even better performance can be achieved. The work of Baquer Gómez already proved that there certainly is room for non-standard waveforms, but the result is difficult to create on a real circuit. However, plenty of synthesizable better performing options might definitely exist.

6.3.3. Recommendations for KHFAC block research and applications

KHFAC stimulation is a very promising technology that can solve a large array of problems that encompass preventing unwanted signals from travelling through the nervous system. Currently, the most promising applications are the ones requiring temporary blocking of a nerve, rather than chronic, as the power requirements are relatively high compared to regular electrical stimulation, as pointed out by Kilgore and Bhadra [3]. Blocking the pudendal nerve during micturition is an excellent example of this. It was also tested as a solution for obese patients to block hunger signals [48]. It might also be an alternative to (local) anaesthesia for patients that are in a heightened risk group. Doctors of different fields should look how patients could benefit from turning of nerves.

Currently, chronic implants require low power usage, as replacing batteries requires surgery and wireless recharging implants is still difficult. By reducing the block thresholds, the current that is needed for the KHFAC waveform can also be reduced; this can lead to large power reductions, as power is proportional to the current squared. If KHFAC stimulation can realistically become part of a chronic implant by the reduced power requirements, it could lead to much more possible applications, especially in chronic pain treatment.

KHFAC block could also work together with a regular stimulation therapy, to ensure one-way stimulation. Asymmetrical charge-balanced square waves could even probably do this by themselves in a bipolar set-up, as the cathodal signal is inverted compared to the anodal signal; meaning if the anode is optimized to have a small block threshold through asymmetry, the cathode will have a high block threshold, which can lead to continuous pulsing in one direction. This type of stimulation can be useful if the operation of nerves that are part of a two-way control system, such as the vagus nerve, must be taken over.

Appendices

A

Electrode design considerations for kilohertz frequency alternating current nerve conduction block therapy in the human pudendal nerve

This appendix contains an essay that was written for the TU Delft course: Themes in Biomedical Electronics (ET4127). The essay provides a complete overview of electrode design considerations for KHFAC stimulation, based on existing literature on general electrode design, and studies that focus on electrode design specifically for KHFAC stimulation. Predictions are made about the effect of high frequency waveforms on both the behaviour of the different electrode types and the electrode-tissue interface model, in order to draw new conclusions. Moreover, the use-case of KHFAC stimulation in the pudendal nerve is used, to demonstrate how the design considerations can be applied to the design of a KHFAC therapy.

Overall, the essay expands the knowledge that was presented in this thesis, and can be useful for developing future KHFAC technologies.

Electrode design considerations for kilohertz frequency alternating current nerve conduction block therapy in the human pudendal nerve

Mini-thesis ET4127: Themes in Biomedical Electronics

Koen Emmer
Student number 4164156

Abstract—**Kilohertz frequency alternating current (KHFAC) stimulation is able to create a temporary conduction block in a nerve, but research on the impact of these high frequency signals on electrode design is limited. This mini-thesis provides a first complete overview of design considerations for KHFAC electrode design, by imposing the high-frequency requirements on electrode geometry and material theory, and by validating the newly found expectations using the few papers that do exist on KHFAC electrode design. By attempting to fully conceptualize a KHFAC electrode design for blocking the pudendal nerve, the gaps in KHFAC electrode design research are laid bare. It was found that Faradaic charge-injection materials are highly preferable to capacitative charge-injection materials for KHFAC stimulation electrodes. Based on current knowledge, a PtIr bipolar lead electrode with large contact surface areas is proposed for the use-case of blocking the pudendal nerve. This mini-thesis reveals that research is still necessary on the viability of efficacious KHFAC block for different electrode types, on optimal waveforms for blocking efficacy and their impact on electrode design, and on the charge-injection limits for KHFAC stimulation.**

I. INTRODUCTION

Kilohertz frequency alternating current (KHFAC) stimulation is a stimulation therapy that creates the function to manually 'turn off' a nerve [1], and has gained a lot of attention over the past 15 years. A limited amount of that attention went into KHFAC electrode design; research has only been carried out on the effect of KHFAC stimulation on electrode material [2, 3] and area [4], and how bipolar electrode design can increase the efficacy of the block [5].

This mini-thesis provides a first complete overview of the design considerations that change when switching from 'normal', low-frequency, excitation stimulation to KHFAC nerve block stimulation. It also shows how these design consideration will translate to a complete stimulating electrode design by using the example of creating a nerve block in the pudendal nerve. This example will reveal that still many aspects of KHFAC electrode design need to be researched, before optimal KHFAC electrodes can be designed.

II. KHFAC NERVE PROPAGATION BLOCK

Whereas electrical stimulation of nerve fibres is often used to trigger action potentials, KHFAC signals can be used to produce the opposite: it creates a temporary and quickly reversible inhibition of action potential conduction in a nerve, an effect that is distinct from synaptic and neural conduction fatigue, as proven by Kilgore and Bhadra [1]. KHFAC signals are able to create a block for frequencies as low as 3 kHz, as long as they are of sufficient amplitude. The minimum amplitude that creates a block under specific stimulation conditions is called a 'block threshold'. The cause for the existence of these nerve blocks is still being researched; in 2007 however, Bhadra et al. [6] found through stimulations that in human axons the inhibition of action potential conduction due to KHFAC stimulation is most likely caused by inactivation of the sodium channels.

Applications of KHFAC stimulation therapy include everything where it is desirable to block action potentials from travelling to the other end of a nerve. Examples are:

- **KHFAC chronic stimulation**: Suppression of phantom pains in patients with amputated limbs. KHFAC stimulation can prevent the pain signals from reaching the brain.
- **KHFAC acute stimulation**: Relaxing the external urethral sphincter in patients with underactive bladder (UAB) to restore bladder functionality. These patients have often lost the ability to voluntarily relax the urethral sphincter; this disables them from emptying the bladder, regardless of their ability to contract the bladder. KHFAC stimulation in the pudendal nerve can potentially suppress the signals that are continuously travelling from the central nervous system (via the pudendal nerve) to the urethra, resulting in relaxation of the sphincter muscle.

This mini-thesis focuses on the case of restoring bladder functionality through KHFAC stimulation in the pudendal nerve.

A. KHFAC block threshold

In KHFAC stimulation, the minimum current amplitude that is necessary at a specific frequency to elicit a nerve propagation block is called 'block threshold'. The effect of different changing conditions and stimulation parameters on the block threshold have been studied; an example is Bhadra et al. [6], who researched block thresholds for varying axon diameters and increasing frequencies. The result can be seen in Figure 1. The thresholds are given in terms of stimulation current (Figure 1a) and in terms of stimulation charge per phase (Figure 1b), which is the total charge in one anodic or cathodic pulse. The formulation of the block threshold as charge per phase will be useful when analysing electrode materials, as will be explained in Section III-B.

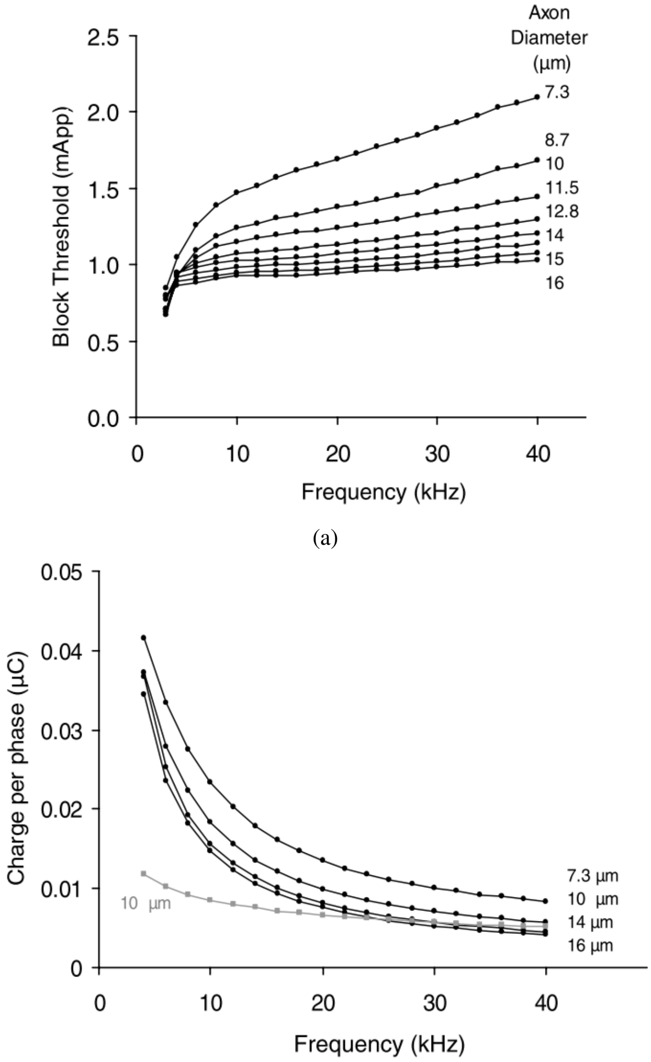

(a)

(b)

Fig. 1: Blocking thresholds for increasing frequencies and different axon diameters [6]. (a) Block threshold over frequency. (b) Block threshold expressed as charge per phase required over frequency.

III. STIMULATION ELECTRODE DESIGN BASICS

Merrill et al. summarized six requirements for the ideal material for use as a stimulating electrode [7]:

1) **Biocompatibility**: The material should not be toxic or necrotic to surrounding tissue when unstimulated.
2) **Mechanical compatibility**: The mechanical characteristics must be acceptable for the application.
3) **Efficacy**: The chosen material and electrode area must be able to inject sufficient charge to elicit action potentials.
4) **Reversibility**: Faradaic reactions should not reach toxic levels during stimulation.
5) **Corrosion threshold compatibility**: Faradaic corrosion reactions should not reach levels that will cause premature failure of the electrode.
6) **Durability**: The material characteristics must be acceptably stable for the duration of the implant.

When focusing on the impact of KHFAC-type signals on the choice of electrode material, requirements 4 and 5 are most important. Requirement 3 should be rewritten for KHFAC stimulation, as the goal is not to elicit action potentials, but to create a nerve conduction block:

3) **Efficacy**: the chosen material and electrode area must be able to inject sufficient charge to elicit a nerve conduction block

The required charge is normally quantified by the strength-duration curve developed by Lapicque [8], but no equal quantisation exists yet for the KHFAC nerve block. However, some earlier research has expressed block threshold data as charge per phase, which can be useful when choosing electrode material.

These requirements can be perceived as more than just requirements for electrode material; they can be seen as requirements for the entire electrode design, as will be done in this mini-thesis.

A. Electrode-tissue interface

When an electrode is placed in tissue, the interface between the electrode and the surrounding tissue is called the electrode-tissue interface (ETI), of which a simple circuit model was described in 1947 by Randles [9] (visible in Figure 2). The equivalent circuit model describes two types of transfer:

1) **Capacitative charge transfer**: When a metal is placed in an electrolyte, a double layer is formed, primarily due to the charge redistribution that occurs of metal ions in the electrolyte combining with the electrode. This is the effect observed at the ETI, and can be modelled as the double layer capacitance C in Figure 2b. When the electrode is driven negative, positive charge is attracted and negative charge is repelled; the opposite occurs at the second electrode, which is driven positive. With sufficiently small charge injected, only charge redistribution occurs within the electrolyte, an effect that is reversible by changing the polarity of the voltage source.
2) **Faradaic charge transfer**: When electrons are transferred across the electrode-electrolyte interface, this is called a Faradaic reaction. This transfer can occur as oxidation, where an electron is removed, a reaction that occurs at the positive electrode. Examples of these anodic processes are the oxidation of water, and corrosion. The opposite type of transfer is reduction, where an

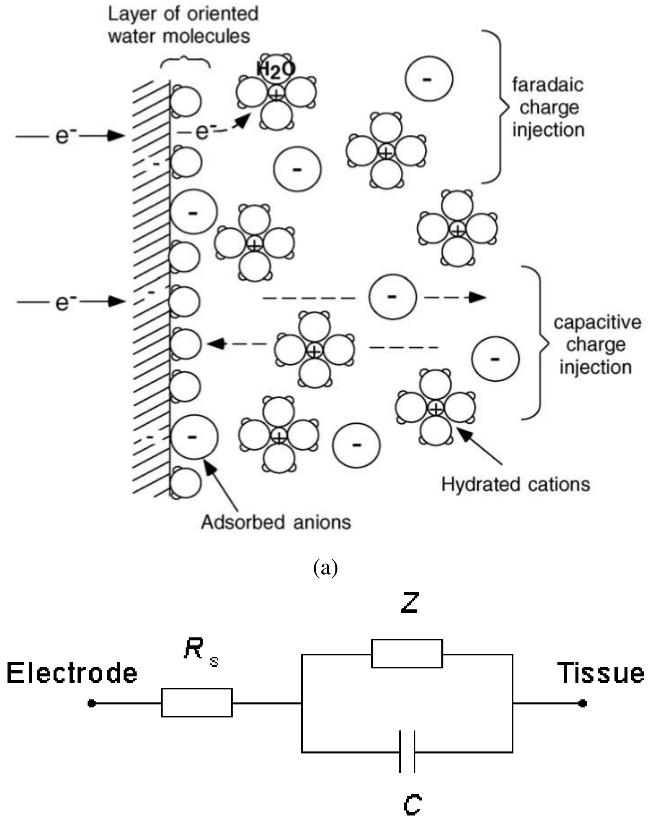
Layer of oriented water molecules
H2O
e⁻
e⁻
e⁻
faradaic charge injection
capacitive charge injection
Hydrated cations
Adsorbed anions
Z
R s
Electrode
Tissue
C

(a)

(b)

Fig. 2: Representation of reactions happening at the electrode-tissue interface. (a) The physical representation [7]. The top reactions represent Faradaic processes, the bottom represents capacitative processes. (b) Simplified circuit model of the electrode tissue interface [10] as conceived by Randles [9]. The double layer capacitance is modelled by C, the Faradaic processes are modelled by impedance Z.

electron is added; this happens at the negative electrode. Examples of these cathodic processes are the reduction of water and oxide formation. Not all Faradaic reactions are reversible. In the circuit representation of Figure 2b, the Faradaic reactions are modelled by the Faradaic impedance Z.

B. Water window and reversible charge storage capacity

The Faradaic impedance is characterized by the current-overpotential equation from Bard and Faulkner [11]:

$$\begin{aligned} i = & i_o \left\{ \frac{C_{O(0,t)}}{C_O^*} e^{-a_c n f \eta} \right. \\ & \left. - \frac{C_{R(0,t)}}{C_R^*} e^{(1-a_c) n f \eta} \right\} \end{aligned} \tag{1}$$

where i is the Faradaic current across the electrode-tissue interface, i_0 is the current density, $C_{O(0,t)}$ and $C_{R(0,t)}$ are the concentrations of respectively the oxidized and reduced species of a redox (reduction-oxidation) couple at the electrode surface as a function of time, C_O^* and C_R^* are the bulk concentrations of the redox species, a_c is the cathodic transfer coefficient, n the number of electrons oxidized, $f = F/RT$ where F is Faraday's constant, R the gas constant and T the absolute temperature, and finally η is the overpotential, described by $\eta = E - E_{eq}$, or the difference between the electrode's potential E and the equilibrium potential E_{eq}.

Equation 1 relates the Faradaic current i to an exponential function of the overpotential. Thus, for small overpotentials, where the electrode's potential is close to the equilibrium potential, the current will mainly flow through the capacitive branch of the circuit of Figure 2b. When the overpotential becomes substantially larger than zero, the right-hand term of Equation 1, involving the concentration of the reduced species, becomes more dominant; when the overpotential instead becomes much smaller than zero, the left-hand term, involving the concentrations of the oxidized species, becomes the dominant factor. These two different processes create a 'safe' margin around the equilibrium potential; this margin is called the 'water window'. If the electrode potential exceeds this water window, the amount of current that flows through the Faradaic branch of the circuit in Figure 2b becomes large enough such that the amount of Faradaic reactions reach unsafe levels, potentially damaging both tissue and electrode.

After Brummer and Turner [12] first asked the question how much charge can be injected without producing any solution product, Rose and Robblee [13] defined the reversible charge injection limit, or reversible charge storage capacity, as the maximum charge density that could be applied without exceeding the water window. The reversible charge storage capacity depends on the electrolyte composition, the waveforms used for stimulation, and the real surface area of the electrode, which depends on the material, size and shape of the electrode (and is different from the geometric surface area (GSA), as was shown by Brummer and Turner [14]).

The water window poses a challenge for the selection of electrode material, and is translated to requirements 4 and 5. As explained, too much anodic charge leads to water oxidation and corrosion, and too much cathodic charge to water reduction, which are both irreversible reactions. An electrode material should thus be chosen such that the reversible charge storage capacity is compliant to the amount of charge that is necessary to initiate a KHFAC block (i.e. the charge per phase, shown in Figure 1b).

C. Double Layer Capacitance

The double layer capacitance C_{dl} (C in Figure 2b) can be quantified to [7]:

$$C_{dl} = (\text{capacitance/area} * \text{area}) \tag{2}$$

where capacitance/area is an intrinsic material option. This capacitance also relates to charge and voltage as:

$$C_{dl} = \frac{dq}{dV} \tag{3}$$

where q is the charge and V is the electrode potential. By increasing the area, C_{dl} increases, such that more charge can be stored at a smaller overpotential. The increased electrode area also reduces the resistance at the electrode-tissue interface, reducing the power that is necessary for efficacious stimulation [15]. This would suggest that a larger electrode area is a safer and therefore better option. However, a smaller electrode area has the ability to stimulate a more precise piece of tissue. Depending on the spatial resolution that is required for the type of stimulation at the stimulation site, the electrode area can thus be chosen to either offer more precise stimulation, or safer stimulation.

However, there is another way to increase electrode area. The double-layer capacitance is namely not dependent on the geometric surface area (as was also stated in Section III-B), but on the electrochemical surface area (ESA). The ESA is the real area of the electrode which can participate in electrochemical reactions. Porous materials have an increased ESA due to the non-flat contour, as shown in Figure 3. The double-layer capacitance can thus be increased not only by choosing larger electrode contacts, but also by choosing a more porous material.

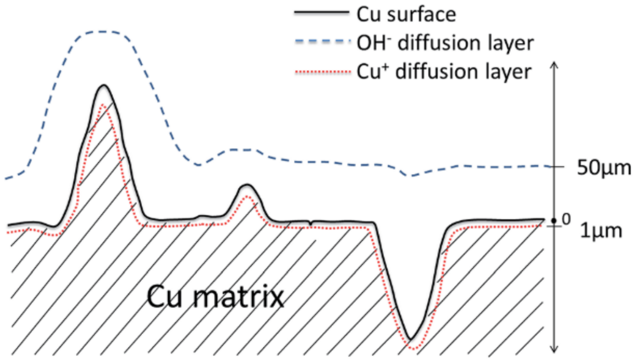

Fig. 3: Schematic contour of porous electrode material [16]. The electrochemical surface area (or 'real' surface area) is much larger than the geometrical surface area, which would be the simplification of this contour as a flat surface.

Interesting for this research, is how the use of high frequency signals combined with the double layer capacitance influence the behaviour of the electrode-tissue interface. At high frequencies a capacitor acts as a short circuit; this implies that, based on the circuit model of Figure 2b, increasing the frequency would force more current to flow through the capacitive branch. This would result in reduced Faradaic reactions, thus making the amount of electrode polarization independent of electrode material selected. This has been confirmed by Ghazavi and Cogan, who researched the polarization of platinum, sputtered iridium oxide (SIROF) and titanium nitride (TiN) using frequencies between 1 kHz and 50 kHz [3]. Ghazavi and Cogan showed that for platinum, electrode polarization decreases with increasing frequency, with overpotentials reaching unsafe levels outside of the water window at 1 kHz, but slowly decreasing to safe levels starting at 5 kHz and higher. SIROF and TiN electrodes were always within safe margins for the stimulation protocols that were used. They concluded that overpotentials associated with faradaic reactions are negligible, and electrode corrosion or the generation of tissue-damaging products during stimulation is unlikely.

D. Characteristics of commonly used electrode material

Cogan reviewed different electrodes used in stimulation [17]. Two main types of electrode material were distinguished:

1) Capacitive charge-injection materials: These are porous materials or materials with high dielectric constant coatings applied, such that they have increased charge-injection capacity, as the double-layer charge per unit area in itself is small. Titanium nitride (TiN) can be fabricated to be very porous by having a high surface roughness; this increases the ESA, and therefore the double-layer capacitance as well, as explained in Section III-C. A tantalum/tantalum oxide capacitor electrode is an example of a capacitor electrode that has a dielectric coating for increased charge injection capabilities. The obvious advantage of capacitive charge-injection materials is that Faradaic reactions can be minimized and neither the tissue nor the electrode are damaged. However, the available charge is limited by pore resistance, the result of deeper pores behaving as delay lines that prevent the total ESA being used during stimulation.

2) Faradaic charge-injection materials: These are often noble metals, noble metal alloys or iridium oxide coatings, which utilize reversible reduction and oxidation reactions to provide high levels of charge for stimulation. Platinum (Pt) and platinum-iridium (PtIr) alloys are the most used noble metals in neural stimulation, which inject charge through both Faradaic and double-layer charging. Iridium oxide coatings include activated iridium oxide films (AIROFs) and sputtered iridium oxide films (SIROFs), and these coatings are used for micro-electrode applications which require higher charge-injection capacities. Although Faradaic charge-injection materials can reach higher levels of charge, the risks for irreversible reactions, and therefore damage to tissue or the electrode, are significantly larger.

IV. ELECTRODE DESIGN CONSIDERATIONS FOR KHFAC STIMULATION

Now that a basic understanding of KHFAC stimulation and electrode design basics have been determined, these two fields can be brought together to see how KHFAC stimulation impacts the design considerations for electrodes. This theory is then brought into practice by choosing design options for a conceptual electrode used for blocking the pudendal nerve.

A. Impact of KHFAC stimulation on electrode geometric design

The most common type of electrode used for eliciting KHFAC blocks in experimental set-ups is a nerve cuff type of electrode; this type of electrodes can circle the entire perimeter of the nerve, as shown in Figure 4a. These type of electrodes have the ability to stimulate a larger part of the nerve with a uniform electric field strength. A cuff type electrode can also mostly prevent electrode migration issues, as the electrode can't move away from the nerve. However, the implantation of these type of electrodes is a highly invasive procedure which can take multiple hours, as the entire nerve needs to be exposed during the operation.

A less invasive electrode is a lead electrode, shown in Figure 4b. This type of electrode can be implanted by making a small incision in the patient, after which the electrode can be directed near the stimulation site in minutes of time. However, it becomes harder to form a uniform field across the entire nerve, as the electrode-axon distance varies more strongly across the nerve.

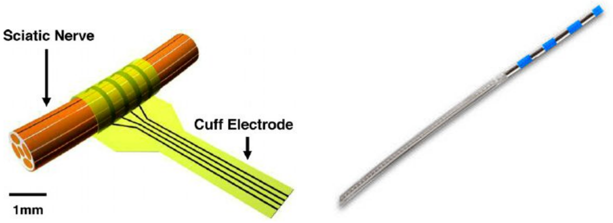

(a) A nerve cuff electrode [18]. (b) A (quadrupolar) lead electrode [19].

Fig. 4: Two basic types of electrodes used in KHFAC block therapy. (a) A cuff electrode that consists of multiple wires that circle the perimeter of the nerve. Other cuff electrode set-ups can consist of pads instead of wires, that circle either the entire nerve, or a part of the nerve. (b) A quadrupolar lead electrode. This type of electrode can also exist with another number of contacts, and can be inserted next to a nerve.

Cuff and lead are not the only electrode styles that are suitable for KHFAC block therapy. Cuellar et al. for example achieved block with a paddle electrode, a bipolar hemi-cuff electrode, a bipolar hook electrode, and a percutaneous cylindrical electrode [20]. Micro-electrode arrays have not been researched for KHFAC nerve block, but could be interesting for blocking specific areas of a nerve.

Not much research has been carried out yet about different electrode geometry set-ups and their effect on the efficacy of the block. However, Patel et al. showed that for cuff electrodes, circumferential coverage significantly reduced block thresholds compared to partial cuffs [4]. This effect was also seen in the simulation study done by Pelot et al. [21], where the efficacy of a partial cuff electrode was compared to a full cuff electrode and a point source for a nerve of $3\,\mathrm{mm}$. In this set-up it became clear that the full cuff electrode produced concentric rings of block thresholds, where the threshold increased closer to the centre of the nerve. The partial cuff electrode produced different 'bands' of similar thresholds, where thresholds close to the partial cuff were lower, and increased for axons placed further away. The point source seemed to produce a similar effect, however for higher amplitudes a more complete block across the entire nerve was accomplished than in any of the other two set-ups.

Most simulations in research so far was done using monopolar research set-ups. In experimental research, bipolar set-ups were used more frequently, but the electrode contact separation distance has often not been documented. This motivated Ackermann et al. [5] to study the effect of electrode contact separation distances in both computational (using a dipole model) and experimental (using cuff electrodes) set-ups. They found that block thresholds could be further reduced by optimizing the distance between the electrode contacts for the implantation site.

B. Impact of KHFAC stimulation on electrode material selection

Only one research looked into the effect of electrode material on the efficacy of KHFAC block therapy. Patel et al. [2] investigated Stainless Steel, Platinum, Platinum-Iridium (90/10), and Titanium Nitride. They found that no benefits were achieved with respect to the block thresholds by choosing different electrode material. This is useful, as this means that the electrode material can be chosen to minimize Faradaic reactions without surrendering efficacy. This offers a possibility for orthogonal design.

Patel et al. also showed in the same research that, even though material characteristics are independent of the blocking thresholds, that the material chosen can substantially influence the power requirements.

In Section III-D, different types of electrode material were discussed. It was noted that capacitative charge-injection materials have the disadvantage that the charge injection is limited, due to the deeper pores behaving as delay-lines. In KHFAC stimulation, this can potentially become a major problem, as the small time periods of the KHFAC waves limit the time available to inject sufficient charge. This effect is also visible in the research by Patel et al. [2], who states: "Although TiN has a high electrochemical surface area (ESA), the high sweep rate used in the CV measurements indicates a significantly lower CSC value for TiN coated electrodes compared to planar, non-coated electrodes" (CV = cyclic voltammetry, CSC = charge storage capacity). Although no direct connection is made by Patel et al., this result acts as a confirmation to the hypothesis that the influence of the delay-line behaviour of porous TiN on the reduction of the CSC becomes more significant under KHFAC stimulation.

C. Preferred electrode design options for KHFAC stimulation in the pudendal nerve

As stated in Section III, there are three requirements of interest for determining suitable electrode parameters:

3) Efficacy
4) Reversibility
5) Corrosion threshold compatibility

There are four different design parameters that have been identified, namely electrode type, set-up, area and material. When combining these with the requirement options, some suggestions can be given on electrode design for KHFAC stimulation.

1) Electrode type: The pudendal nerve is partly situated in the pudendal canal (or Alcock's canal), which is a sheath of fascia that tightly encloses the pudendal nerve [22]. When an electrode is implanted here, electrode migration can be minimized due to the tight enclosure of the sheath. In this regard, a lead electrode thus almost performs as well as a cuff electrode. As the lead electrode is relatively much easier to implant, this is the preferred electrode type to be used, provided that the lead electrode will be able perform a full pudendal nerve block as well as a cuff electrode.

2) Electrode set-up: In Figure 5 the quadratic relationship between the electrode-to-axon distance and the block threshold can be observed. The pudendal nerve itself is on average 4.67 ± 1.17 mm [22], meaning some axons are situated maximally almost three times as far as shown in Figure 5. For blocking the furthest axons, stimulation amplitudes that are substantially larger than necessary for the closest axons are needed, especially in the case of a lead electrode.

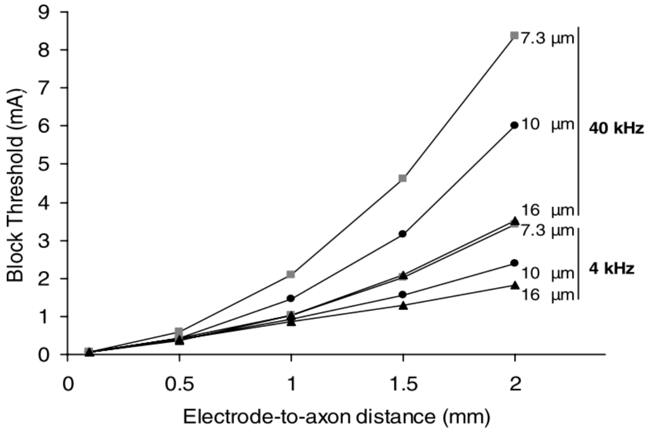

Fig. 5: The influence of perpendicular electrode-to-axon distance on the block threshold for three axon diameters under two different frequencies [6].

With a bipolar set-up, the electric field can be altered to be more uniform across the diameter of the nerve. The field strength along the diameter of the pudendal nerve can be varied by changing the distance between contacts, ensuring that the potentials at the nodes of Ranvier of axons closest to the electrode better resemble the potentials at the nodes of Ranvier of axons furthest away from the electrode. For a lead electrode, maybe even multiple bipolar set-ups, such as a quadrupolar set-up, can be adjusted to utilize different stimulation protocols that optimize the block for axons close or far away from the electrode, however, this should first be further researched.

3) Electrode contact area size: As explained in Section III-C, a larger electrode area increases the safety, but lowers spatial resolution. For the pudendal nerve a low spatial resolution is sufficient. Increasing the area will also decrease the power necessary to reach the block thresholds. Thus, a large area is preferred, as long as it fits within the available geometrical space of the pudendal canal and is not as large that surrounding nerves are also stimulated or blocked.

4) Electrode material: Two common electrode material types were discussed in Section III-D: capacitative and Faradaic charge-injection material. In Section IV-B it was explained that the delay-line behaviour of porous materials can reduce the charge storage capacity of the material when using KHFAC stimulation. The same Section also explained that choosing different materials had little impact on blocking efficacy, which offers the possibility to choose between these type of materials based on other aspects, such as long-term safety, without compromising efficacy. Section III-C discussed how at KHFAC frequencies more current flows through the capacitative branch of the electrode-tissue interface, reducing Faradaic reactions, especially for capacitative porous electrodes and Faradaic iridium oxide coatings.

Taking everything into account, Faradaic iridium oxide coated electrodes such as SIROF seem very promising, due to their high charge-injection capacities (which improves efficacy), and since Faradaic reactions are reduced under KHFAC stimulation. SIROF is however a material that is more suitable for microelectrodes. Patel et al. [2] suggested PtIr alloys, a material already used in clinically available KHFAC devices, but has not been researched in the research by Ghazavi and Cogan [3] which looked into which branch of the electrode-tissue interface the current flows under KHFAC signals. This could be a material that better fits the large electrode contact area that was preferred.

V. DISCUSSION

Section IV-C discussed that the best electrode design, based on current knowledge, should be a PtIr bipolar lead electrode with large contact surface areas. There are still some aspects that need verification:

- There is no research yet that confirms if a nerve with thickness equal to the pudendal nerve can be blocked with a lead electrode without having to increase the amplitude to dangerous levels. This should be validated, together with the effect of using different bipolar electrode pairs optimized for different electrode-to-axon distances, to see whether a quadrupolar electrode might be more effective than a bipolar electrode for blocking the entire pudendal nerve.
- The limits to which the area of the electrode can be increased without exciting or blocking other nerves neighbouring the pudendal nerve should be studied.
- It is still unclear which waveforms are optimal for efficacious KHFAC block. When more is known about this subject, the performance of different electrode materials when using these waveforms should be tested.
- Figure 1b gives an indication of the charge per phase that is necessary to block an axon that is situated 1 mm from the nerve. The charge per phase necessary to block the entire pudendal nerve should be determined, and then it

should be checked which materials have a charge storage capacity under KHFAC stimulation that is sufficient.

A. Future electrode material technology

This mini-thesis so far only focused on available electrode technology, but there are also a lot of materials that are emerging.

Polyethylenedioxythiophene (PEDOT) is a polymer that can be used as a coating for electrodes that can significantly reduce electrode impedance [17]. It is the most promising electrically conducting polymer when looking at biocompatibility.

Carbon nanotubes can be placed in a micro-electrode array to greatly improve the charge injection limit as they create a large electrochemical surface area [23].

Graphene is a new electrode material technology which is said to outperform traditional electrode material derived from metals [24]. It is mostly interesting for recording due to a low SNR, but graphene can also be shaped to resemble nanotubes for increased capacitance [25], which is useful for stimulation.

These emerging electrode materials bring interesting characteristics to the table, but are all technologies used in micro-electrode arrays, which is an electrode type that has not been used in KHFAC experimental research. If micro-electrode arrays become valid options for KHFAC stimulation, or if these materials might develop in the future to replace single electrode technology (such as lead or cuff electrodes) these technologies should be re-evaluated.

B. Influence of DC contamination

Franke et al. [26] discussed that care should be taken when using off-the-shelf stimulators, as they do not always produce perfectly charge-balanced waveforms, which results in a direct current component in the KHFAC signal. This direct current can build up charge at the electrode-tissue interface, which can result in irreversible Faradaic reactions. If perfectly charge-balanced stimulators are not available, it is thus necessary to design the electrode (and stimulation protocol) such that all the charge that is built up during the stimulation periods because of the DC component can be stored reversibly.

VI. CONCLUSION

This mini-thesis focused on finding how design parameters change for KHFAC nerve propagation block therapy, and explored the use-case of a KHFAC electrode in the human pudendal nerve. The high frequency reduces the current flowing through the Faradaic branch of the electrode-tissue interface, which results in that Faradaic charge-injection materials become more feasible options. Another aspect of the high frequencies was that the charge storage capacity of porous capacitative charge-injection materials is reduced, making them less desirable.

For KHFAC nerve propagation block therapy, the advice would thus be to use a platinum-iridium alloy (or an iridium oxide coating, which is now primarily used in micro-electrodes) as electrode material. For applying this type of stimulation in the pudendal nerve, a lead electrode would be preferred for its ease of implantation, in a bipolar set-up in order to achieve an as uniform as possible electric field through the entire nerve. The electrode should have a large contact area to decrease power usage and increase the charge storage capacity.

At this moment the research on the impact of KHFAC on electrode material behaviour is still very limited, and more verification is needed. There is also still too much uncertainty on the exact stimulation parameters that will be used in creating pudendal nerve propagation blocks. The knowledge available is sufficient to create working KHFAC electrodes, but there is a long road of improvements ahead of now.

REFERENCES

[1] K. L. Kilgore and N. Bhadra, “Nerve conduction block utilising high-frequency alternating current,” *Medical & Biological Engineering & Computing*, vol. 42, no. 3, pp. 394–406, may 2004.

[2] Y. A. Patel, B. S. Kim, and R. J. Butera, “Kilohertz Electrical Stimulation Nerve Conduction Block: Effects of Electrode Material,” *IEEE Transactions on Neural Systems and Rehabilitation Engineering*, vol. 26, no. 1, pp. 11–17, jan 2018.

[3] A. Ghazavi and S. F. Cogan, “Electrochemical characterization of high frequency stimulation electrodes: role of electrode material and stimulation parameters on electrode polarization,” *Journal of Neural Engineering*, vol. 15, no. 3, p. 036023, jun 2018.

[4] Y. A. Patel, B. S. Kim, W. S. Rountree, and R. J. Butera, “Kilohertz Electrical Stimulation Nerve Conduction Block: Effects of Electrode Surface Area,” *IEEE Transactions on Neural Systems and Rehabilitation Engineering*, vol. 25, no. 10, pp. 1906–1916, oct 2017.

[5] D. M. Ackermann, E. L. Foldes, N. Bhadra, and K. L. Kilgore, “Effect of bipolar cuff electrode design on block thresholds in high-frequency electrical neural conduction block,” *IEEE Transactions on Neural Systems and Rehabilitation Engineering*, vol. 17, no. 5, pp. 469–477, 2009.

[6] N. Bhadra, E. A. Lahowetz, S. T. Foldes, and K. L. Kilgore, “Simulation of high-frequency sinusoidal electrical block of mammalian myelinated axons,” *Journal of Computational Neuroscience*, vol. 22, no. 3, pp. 313–326, may 2007.

[7] D. R. Merrill, M. Bikson, and J. G. Jefferys, “Electrical stimulation of excitable tissue: Design of efficacious and safe protocols,” *Journal of Neuroscience Methods*, vol. 141, no. 2, pp. 171–198, 2005.

[8] L. Lapicque, “Recherches quantitatives sur l’excitation électrique des nerfs traitée comme une polarisation,” *J. Physiol. Pathol. Gen*, 1907.

[9] J. E. B. Randles, “Kinetics of rapid electrode reactions,” *Discussions of the Faraday Society*, vol. 1, p. 11, 1947.

[10] J. Malmivuo and R. Plonsey, *Bioelectromagnetism: Principles and Applications of Bioelectric and Biomagnetic Fields*. New York: Oxford University Press, 2012. [Online]. Available: http://www.bem.fi/book/book.pdf

[11] A. J. Bard and L. R. Faulkner, *Electrochemical methods : fundamentals and applications*. New York: John Wiley and Sons, 1980.

[12] S. Brummer and M. Turner, “Electrical stimulation of the nervous system: The principle of safe charge injection with noble metal electrodes,” *Bioelectrochemistry and Bioenergetics*, vol. 2, no. 1, pp. 13–25, jan 1975.

[13] T. Rose and L. Robblee, “Electrical stimulation with Pt electrodes. VIII. Electrochemically safe charge injection limits with 0.2 ms pulses (neuronal application),” *IEEE Transactions on Biomedical Engineering*, vol. 37, no. 11, pp. 1118–1120, 1990.

[14] S. B. Brummer and M. J. Turner, “Electrical Stimulation with Pt Electrodes: AMethod for Determination of ”Real” Electrode Areas,” *IEEE Transactions on Biomedical Engineering*, vol. BME-24, no. 5, pp. 436–439, sep 1977.

[15] C. Alon, G. Kantor, and H. S. Ho, “Effects of Electrode Size on Basic Excitatory Responses and on Selected Stimulus Parameters,” *Journal of Orthopaedic & Sports Physical Therapy*, vol. 20, no. 1, pp. 29–35, jul 1994.

[16] P. Zhu and Y. Zhao, “Effects of electrochemical reaction and surface morphology on electroactive surface area of porous copper manufactured by Lost Carbonate Sintering †,” *RSC Advances*, vol. 7, no. 42, pp. 26 392–26 400, 2017.

[17] S. F. Cogan, “Neural Stimulation and Recording Electrodes,” *Annual Review of Biomedical Engineering*, vol. 10, no. 1, pp. 275–309, aug 2008.

[18] S. H. Lee, J. H. Jung, Y. M. Chae, J.-K. F. Suh, and J. Y. Kang, “Fabrication and characterization of implantable and flexible nerve cuff electrodes with Pt, Ir and IrOx films deposited by RF sputtering,” *Journal of Micromechanics and Microengineering*, vol. 20, no. 3, p. 035015, mar 2010.

[19] Medtronic, “Spinal neurostimulation lead / quadrupolar - 3889, 3093 - Medtronic.” [Online]. Available: http://www.medicalexpo.com/prod/medtronic/product-70691-503182.html

[20] J. M. Cuellar, K. Alataris, A. Walker, D. C. Yeomans, and J. F. Antognini, “Effect of high-frequency alternating current on spinal afferent nociceptive transmission,” *Neuromodulation*, vol. 16, no. 4, pp. 318–327, jul 2013.

[21] N. A. Pelot, C. E. Behrend, and W. M. Grill, “Modeling the response of small myelinated axons in a compound nerve to kilohertz frequency signals,” *Journal of Neural Engineering*, vol. 14, no. 4, p. 046022, aug 2017.

[22] P. Mahakkanukrauh, P. Surin, and P. Vaidhayakarn, “Anatomical study of the pudendal nerve adjacent to the sacrospinous ligament,” *Clinical Anatomy*, vol. 18, no. 3, pp. 200–205, apr 2005.

[23] K. Wang, H. A. Fishman, H. Dai, and J. S. Harris, “Neural Stimulation with a Carbon Nanotube Microelectrode Array,” *Nano Letters*, vol. 6, no. 9, pp. 2043–2048, sep 2006.

[24] S. Walston, “Creating a Graphene-Based Neural Interface,” 2018. [Online]. Available: https://www.rdmag.com/article/2018/05/creating-graphene-based-neural-interface

[25] Y. Zhu, L. Li, C. Zhang, G. Casillas, Z. Sun, Z. Yan, G. Ruan, Z. Peng, A.-R. O. Raji, C. Kittrell, R. H. Hauge, and J. M. Tour, “A seamless three-dimensional carbon nanotube graphene hybrid material,” *Nature Communications*, vol. 3, no. 1, p. 1225, jan 2012.

[26] M. Franke, N. Bhadra, N. Bhadra, and K. Kilgore, “Direct current contamination of kilohertz frequency alternating current waveforms,” *Journal of Neuroscience Methods*, vol. 232, pp. 74–83, 2014.

B

Simulation system code

All code that was used for the project will be made available together with the electronic version of this thesis at `http://repository.tudelft.nl/`. This appendix provides an overview of the most important files that make up the simulations that were done for this thesis. An installation of Neuron is necessary for the simulator to work, refer to `https://www.neuron.yale.edu/neuron/` for instructions on installing Neuron. Furthermore, the Python code runs on Python version 2.7.

All code can also be uploaded on Brainframe, which has Neuron pre-installed and does not require compilation of files like AXNODE.mod and ipulse1.mod (they do however need to be included to the upload).

main.py

The main file is the starting file for python. It contains all functions that are necessary to reproduce the data that was necessary for this research, as well as the functions that generate the plots that can be found in this thesis. All functions should be commented, but by uncommenting and running each function one by one, from top to bottom, all files should be generated first, that are later necessary to create the plots with the functions that are further down the main file.

blockdetection.py

This file contains the block determination functions, both using the classic method and the proposed gate-dependent method. The function 'blockeffectiveness' returns a percentage representing the effectiveness of the block based on the spikes counted at the end of the axon, and only works for the classic method. The percentage can be compared with a threshold (e.g. 90%) to determine whether block has been reached. The function 'is_blocked' implements the proposed gate-dependent block-determination model as described in Section 3.2, and returns a boolean containing 'True' for a successful block or 'False' for an unsuccessful block.

The other functions are used to return values that were used in the calibration process of the proposed model (e.g. h_{max} of the measurement time frame).

monopolar_simulations.py and bipolar_simulations.py

This file contains the functions that were used to run the monopolar simulations of Section 5.2 and the bipolar simulations of Section 5.3. For some of the monopolar simulations, the file simulationfunctions_proposed-model.py is called, so this file is needed as well. Both files also contain a function that can be called to plot the results of the monopolar and bipolar simulations; plottingfunctions_results.py is needed for that the plots to generate.

waveforms.py

This file contains functions that generate waveforms in the correct format for Neuron, a process that was described in Section 4.1.

configoptions.py

This file contains the standard variable configurations that are used for simulations.

MRG_Model.py

This file contains the functions that are necessary to let Python interface with Neuron.

MRG_MODEL_edit.hoc

This file is an adapted version of the original MRG model file created by McIntyre et al. [13]. It has been extended to support monopolar and bipolar extracellular stimulation, and intracellular pulse trains have been implemented as well.

The file needs two other files to work correctly:

- AXNODE.mod, found in the original upload of the MRG Model:
  `https://senselab.med.yale.edu/ModelDB/showmodel.cshtml?model=3810`
- ipulse1.mod, which original file is lost but can be found as part of other models, for example at:
  `https://senselab.med.yale.edu/ModelDB/ShowModel.cshtml?model=225086&file=/GC-gna_distribution/ipulse1.mod`

Overview of other files

The rest of the files that are in the repository are:

- **datasetsformodeldesign.py** tests huge datasets for block and saves these results; these can be used to create thresholds conditions as in Equation (3.1) by quickly testing different threshold conditions, without the need for redoing new simulations.
- **plottingfunctions.py** and other Python files that start with ‘plottingfunctions’ are responsible for the different plots in this thesis.
- **simulationfunctions.py** contains simulation functions to determine block thresholds with the classic method.
- **x86_64** is a folder containing compiled versions of AXNODE.mod and ipulse1.mod; this could be useful when you want to run simulations locally and do not know how to compile these files.

Glossary

action potential The change in electrical potential resulting from an electrical impulse travelling through the membrane of a cell..

afferent / efferent Travelling respectively to / from the central nervous system..

anode / cathode Respectively the positive / negative electrode. However, since this thesis deals with alternating current waveforms, which means that anode and cathode would continuously switch roles, this thesis refers to the anode as the electrode that stimulates using the ‘original’ waveform, and to the cathode as the electrode that stimulates using the ‘inverted’ waveform. This is especially important when using charge-balanced asymmetrical waveforms or adding anodic and cathodic interphase delays of different size.

anode fraction The fraction of the waveform that makes up the period of the anodic pulse, thus given by $\frac{T_{\text{anodal}}}{T_{\text{anodal}}+T_{\text{cathodal}}}$.

anodic / cathodic interphase delay The interphase delay that follows directly after respectively the anodic / cathodic pulse.

anodic/cathodic pulse Respectively the positive/negative amplitude part of the waveform.

axon a nerve fiber that conducts electrical impulses (action potentials) originating from the nerve cell body..

block threshold The minimum current amplitude of a waveform that produces a KHFAC block under for a set of specific conditions.

block threshold charge per phase the charge per phase of the waveform when the amplitude is equal to the block threshold.

charge per phase The amount of charge that is generated during a single anodic or cathodic pulse. It is calculated as the integral of the current over the time of the pulse.

charge-balanced waveform A waveform that has equal positive and negative charge.

interpolar distance The distance between the two electrodes of a bipolar electrode set-up.

KHFAC node The node of Ranvier that is closest to the origin of the KHFAC stimulation signal.

KHFAC stimulation KiloHertz Frequency Alternating Current stimulation, a type of electrical stimulation that utilizes alternating current signals with frequencies in the kilohertz range which is primarily used to create a action potential propagation block in the nerve, or KHFAC block.

membrane voltage The difference in electric potential between the interior and exterior of a cell.

myelinated nerve A nerve with myelinated axons. These axons are covered with an insulating ‘myelin sheath’, except at the nodes of Ranvier. The insulation alters the electric fields that are created by the action potentials, which allows faster conduction of electrical impulses.

node of Ranvier Short unmyelinated segments of a myelinated axon. Because the insulating myelin sheath is missing at these segments, the nodes of Ranvier are the only part of a myelinated axon that can conduct electricity.

REVaIUE REstore Voiding Urinary REtention; the collaboration project between Erasmus MC and TU Delft that aims to restore the ability to relax the external urethral sphincter by applying KHFAC stimulation to the pudendal nerve.

virtual anode One of the two nodes adjecent to the KHFAC node.

Bibliography

[1] D. E. Irwin, Z. S. Kopp, B. Agatep, I. Milsom, and P. Abrams, “Worldwide prevalence estimates of lower urinary tract symptoms, overactive bladder, urinary incontinence and bladder outlet obstruction,” *BJU International*, vol. 108, no. 7, pp. 1132–1138, oct 2011.

[2] Y.-H. Chang, J. J.-Y. Siu, P.-J. Hsiao, C.-H. Chang, and E. C.-L. Chou, “Review of underactive bladder,” *Journal of the Formosan Medical Association*, vol. 117, no. 3, pp. 178–184, mar 2018.

[3] K. L. Kilgore and N. Bhadra, “Reversible nerve conduction block using kilohertz frequency alternating current,” *Neuromodulation*, vol. 17, no. 3, pp. 242–254, 2014.

[4] K. L. Kilgore and N. Bhadra, “Nerve conduction block utilising high-frequency alternating current,” *Medical & Biological Engineering & Computing*, vol. 42, no. 3, pp. 394–406, may 2004.

[5] TU Delft, “REValUE | TU Delft Repositories.” [Online]. Available: https://repository.tudelft.nl/islandora/search/project:REValUE

[6] N. Bhadra, E. A. Lahowetz, S. T. Foldes, and K. L. Kilgore, “Simulation of high-frequency sinusoidal electrical block of mammalian myelinated axons,” *Journal of Computational Neuroscience*, vol. 22, no. 3, pp. 313–326, may 2007.

[7] S. Zhao, G. Yang, J. Wang, J. R. Roppolo, W. C. de Groat, and C. Tai, “Conduction block in myelinated axons induced by high-frequency (kHz) non-symmetric biphasic stimulation,” *Frontiers in Computational Neuroscience*, vol. 9, p. 86, jul 2015.

[8] X. Zhang, J. Roppolo, W. De Groat, and C. Tai, “Simulation Analysis of Conduction Block in Myelinated Axons Induced by High-Frequency Biphasic Rectangular Pulses,” *IEEE Transactions on Biomedical Engineering*, vol. 53, no. 7, pp. 1433–1436, jul 2006.

[9] J. Wang, B. Shen, J. R. Roppolo, W. C. Groat, and C. Tai, “Influence of frequency and temperature on the mechanisms of nerve conduction block induced by high-frequency biphasic electrical current,” *Journal of Computational Neuroscience*, vol. 24, no. 2, pp. 195–206, 2008.

[10] Y. A. Patel, B. S. Kim, W. S. Rountree, and R. J. Butera, “Kilohertz Electrical Stimulation Nerve Conduction Block: Effects of Electrode Surface Area,” *IEEE Transactions on Neural Systems and Rehabilitation Engineering*, vol. 25, no. 10, pp. 1906–1916, oct 2017.

[11] D. M. Ackermann, E. L. Foldes, N. Bhadra, and K. L. Kilgore, “Effect of bipolar cuff electrode design on block thresholds in high-frequency electrical neural conduction block,” *IEEE Transactions on Neural Systems and Rehabilitation Engineering*, vol. 17, no. 5, pp. 469–477, 2009.

[12] D. R. Merrill, M. Bikson, and J. G. Jefferys, “Electrical stimulation of excitable tissue: Design of efficacious and safe protocols,” *Journal of Neuroscience Methods*, vol. 141, no. 2, pp. 171–198, 2005.

[13] C. C. McIntyre, A. G. Richardson, and W. M. Grill, “Modeling the Excitability of Mammalian Nerve Fibers: Influence of Afterpotentials on the Recovery Cycle,” *Journal of Neurophysiology*, vol. 87, no. 2, pp. 995–1006, feb 2002.

[14] S. R. Muellner, “The Physiology of Micturition,” *Journal of Urology*, vol. 65, no. 5, pp. 805–810, may 1951.

[15] W. de Groat, M. Fraser, M. Yoshiyama, S. Smerin, C. Tai, M. B. Chancellor, N. Yoshimura, and J. Roppolo, “Neural Control of the Urethra,” *Scandinavian Journal of Urology and Nephrology*, vol. 35, no. 207, pp. 35–43, jan 2001.

[16] M. J. Semins and M. B. Chancellor, “Diagnosis and management of patients with overactive bladder syndrome and abnormal detrusor activity,” *Nature Clinical Practice Urology*, vol. 1, no. 2, pp. 78–84, dec 2004.

[17] J. T. Stoffel, "Detrusor sphincter dyssynergia: a review of physiology, diagnosis, and treatment strategies." *Translational andrology and urology*, vol. 5, no. 1, pp. 127–135, feb 2016.

[18] G. Baquer Gómez, "Optimal stimulation waveform for efficacious high frequency block of the pudendal nerve with electrochemical damage," Master Thesis, TU Delft, 2018. [Online]. Available: http://resolver.tudelft.nl/uuid:5c875b14-08a3-4ef0-8e90-4fc997dc19d3

[19] J. A. Tanner, "Reversible Blocking of Nerve Conduction by Alternating-Current Excitation," *Nature*, vol. 195, no. 4842, pp. 712–713, aug 1962.

[20] Nevro, "Senza System." [Online]. Available: https://www.nevro.com/English/Physicians/Senza-System/default.aspx

[21] X. Zhang, J. R. Roppolo, W. C. De Groat, and C. Tai, "Mechanism of nerve conduction block induced by high-frequency biphasic electrical currents," *IEEE Transactions on Biomedical Engineering*, vol. 53, no. 12, pp. 2445–2454, 2006.

[22] B. Frankenhaeuser and A. F. Huxley, "The action potential in the myelinated nerve fibre of Xenopus laevis as computed on the basis of voltage clamp data," *The Journal of Physiology*, vol. 171, no. 2, pp. 302–315, jun 1964.

[23] J. R. Schwarz and G. Eikhof, "Na currents and action potentials in rat myelinated nerve fibres at 20 and 37° C," *Pflügers Archiv European Journal of Physiology*, vol. 409, no. 6, pp. 569–577, 1987.

[24] A. L. Hodgkin and A. F. Huxley, "A quantitative description of membrane current and its application to conduction and excitation in nerve," *J. Physiol.*, vol. 117, pp. 500–544, 1952.

[25] J. G. Betts, P. Desaix, E. Johnson, J. E. Johnson, O. Korol, D. Kruse, B. Poe, J. A. Wise, M. Womble, and K. A. Young, *Anatomy and Physiology*, 1st ed. OpenStax, 2017.

[26] J. B. Ranck, "Which elements are excited in electrical stimulation of mammalian central nervous system: A review," *Brain Research*, vol. 98, no. 3, pp. 417–440, nov 1975.

[27] M. Franke, T. Vrabec, J. Wainright, N. Bhadra, N. Bhadra, and K. Kilgore, "Combined KHFAC +DC nerve block without onset or reduced nerve conductivity after block," *Journal of Neural Engineering*, vol. 11, no. 5, p. 056012, 2014.

[28] E. H. Lothet, K. L. Kilgore, N. Bhadra, N. Bhadra, T. Vrabec, Y. T. Wang, E. D. Jansen, M. W. Jenkins, and H. J. Chiel, "Alternating current and infrared produce an onset-free reversible nerve block," *Neurophotonics*, vol. 1, no. 1, p. 011010, jul 2014.

[29] J. D. Miles, K. L. Kilgore, N. Bhadra, and E. A. Lahowetz, "Effects of ramped amplitude waveforms on the onset response of high-frequency mammalian nerve block," *Journal of Neural Engineering*, vol. 4, no. 4, pp. 390–398, 2007.

[30] R. P. Williamson and B. J. Andrews, "Localized electrical nerve blocking," *IEEE Transactions on Biomedical Engineering*, vol. 52, no. 3, pp. 362–370, 2005.

[31] Medtronic, "Spinal neurostimulation lead / quadrupolar - 3889, 3093 - Medtronic." [Online]. Available: http://www.medicalexpo.com/prod/medtronic/product-70691-503182.html

[32] P. Mahakkanukrauh, P. Surin, and P. Vaidhayakarn, "Anatomical study of the pudendal nerve adjacent to the sacrospinous ligament," *Clinical Anatomy*, vol. 18, no. 3, pp. 200–205, apr 2005.

[33] D. M. Ackermann, N. Bhadra, M. Gerges, and P. J. Thomas, "Dynamics and sensitivity analysis of high-frequency conduction block," *Journal of Neural Engineering*, vol. 8, no. 6, p. 65007, 2011.

[34] G. van Rossum, "Python tutorial," Centrum voor Wiskunde en Informatica (CWI), Amsterdam, Tech. Rep., 1995.

[35] B. W. Kernighan and J. R. Mashey, "The UNIX™ programming environment," *Software: Practice and Experience*, 1979.

[36] M. L. Hines and N. T. Carnevale, "The NEURON simulation environment." *Neural computation*, vol. 9, no. 6, pp. 1179–209, aug 1997.

[37] A. Graham, "HyperPhysics," 2003. [Online]. Available: http://hyperphysics.phy-astr.gsu.edu/hbase/electric/equipot.html

[38] A. G. Richardson, C. C. Mclntyre, W. M. Grill, G. A˜cial, and G. Ga, "Modelling the effects of electric fields on nerve fibres: influence of the myelin sheath," *Medical & Biological Engineering & Computing*, vol. 38, no. 4, pp. 438–446, 2000.

[39] D. R. McNeal, "Analysis of a Model for Excitation of Myelinated Nerve," *IEEE Transactions on Biomedical Engineering*, vol. BME-23, no. 4, pp. 329–337, jul 1976.

[40] S. Y. Chiu, J. M. Ritchie, R. B. Rogart, and D. Stagg, "A quantitative description of membrane currents in rabbit myelinated nerve." *The Journal of physiology*, vol. 292, pp. 149–66, jul 1979.

[41] J. D. Sweeney, J. T. Mortimer, and D. M. Durand, "Modeling of mammalian myelinated nerve for functional neuromuscular stimulation," *IEEE 9th Annual Conference of the Engineering in Medicine and Biology Society*, 1987.

[42] J. R. Schwarz, G. Reid, and H. Bostock, "Action potentials and membrane currents in the human node of Ranvier," *Pflügers Archiv European Journal of Physiology*, vol. 430, no. 2, pp. 283–292, 1995.

[43] C. H. Berthold and M. Rydmark, "Anatomy of the paranode-node-paranode region in the cat," *Experientia*, vol. 39, no. 9, pp. 964–976, sep 1983.

[44] G. Smaragdos, G. Chatzikonstantis, R. Kukreja, H. Sidiropoulos, D. Rodopoulos, I. Sourdis, Z. Al-Ars, C. Kachris, D. Soudris, C. I. De Zeeuw, and C. Strydis, "BrainFrame: a node-level heterogeneous accelerator platform for neuron simulations," *Journal of Neural Engineering*, vol. 14, no. 6, p. 066008, dec 2017.

[45] N. Bhadra and K. L. Kilgore, "High-frequency electrical conduction block of mammalian peripheral motor nerve," *Muscle & Nerve*, vol. 32, no. 6, pp. 782–790, dec 2005.

[46] C.-W. Peng, S.-C. Chen, W.-J. Fan, C.-H. Lai, and J.-J. Chen, "Influence of stimulus waveforms of high-frequency electrical current on nerve conduction block," in *2009 4th International IEEE/EMBS Conference on Neural Engineering*. IEEE, apr 2009, pp. 72–75. [Online]. Available: http://ieeexplore.ieee.org/document/5109237/https://ieeexplore.ieee.org/stamp/stamp.jsp?tp={&}arnumber=5109237

[47] N. A. Pelot, C. E. Behrend, and W. M. Grill, "Modeling the response of small myelinated axons in a compound nerve to kilohertz frequency signals," *Journal of Neural Engineering*, vol. 14, no. 4, p. 046022, aug 2017.

[48] S. A. Shikora, B. M. Wolfe, C. M. Apovian, M. Anvari, D. B. Sarwer, R. D. Gibbons, S. Ikramuddin, C. J. Miller, M. B. Knudson, K. S. Tweden, M. G. Sarr, and C. J. Billington, "Sustained Weight Loss with Vagal Nerve Blockade but Not with Sham: 18-Month Results of the ReCharge Trial," *Journal of Obesity*, vol. 2015, pp. 1–8, jul 2015.